UNIVERSITY OF SOUTHAMPTON

Faculty of Engineering, Science and Mathematics

School of Ocean & Earth Sciences

Saturation effects on frequency-dependent seismic anisotropy in fractured porous rocks

by

Kelvin I. Amalokwu

Doctor of Philosophy

January 2016

UNIVERSITY OF SOUTHAMPTON

Abstract

FACULTY OF ENGINEERING, SCIENCE & MATHEMATICS

SCHOOL OF OCEAN & EARTH SCIENCES

Doctor of Philosophy

SATURATION EFFECTS ON FREQUENCY-DEPENDENT SEISMIC ANISOTROPY IN FRACTURED POROUS ROCKS

by Kelvin I. Amalokwu

The response of Earth materials to seismic wave propagation is the most commonly used geophysical method for studying the Earth's crust. Rocks making up the Earth's crust are porous, with fluids occupying the pore space. The saturation of the pore space can be multiphase, for example, in gas reservoirs and gas bearing oil reservoirs where gas and liquid occupy the pore space. Additional voids such as aligned fractures are common in the Earth's crust and are known to cause seismic anisotropy. Knowledge of the effects of pore fluids and of aligned fractures on seismic wave propagation is needed for the interpretation of seismic data in terms of these physical properties. This information is particularly useful for the hydrocarbon industry as the presence of either natural or artificially induced fractures can play a major role in the safe and efficient exploration and production of hydrocarbons. Therefore, it is important to be able to remotely characterise fractures in fluid-filled reservoir rocks.

Theoretical models are used to relate seismic measurements to the physical properties of rocks such as porosity, saturation, and fracture properties. Previous studies have either focused on multiphase saturation effects in non-fractured isotropic rocks or on single fluid phase saturation effects in fractured anisotropic rocks. Therefore, the combined effect of multiphase saturation and aligned fractures is still poorly understood. This thesis focuses on improving the understanding of the effect of saturation on fracture-induced seismic anisotropy

by using novel synthetic sandstones with known fracture properties to conduct controlled laboratory experiments. Although controlled laboratory experiments are usually carried out in order to validate, calibrate or extend existing theoretical models, this thesis takes a different approach of making experimental observations in the absence of suitable theoretical models. The results are intended not only to improve our understanding of this aspect, but also to help inform the development of suitable theoretical models.

I present ultrasonic laboratory data investigating certain aspects of water saturation effects on the seismic response of rocks containing aligned fractures. The results are analysed from a theoretical but yet qualitative approach where possible. Despite experimental limitations such as the violation of the equivalent media criteria, certain new phenomena are observed which are in agreement with theoretical mechanisms. Variations are observed between the compressional and shear attenuation versus water saturation relationships of a non-fractured rock, and a rock containing fractures aligned parallel to wave propagation. Thomsen's P-wave anisotropy parameter ε, and shear wave splitting at 45° to the fracture normal were found to be sensitive to water saturation. These results have implications for gas saturation estimation in hydrocarbon reservoirs. Attempts to study the implications of changing porosities on saturation effects in rocks containing aligned fractures yielded ambiguous results due to unexpected experimental limitations. However, the study showed that it is possible to achieve the non-trivial task of varying the porosity of the synthetic sandstones within a good range 17% - 27%, and sets the scene for future studies of a similar kind.

Table of Contents

List of Figures

Declaration of Authorship

I, *Kelvin I. Amalokwu,* declare that this thesis entitled:

Saturation effects on frequency-dependent seismic anisotropy in fractured porous rocks

and the work presented in it are my own and has been generated by me as the result of my own original research. I confirm that:

1. This work was done wholly or mainly while in candidature for a research degree at this University;
2. Where any part of this thesis has previously been submitted for a degree or any other qualification at this University or any other institution, this has been clearly stated;
3. Where I have consulted the published work of others, this is always clearly attributed;
4. Where I have quoted from the work of others, the source is always given. With the exception of such quotations, this thesis is entirely my own work;
5. I have acknowledged all main sources of help;
6. Where the thesis is based on work done by myself jointly with others, I have made clear exactly what was done by others and what I have contributed myself;
7. Parts of this work have been published as:

Journal Publications:

Amalokwu, K., A. I. Best, J. Sothcott, M. Chapman, T. Minshull, and X.-Y. Li. 2014, Water saturation effects on elastic wave attenuation in porous rocks with aligned fractures. Geophysical Journal International, 197, no. 2,943-947. doi: 10.1093/gji/ggu076.

Amalokwu, K., M. Chapman, A. I. Best, J. Sothcott, T. A. Minshull, and X.-Y. Li. 2015, Experimental observation of water saturation effects on shear wave

splitting in synthetic rock with fractures aligned at oblique angles. Geophysical Journal International, 200, no. 1,17-24. doi: 10.1093/gji/ggu368.

Amalokwu, K., M. Chapman, A. I. Best, T. A. Minshull, and X.-Y. Li. 2015, Water saturation effects on P-wave anisotropy in synthetic sandstone with aligned fractures. Geophysical Journal International, 202, no. 2,1088-1095. doi: 10.1093/gji/ggv192.

Conference proceedings:

Amalokwu, K., Best, A.I., Sothcott, J., Chapman, M., Minshull, T. & Li, X.-Y., 2014. A Laboratory Study of Qs/Qp and Vp/Vs Ratios for Water Saturation Estimate in Fractured and Non-fractured Sandstones. 76th EAGE Conference and Exhibition, Amsterdam.

Amalokwu, K., Best, A.I., Sothcott, J., Chapman, M., Minshull, T. & Li, X.-Y., 2014. Water saturation effects on wave velocity and attenuation in porous rock with aligned fractures. 84th SEG Annual meeting, Denver.

Amalokwu, K., Best, A.I., Chapman, M., Papageorgiou, G, 2015. Water saturation effects on shear wave splitting in synthetic rock with fractures aligned at oblique angles. 3rd international workshop on rock physics, Perth.

Amalokwu, K., Best, A.I., Chapman, M., Minshull, T. & Li, X.-Y., 2015. Partial gas saturation effects on P-wave anisotropy in porous rock with aligned fractures. 85th SEG Annual Meeting, New Orleans.

Journal publications during PhD candidature but not included in this thesis:

Amalokwu, K., Best, A.I., Chapman, M., 2016. Effects of aligned fractures on the response of velocity and attenuation ratios to water saturation variation: A laboratory study using synthetic sandstones, Geophysical prospecting, in press.

Falcon-Suarez, I., North, L., Amalokwu, K. & Best, A.I., 2016. Integrated Geophysical and Hydromechanical Assessment for CO_2 Storage: Shallow Low Permeable - Reservoir Sandstones, Geophysical prospecting, in press.

Papageorgiou, G., Amalokwu, K. & Chapman, M., 2016. Theoretical Derivation of a Brie-like Fluid Mixing Law, Geophysical prospecting, in press.

Reports during PhD candidature but not included in this thesis:

Amalokwu, K., Best, A.I., 2015. A procedure for manufacturing silica-cemented synthetic porous rocks (sandstones). National Oceanography Centre Research & Consultancy Report No. 47.

Signed: .....

Date: .....

Acknowledgements

I would like to thank my supervisors Dr. Angus Best, Dr. Mark Chapman and Prof. Tim Minshull for their continuous guidance, support and encouragement throughout my PhD. I would like to thank Angus for giving me this opportunity and for always having his door open for any discussions. I would like to thank Mark for many stimulating discussions, and for always being accommodating and welcoming, especially during my visits to Edinburgh.

I would like to thank Jeremy Sothcott for his technical help with the experiments, his many jokes which helped ease the pain of several experimental disappointments, and for helping me settle-in at NOCS when I arrived. Without his help, the laboratory experiments in this thesis would not have been possible. His insights and expertise also led to the advances in the synthetic rocks.

Help from Laurence North, Bob Jones and John Ford with various aspects of sample preparation and experimentation is gratefully acknowledged. I would also like to thank my colleagues and office mates at NOCS for making my time here enjoyable, and for many stimulating discussions (scientific and non-scientific).

I would like to thank the sponsors of the Edinburgh Anisotropy Project for funding this project through a NERC-BGS PhD studentship.

Finally, I wish to express my sincere gratitude to my family, Kathryn Locke, and Mr. and Mrs. Locke for their support and encouragement which has greatly helped me through this PhD.

Notations and Conventions

The Einstein summation convention, i.e. summation over repeated indices, applies throughout this thesis.

Chapter 1: Introduction

The Earth's interior is studied for many reasons including understanding the Earth's dynamics, geohazards, and for natural resource exploitation. Seismic methods are the most widely used for this purpose and form the core of geophysical studies. The properties of seismic waves propagating through a medium are controlled by the properties of the medium. This means that in principle, it is possible to infer information about the properties of the medium from its seismic response.

Crustal rocks are porous, with fluids (sometimes multiphase) occupying these pore spaces and the seismic properties of the fluid saturated rock will depend on the rock and fluid properties. This sensitivity of seismic properties to pore fluid properties is exploited for hydrocarbon exploration and production, monitoring geologic storage of carbon dioxide (CO_2), volcanology, and geothermal reservoir management (Ensley, 1984, Simiyu, 2000, Castagna et al., 2003, Arts et al., 2004, Sodagar and Lawton, 2014).

When the pore space of a rock contains fluids of different phases (e.g. liquid and gas), the seismic response of the fluid saturated rock not only depends on the rock-fluid properties, but also on the spatial distribution of fluid phases (Knight and Nolen-Hoeksema, 1990, Knight et al., 1998, Mavko and Mukerji, 1998). Partial liquid/gas saturation can occur in gas reservoirs, oil reservoirs where the gas has come out of solution, and in oil/water reservoirs where gas (e.g. CO_2, natural gas) has been injected either to stimulate production or for geologic sequestration. This partial fluid saturation can cause velocity dispersion and attenuation due to wave-induced fluid flow.

A lot of effort has gone into quantifying these effects both theoretically and experimentally, and is still an active area of research (Domenico, 1974, White, 1975, 1976, Mavko and Nur, 1979, Murphy, 1982, 1984, Murphy et al., 1986, Miksis, 1988, Norris, 1993, Cadoret et al., 1995, 1998, Müller and Gurevich, 2004, Pride et al., 2004, Qi et al., 2014, Papageorgiou and Chapman, 2015). However, research into partial saturation effects in rocks and their applications have mainly focused on non-fractured isotropic rocks even though subsurface rocks are known to be anisotropic.

Aligned cracks are believed to be the main cause of the widespread occurrence of seismic anisotropy in the Earth's crust (Crampin, 1994, 1999, Crampin and Peacock, 2005). In subsurface reservoirs, fractures can significantly control fluid flow during both production, and injection for recovery stimulation (Reiss, 1980, Nelson, 2001). Depending on the interplay between the fracture, rock and fluid properties, the presence of fractures could either aid or limit recovery (Reiss, 1980, Allan and Sun, 2003). In general, where the net result of the presence of fractures is an increase in permeability, an increase in recovery would be expected. However, this is not always the case, for example, in stimulation by waterflooding, fractures could lead to a reduction in sweep efficiency. Also, increased rate of production due to the presence of fractures could lead to a rapid decline in reservoir pressure, leading to gas coming out of solution, leaving the oil more dense and viscous thereby reducing recovery (Fernø, 2012). During the injection of waste gases such as carbon dioxide for geologic sequestration, leakage pathways due to the presence of fractures is undesirable as the gases could make it back to the surface or contaminate subsurface aquifers. It is clear that knowledge of the location of the fractures and their properties (e.g. orientation and density) are important for the optimisation of field development and production, and monitoring of geologic disposal of fluids (e.g. CO_2, acid gases).

The orientation of fractures in the Earth's crust is believed to be related to the stress field in the subsurface, as open fractures will tend to be aligned parallel to the direction of maximum in-situ stress (so normal to minimum in-situ stress) (Crampin, 1987, Thomsen, 2002). When a medium contains aligned fractures, its overall properties as experienced by long-wavelength waves will be anisotropic (Hudson et al., 2001). The presence of aligned fractures has been shown to cause seismic anisotropy which as a result has been widely used for fractured rock characterisation. This has the advantages of relatively low cost, deeper penetration, and much wider spatial coverage compared to logging tools such as the borehole televiewer and formation microimager (Schlumberger, 1991) which are designed to view fractures which the boreholes have intersected. These borehole logging methods provide the only direct information about the fracture properties such as fluid content, vertical extent, geometry and connectivity; however, this information is limited by the high costs and small sampling coverage.

Over the past three decades, the use of seismic anisotropy for fractured rock characterisation has received considerable interest and has seen a great deal of progress. Different techniques for obtaining measurements of seismic anisotropy have been developed including shear wave splitting, variation of seismic velocities with azimuth, and the azimuthal variation of AVO gradients (Crampin et al., 1980b, Crampin, 1985, Alford, 1986, Crampin et al., 1986, Thomsen, 1986, Lynn and Thomsen, 1990, Queen and Rizer, 1990, Winterstein and Paulsson, 1990, Mueller, 1991, Lynn et al., 1996, Rüger, 1997, Sayers and Rickett, 1997, Bakulin et al., 2000, Winterstein et al., 2001, Thomsen, 2002).

Equivalent medium theories are used to relate the measured seismic anisotropy to fracture properties. This approach considers the wavelength to be long enough so that a heterogeneous medium can be represented as a homogeneous medium with equivalent effective properties as the heterogeneous medium. If the heterogeneities (e.g. fractures, bedding planes, crystals) have a preferred alignment, the effective properties of the equivalent medium would be anisotropic. Seismic wavelengths can be on the order of a few kilometres and as such the heterogeneities that can be modelled using equivalent medium theories can range from microscale to macroscale. Detailed fractured reservoir characterization requires knowledge of the background rock matrix property (e.g. lithology, porosity), fracture properties (e.g. crack density, size, orientation, connectivity), and their fluid fill (Hudson et al., 2001). Therefore, interpreting seismic data in terms of these physical properties requires an understanding of the seismic response in porous saturated fractured media.

The effects of fluid saturation on the anisotropic response of rocks containing fractures have received considerable attention already (Hudson, 1981, Rathore et al., 1995, Thomsen, 1995, Hudson et al., 1996, Xu, 1998, Chapman, 2003, Gurevich, 2003, Jakobsen, 2004, Gurevich et al., 2009, Tillotson et al., 2011, 2012). However, these studies have focused on single phase fluid saturation. As such, the effects of multiphase fluid saturation (e.g. liquid and gas) on fracture-induced seismic anisotropy are still poorly understood even though both aligned fractures and partial saturation are likely to be present at the same time in subsurface reservoirs. One way to improve our understanding of saturation effects on fracture-induced anisotropy is through controlled laboratory experiments, which could also help inform the development of suitable theoretical models.

Controlled laboratory studies of fracture-induced seismic anisotropy are limited and only a handful have investigated fluid effects using porous rocks containing aligned fractures (e.g. Rathore et al., 1995, Tillotson et al., 2011, 2012, 2014). The limited number of fractured rock experiments is due to the difficulty of obtaining rock samples possessing a realistic background material with known and controlled fracture properties. A significant advance at addressing this difficulty was made by Rathore et al. (1995), who made synthetic porous epoxy-cemented sandstone samples containing aligned penny-shaped voids. Tillotson et al. (2012) improved on this approach by making synthetic silica-cemented porous sandstone samples. These studies focused on validating certain aspects of equivalent medium fractured rock theories. The work of Tillotson et al. (2012) has paved the way for more studies into fluid effects on fracture-induced anisotropy and the effects of partial saturation is one of interest. The synthetic rocks represent an analogue of naturally occurring sandstones and as such would be expected to saturate in a similar way to natural sandstones that have been used for partial saturation studies. These novel synthetic fractured sandstones have paved the way for further experimental studies of other aspects of fracture-induced seismic anisotropy using more realistic rock materials.

The aim of this work is to study the effects of partial liquid/gas saturation on fracture-induced seismic anisotropy by carrying out controlled laboratory experiments using synthetic porous sandstones containing aligned penny-shaped fractures. Effects of water saturation on P- and S- wave velocity and attenuation anisotropy were investigated. The experimental results show several new phenomena. Although there is a lack of suitable theories with which to model our results, existing theoretical mechanisms were found to be successful in explaining the experimental observations. There is still no general consensus on the theoretical mechanisms responsible for dispersion and attenuation in the isotropic case (Batzle et al., 2006, Wu et al., 2014), let alone the anisotropic case. Which mechanism dominates over which at various frequencies, or is the dispersion a result of multiple mechanisms? If there are multiple mechanisms, how do they combine? These are still open research questions and the presence of fractures adds further complexities. Therefore, the focus of the interpretation of the experimental results will be more qualitative even though theoretical models are employed to interpret the data where possible. Dispersion is acknowledged and some mechanisms are adopted without limiting the cause of dispersion to any particular mechanism.

I begin this thesis with reviews of saturation effects and seismic anisotropy in rocks. I introduce the concepts of poroelasticity, velocity dispersion and attenuation, and discuss the effects of partial saturation on seismic properties of rocks. I describe wave propagation in anisotropic media, methods of seismic fracture detection, and equivalent medium representation of fractured rocks. I then discuss frequency-dependent seismic anisotropy due to wave induced fluid flow. A review of laboratory measurements of fractured rock anisotropy is presented, and the need for synthetic rocks is discussed. The chapter then concludes with a description of the models of White (1975) and Chapman (2003) which are used in this thesis.

The remainder of the thesis is a collection of self-contained papers (or studies).

The set of experimental results presented by Amalokwu et al. (2014) forms chapter three. The results show that the presence of fractures aligned parallel to the direction of wave propagation can change the attenuation versus water saturation relationships from those observed in non-fractured rocks. Important interpretations of the possible mechanisms involved are inferred from the results. Results for the non-fractured rock sample corroborate previous works.

Chapter four represents the paper by Amalokwu et al. (2015b), which presents the effects of water saturation on shear wave splitting when fractures are aligned at oblique angles to wave propagation direction. Previous work has shown that shear wave splitting in this direction can be sensitive to the fluid properties but only for full saturation with a single fluid. The results show shear wave splitting due to fractures aligned at oblique angles to wave propagation can be sensitive to water saturation. In seeking to explain these observations, we find the concept of wave induced fluid flow to be useful.

Chapter five deals with the effects of water saturation on P-wave anisotropy, which represents the paper by Amalokwu et al. (2015a). The samples were in the shape of octagonal prisms which allowed measurements in different directions relative to the fracture orientations, and were made at the National Oceanography Centre, Southampton. The results showed a sensitivity of P-wave anisotropy to water saturation. Again, the concept of wave-induced fluid flow was found to be useful in interpreting the results. Two frequency-dependent models were combined to interpret the results. The modelling suggests that although the

saturation distribution in the background rock could be important, the saturation distribution at the pore/fracture scale could also have significant effects.

Background porosity has been shown to affect fracture-induced P-wave anisotropy in saturated rocks due to wave induced fluid flow. Chapter six was aimed at investigating the effects of saturation on rocks with similar fracture properties but different background properties. I describe the making of synthetic rocks with varying background rock properties but similar fracture properties. On first tests of the elastic properties of the rocks, I found that the results on the porosity effects on P-wave anisotropy were ambiguous due to unforseen limitations associated with the manufacturing process. However, this study did show it is possible to vary porosities of the synthetic sandstones within a good range 17% - 27%, which is not trivial.

Chapter seven summarises the results and discusses the significance of the findings and their implications for seismic exploration.

Chapter 2: Review of saturation effects and seismic anisotropy in rocks

Summary: The aim of this chapter is to introduce the effects of fluid saturation (including partial saturation) and the effects of aligned fractures on the seismic response of rocks, setting the scene for subsequent chapters. I begin by introducing poroelasticity and discussing the concept of dynamic poroelasticity (frequency-dependent behaviour). Partial saturation effects on the seismic response of rocks are then discussed. I go on to review some basic theoretical fundamentals of seismic anisotropy, after which methods used for seismic fracture detection are summarized. The concept of frequency-dependent seismic anisotropy due to wave induced fluid flow is discussed, and a brief review of laboratory experimental fractured rock studies is presented. This chapter concludes with a discussion of the models of White (1975) and Chapman (2003), which are used in this thesis.

2.1 Poroelasticity

Sedimentary rocks are porous (and permeable) materials and when fluid saturated, elasticity theory is not sufficient to describe their seismic response. Poroelasticity deals with describing the response of fluid saturated porous media to deformation. Terzaghi (1923) provided the earliest theory to account for the influence of pore fluids in porous rocks when he proposed a quasi-static deformation model for describing one-dimensional consolidation of soils (clay). However, the modern development of poroelasticity and three-dimensional generalization is due to M.A. Biot who in a series of works (Biot, 1941, 1956) was the first to develop a linear theory of poroelasticity to account for the effects of dynamic loading and stress waves (Detournay and Cheng, 1993, Rice, 1998). In seismic exploration, the problem of estimating the impact of changing fluid saturation on seismic response is known as fluid substitution. The theory of Gassmann (1951) which is consistent with the low-frequency theory of Biot (1956) is the most widely used poroelastic model for fluid substitution.

Gassmann (1951) gave explicit solutions for the saturated bulk modulus of a fluid saturated isotropic porous medium which can be written as (Wang, 2001, Mavko et al., 2009)

$$K_{sat} = K_{dry} + \frac{\left(1 - \frac{K_{dry}}{K_m}\right)^2}{\frac{\phi}{K_f} + \frac{(1-\phi)}{K_m} - \frac{K_{dry}}{K_m^2}}, \tag{2.1}$$

where K_{sat} is the bulk modulus of a porous medium with a frame bulk modulus K_{dry}, saturated with a fluid of bulk modulus K_f; K_m is the matrix material bulk modulus, and ϕ is the porosity. The shear modulus is predicted not to be affected by saturation (e.g. Mavko and Jizba, 1991, Berryman, 1999) so that

$$\mu_{sat} = \mu_{dry}\,. \tag{2.2}$$

There are some assumptions associated with Gassmann's equations. The model assumes that the matrix mineral and frame moduli are macroscopically homogeneous which assures the wavelength is long compared to the grain and pore sizes. Brown and Korringa (1975) generalised Gassmann's relations to the case where the rock matrix mineral is heterogeneous. The pore space is also assumed to be statistically isotropic and completely connected, and filled with a non-viscous fluid, which ensures equilibration of wave-induced fluid flow. The

model also assumes the rock-fluid system is undrained and that there is no chemical interaction between the fluid and the solid that would result in a change in the frame properties. In the static limit, the assumption of complete pore pressure equalization is valid for most rocks; however, for seismic wave propagation this assumption might not always be valid. Depending on the seismic wave frequency relative to the pore space interconnectivity and viscosity of the pore fluid, the assumption of pore pressure equilibration might not be valid. The frequency of the seismic wave needs to be low enough to ensure pore pressures are equalised within the time frame of half a wave period (Wang, 2001, Smith et al., 2003). Seismic frequencies are generally considered low enough for Gassmann's assumption of pore pressure equalisation to be valid (e.g. Domenico, 1976, Murphy, 1984, Winkler, 1985, Wang and Nur, 1992, Mavko and Nolen - Hoeksema, 1994, Nolen - Hoeksema, 2000, Wang, 2001, Smith et al., 2003); however, this might not always be the case (Batzle et al., 2006). At higher frequencies such as sonic (logging) or ultrasonic frequency ranges, the measured bulk moduli or velocities are usually higher than those calculated with Gassmann's equations (e.g. Murphy, 1985, Winkler, 1985, Winkler, 1986, Wang and Nur, 1990, Gist, 1994a, Sams et al., 1997, Adelinet et al., 2010). This is due to dispersion as a result of wave-induced fluid flow.

In addition to the equations for fluid substitution in isotropic rocks, Gassmann (1951) also gave equations for anisotropic porous rocks. Brown and Korringa (1975) generalised the anisotropic Gassmann equations to allow for an anisotropic mineral. This generalised Gassmann equation is given in the compliance domain as (Mavko et al., 2009)

$$S_{ijkl}^{sat} = S_{ijkl}^{dry} - \frac{\left(S_{ijaa}^{dry} - S_{ijaa}^{0}\right)\left(S_{bbkl}^{dry} - S_{bbkl}^{0}\right)}{\left(S_{ccdd}^{dry} - S_{ccdd}^{0}\right) + \phi\left(\beta_{fl} - \beta_{0}\right)}, \tag{2.3}$$

where S_{ijkl}^{dry} is the effective elastic compliance tensor element of the dry rock, S_{ijkl}^{sat} is the effective compliance tensor of the saturated rock, S_{ijkl}^{0} is the effective elastic compliance element of the solid mineral, β_{fl} is the fluid compressibility, β_0 is the mineral compressibility, and ϕ is the porosity.

2.1.1 Dynamic poroelasticity: attenuation and dispersion mechanisms

When seismic waves propagate through a fluid saturated rock, the finite wavelength (or finite frequency) and the high contrast in elastic moduli between

the solid matrix and the pore fluid causes relative motion between the solid matrix and the pore fluid, causing dispersion and attenuation (Wang, 2001). This wave induced fluid flow can occur at different length scales; from the macroscopic scale down to the microscopic scale. Viscous dissipation and dispersion due to wave induced fluid flow has long been recognised and has led to the development of dynamic theories for wave propagation in fluid saturated porous media.

Biot (1956) was the first to develop a theory for wave propagation in fluid saturated porous media which quantified viscous dispersion and attenuation. He developed a theory that covers the whole frequency range and showed that the relative motion between the pore fluid and the rock matrix, and the viscous coupling between them, can result in velocity dispersion and associated attenuation. Biot considered wavelength-scale wave-induced fluid pressure equilibration between peaks and troughs of the passing seismic wave (Pride et al., 2003) and as such, this type of mechanism is usually referred to as global flow or macroscopic fluid flow. Biot's theory reduces to Gassmann's theory in the low frequency limit. Biot defined the critical frequency where the transition from the low-frequency to the high-frequency regime occurs as

$$f_c = \frac{\eta\phi}{2\pi k\rho_f}, \tag{2.4}$$

where η and ρ_f are the viscosity and density of the pore fluid, respectively, and ϕ and k are the porosity and permeability of the rock, respectively. For typical rocks, the values for the critical frequency are above 100 kHz and could reach frequencies on the order of gigahertz (Wang and Nur, 1992, Mavko et al., 2009, Müller et al., 2010). Biot's theory also predicts the existence of a third body wave, a slow compressional wave which has been observed experimentally (Plona, 1980, Klimentos and McCann, 1988, Johnson et al., 1994, Kelder and Smeulders, 1997). Although Biot's theory predicts that an elastic wave propagating through a fluid-saturated porous medium is both dispersive and dissipative, it under-predicts the magnitude of dispersion and attenuation (Winkler, 1985, Winkler, 1986, Wang and Nur, 1990, Wang and Nur, 1992, Winkler and Murphy, 1995, King et al., 2000). Biot's theory also predicts that the critical frequency is directly proportional to the viscosity of the fluid which implies lower velocities for higher fluid viscosities. This is in contradiction to experimental observations (e.g. Winkler, 1985, Batzle et al., 2001, 2006).

Another wave induced fluid flow mechanism that has been proposed to account for dispersion and attenuation in rocks is the "local" or "squirt" flow mechanism which is based on microscopic fluid motion at the grain scale. The pore space of rocks are generally heterogeneous and consist of stiff (intergranular pores) and compliant regions (microcracks and grain contacts) adjacent to one another. As a result, local pressure gradients could arise due to the compression of the compliant regions to a much greater extent than the stiff regions, causing fluid flow which results in viscous dissipation and dispersion. When there is not enough time for the fluid pressure gradients to relax, the rock appears stiffer than when the fluid pressure gradients are relaxed. Unlike in the Biot theory, the pressure gradients do not necessarily point in the direction of wave propagation (Mavko and Nur, 1979, Winkler and Nur, 1982, Chapman et al., 2002, Pride et al., 2003). Velocities and attenuation depend on the frequency of the elastic wave relative to the particular timescale it takes the pressure gradients to relax. Mavko and Nur (1975) were the first to analyse this mechanism that has since received further theoretical treatment (e.g. O'Connell and Budiansky, 1977, Johnston et al., 1979, Mavko and Nur, 1979, Palmer and Traviolia, 1980, Murphy et al., 1986, Tutuncu and Sharma, 1992, Dvorkin et al., 1995, Chapman et al., 2002, Pride et al., 2004, Gurevich et al., 2010). The interest in this mechanism has been driven primarily by two reasons; it predicts much higher magnitudes of dispersion and attenuation than Biot's theory and as such has been able to explain dispersion and attenuation observed at higher frequencies (e.g. Winkler and Nur, 1979, Winkler and Nur, 1982, Winkler, 1983, Murphy, 1984, Winkler, 1985, Winkler, 1986, Wang and Nur, 1990, Sams et al., 1997, Adelinet et al., 2010). Secondly, Biot's theory predicts that the characteristic frequency is directly proportional to viscosity and inversely proportional to permeability, while the squirt mechanism predicts an opposite relationship which has been shown to be more consistent with experimental observations (Winkler, 1985, Batzle et al., 2001, 2006). Despite the success of the squirt mechanism in explaining the magnitude of dispersion and attenuation in data, its quantitative use is still hindered by its strong dependence on details of the microstructure that are not readily available or cannot be adequately measured (Winkler and Murphy, 1995, Dvorkin and Mavko, 2006).

A third mechanism is the wave induced flow at mesoscopic scales due to heterogeneities larger than the pore scale but much smaller than the wavelength. At this scale, variations in rock compliance can occur, for example, due to heterogeneities in saturating fluid distribution or due to heterogeneities in rock

properties. The physical representation of this mechanism is similar to the local (squirt) flow concept in that the more compliant region is compressed to a greater extent than the stiffer region. This difference creates fluid pressure gradients that drive mesoscopic fluid flow which causes viscous dissipation and dispersion. When a rock is saturated with regions (or patches) of two immiscible fluids having substantially different compressibilities (e.g. water and gas), different fluid pressures are induced in each region, causing fluid flow, which need to be equilibrated over some timescale imposed by the passing seismic wave (White, 1975, Johnson, 2001, Pride et al., 2003, Müller et al., 2010). Mesoscopic flow can also occur when there are heterogeneities in the rock properties at a scale much smaller than the wavelength but larger than the pore scale. This could be due to, for example, interbedded shales and sands, the presence of fractures/joints, or the presence of less well cemented regions in an otherwise well cemented rock (Berryman and Wang, 2000, Pride and Berryman, 2003a, 2003b, Pride et al., 2003). The more compliant mesoscopic regions are compressed to a much greater extent than the stiffer regions, causing mesoscopic fluid flow. This could cause viscous dissipation and dispersion if the wave induced fluid pressure does not have enough time to equilibrate. If the meso-scale heterogeneities are aligned (such as aligned fractures), then the resulting wave induced fluid flow will cause frequency-dependent anisotropy (Müller et al., 2010). Fracture characterisation using seismic anisotropy is an important aspect of reservoir characterisation and as such frequency-dependent seismic anisotropy (see section 2.6) has received considerable interest (e.g. Chapman et al., 2003, Gurevich et al., 2009, Carcione et al., 2013).

2.2 Partial saturation effects

Elastic properties of rocks are affected by the presence of pore fluids and this is exploited for reservoir characterisation in terms of fluid properties. The low frequency limit is well described by the equations of Gassmann (1951) which was developed for a single fluid phase under the assumption that the increment of pore fluid pressure due to external stress is equal throughout the pore space. However, rocks in the subsurface might not always be saturated with a single fluid phase as gas and liquid could simultaneously occupy the pore space. Therefore, there have been many studies (both theoretical and experimental) looking at the effect of varying amounts of water saturation on elastic wave properties (Domenico, 1974, White, 1975, Domenico, 1976, Gregory, 1976,

Mavko and Nur, 1979, Murphy, 1982, Winkler and Nur, 1982, Murphy, 1984, Knight and Nolen-Hoeksema, 1990, Mavko and Nolen – Hoeksema, 1994, Cadoret et al., 1995, 1998, Knight et al., 1998).

Quantifying the effects of multiphase saturation on elastic wave properties is not trivial as this dependence is not only on the amount of saturation but also on the spatial distribution of saturation. Domenico (1976) suggested multiple fluid phases can be modelled using Gassmann's equations by taking an effective fluid modulus given by the Reuss (1929) average of the different constituents (also known as Wood's formula). This is only applicable when the gas and liquid are mixed uniformly at a very small scale so that any wave-induced increments of pore pressure in each phase have enough time to diffuse and equilibrate during a seismic period (Mavko and Mukerji, 1998). This pore pressure equilibration can only be achieved if the wave frequency is low enough so that the characteristic length of fluid diffusion is large compared to any saturation heterogeneity (Mavko and Mukerji, 1998, Müller et al., 2010). The length scale can be expressed as $\sqrt{kK_f/f\eta}$, where k is the permeability, η and K_f are the viscosity and bulk modulus of the most viscous fluid phase (Mavko and Mukerji, 1998). Similar expressions have been given elsewhere in the literature (e.g. Norris, 1993, Pride et al., 2004, Batzle et al., 2006). For saturations that are heterogeneous over scales larger than the characteristic length of fluid diffusion (wave frequency not low enough), wave induced pore pressures cannot equilibrate, resulting in velocity dispersion and attenuation.

White (1975) was the first to show theoretically that the presence of gas pockets in otherwise liquid saturated rocks can lead to significant velocity dispersion and attenuation. The effects of partial gas saturation have been studied more extensively since then and is still an actively developing field (Müller et al., 2010). Experimental studies have also shown the saturation dependence of elastic wave properties is frequency-dependent (e.g. Murphy, 1982, Winkler and Nur, 1982, Murphy, 1984) and the observed velocities are not consistent with the theoretical predictions using a Reuss averaged bulk modulus in Gassmann's equations, especially at ultrasonic frequencies (e.g. Domenico, 1976, Gregory, 1976, Gist, 1994b, Cadoret et al., 1995). A huge amount of effort has gone into trying to reconcile these differences and explain these observations using theoretical models. Several physical mechanisms have been proposed and described mathematically with varying degrees of detail (Murphy et al., 1986). However, the widely accepted approaches can be broadly classified into three

different categories. Two approaches consider frequency-dependent effects of wave-induced fluid flow due to saturation distribution at two different scales (microscopic and mesoscopic), while the third category deals with defining an effective fluid modulus.

As discussed in section 2.1.1, rocks contain thin grain contacts or micro-cracks that are more compliant than the rounder 'equant' pores. In the presence of two immiscible fluids (e.g. gas and water), saturation distribution heterogeneities can exist at the grain scale, as wetting fluid such as water would preferentially occupy thin cracks and grain contacts while non-wetting fluids such as gas would occupy the rounder pore space. So when the rock is compressed under wave excitation, fluid flow occurs from the more compliant region to the rounder pores due to spatial pressure gradients from the compliant cracks being compressed to a greater extent than the rounder pores. The presence of a small fraction of free gaseous phase in a single crack permits the liquid to flow freely when the crack is compressed (so no fluid exchange between crack and rounder pores). This case was treated by Mavko and Nur (1979) and would only be relevant for low water saturation (Murphy et al., 1986). This wave-induced fluid flow at the pore scale (also known as local or squirt flow) causes significant attenuation and velocity dispersion if the fluid pressure gradients do not equilibrate by fluid flow on the timescale of the seismic wave (Winkler and Nur, 1982, Müller et al., 2010). When there is enough time (low enough wave frequency) for fluid pressure equilibration, then there is no effect on the rock stiffness. When the wave frequency is too high so that there is not enough time for the fluid to flow, then the rock appears stiffer. At intermediate wave frequencies, the effective stiffness (and hence velocity) of the rock is frequency-dependent and attenuation is a maximum (Toms et al., 2006).

Fluid heterogeneities could also exist at scales greater than the pore scale but smaller than the wavelength (so-called mesoscopic scale). This mesoscopic distribution of fluid saturation can be caused by spatial variations in porosity, permeability, wettability, shaliness, etc. This could lead to the immiscible fluids forming saturation 'patches' in different regions of the pore space. Mesoscopic distribution of fluid heterogeneities is therefore also referred to as "patchy saturation". This effect has been modelled using a periodic distribution of idealised geometry (e.g. White, 1975, Dutta and Odé, 1979b, Johnson, 2001) or a random distribution (e.g. Müller and Gurevich, 2004, Toms et al., 2007, Müller et al., 2008). When a seismic wave compresses the medium, pressure gradients

arise due to the significant differences in compressibilities between the fluid phases, causing fluid flow between different patches which if unequilibrated can lead to significant attenuation and velocity dispersion. Effects of patchy distribution of saturation have been observed in experimental studies (e.g. Cadoret et al., 1995, 1998, Monsen and Johnstad, 2005, Lebedev et al., 2009). These experiments showed that the distribution of saturation heterogeneities had a significant effect on velocity and attenuation, and that the saturation distribution depends on the saturation procedure. Imbibition where the wetting phase (e.g. water) displaces the non-wetting phase (e.g. gas) has been shown to produce a more uniform (homogeneous) distribution of water saturation as opposed to drainage or drying which produces a more heterogeneous saturation distribution. Bourbie and Zinszner (1984) also showed that desaturation using a centrifuge could also produce heterogeneous distribution of gas patches.

The effects of partial saturation can be modelled using the equations of Gassmann (1951) with an effective fluid modulus. When the rock is saturated by two or more fluid phases, the mixture of the different fluid moduli can be replaced with an effective fluid modulus which is determined by taking an average of the modulus of individual fluid constituents. Domenico (1976) suggested using the Reuss averaged modulus of the different fluid phases as the effective fluid modulus. Mavko and Mukerji (1998) showed that this is a lower limit which is only valid for homogeneous saturation distribution when the fluid phases are mixed at a very fine scale so that any wave-induced pore pressure increments are equilibrated. They showed that a rock with heterogeneous (patchy) saturation distribution has spatially varying bulk modulus and spatially uniform shear modulus so that the effective modulus is described exactly by the mixing law given by Hill (1963). In order to obtain a better fit with well log observations, Brie et al. (1995) introduced an empirical averaging law which varies the effective fluid modulus using an exponent which does not have any physical meaning. The empirical law of Brie et al. (1995) has since been used to account for velocity dispersion and to obtain a better fit with laboratory data (e.g. Monsen and Johnstad, 2005, Doan et al., 2011). Although the approach of Brie et al. (1995) can be useful for practical purposes, it is strictly empirical and must be calibrated and tested locally (i.e. for individual situations) (Castagna, 2001). There is no explicit frequency-dependence of the effective rock stiffness due to any specific mechanism in these averaging methods and as such no estimate of attenuation is obtainable.

2.3 Wave propagation in anisotropic media

Seismic anisotropy can be defined as the variation of elastic properties of a medium with direction (or angle). The idea of anisotropic propagation of elastic waves dates back to the early 19th century, with roots in crystal optics and crystal elasticity and only entered seismology towards the end of the 19th century, but has only become important in exploration seismology in more recent years (Winterstein, 1990, Helbig and Thomsen, 2005). The earliest observations of seismic anisotropy were of the variation of P-waves in the upper mantle by investigators such as Hess (1964) and Raitt et al. (1969) (discussed by Crampin (1984))

Helbig and Thomsen (2005) give a detailed overview of the historical developments of seismic anisotropy.

In a linear, elastic medium the anisotropic Hooke's law relates the stress tensor σ_{ij} to the strain tensor ε_{kl} through the stiffness tensor C_{ijkl} as follows:

$$\sigma_{ij} = C_{ijkl}\varepsilon_{kl}\,, \tag{2.5}$$

where the strain (the symmetric part of the deformation) is given by (e.g., Thomsen, 2002)

$$\varepsilon_{kl} = \frac{1}{2}\left(\frac{\partial u_k}{\partial x_l} + \frac{\partial u_l}{\partial x_k}\right). \tag{2.6}$$

The stiffness tensor is a fourth rank tensor (hence 81 components) with two indices corresponding to the indices of stress and the other two corresponding to the indices of strain. The symmetry of stress and strain requires that

$$C_{ijkl} = C_{jikl} = C_{ijlk} = C_{jilk}\,, \tag{2.7}$$

reducing the number of independent constants to 36. The existence of a unique strain energy potential also requires that

$$C_{ijkl} = C_{klij}\,, \tag{2.8}$$

further reducing the number of independent constants to 21 (Thomsen, 2002, Mavko et al., 2009). These considerations allows for the replacement of the 3 × 3 × 3 × 3 tensor C_{ijkl} with a 6 × 6 matrix C_{IJ}, using the Voigt notation, where the scheme for conversion of the indices is given by:

ij or kl	11	22	33	23 = 32	31 = 13	12 = 21
I or J	1	2	3	4	5	6

Equation 2.5 can then be written as follows:

$$\sigma_I = C_{IJ}\varepsilon_J\,, \tag{2.9}$$

where C_{ij} is a 6 × 6 symmetric matrix and from equations 2.7 and 2.8, the number of independent elastic constants reduces to 21 for the most general anisotropic case.

The equation of motion from Newton's second law of motion is given by (e.g., Tsvankin et al., 2001, Thomsen, 2002)

$$\rho\frac{\partial^2 u_i}{\partial t^2} = \frac{\partial \sigma_{ij}}{\partial x_j}, \tag{2.10}$$

where ρ is the density of the material. Combining Hooke's law with Newton's second law of motion yields the elastodynamic wave equation which relates stiffness to displacement **u**:

$$C_{ijkl}\frac{\partial^2 u_k}{\partial x_l \partial x_j} = \rho\frac{\partial^2 u_i}{\partial t^2}. \tag{2.11}$$

Assuming a plane wave solution given by,

$$u_k = U_k e^{i\omega(t-p_j x_j)}\,, \tag{2.12}$$

where U is the polarization vector, $p = \boldsymbol{n}/v$ is the slowness vector and ω is the angular frequency, we can then recast the problem as an eigenvalue problem (commonly referred to as the Kelvin-Christoffel equation) as follows (e.g. Auld, 1973):

$$(\Gamma_{ik} - \rho v^2\delta_{ik})U_k = 0\,, \tag{2.13}$$

where

$$\Gamma_{ik} = C_{ijkl}\boldsymbol{n}_j\boldsymbol{n}_l\,, \tag{2.14}$$

where $\boldsymbol{n}$ is the unit vector normal to the wavefront, v is the phase velocity, Γ_{ik} is known as the Christoffel matrix and δ_{ik} represents the Kroneckar delta function which equals 1 for $i = k$, and 0 for $i \neq k$. Γ_{ik} is a 3 × 3 matrix and solving the eigenvalue problem therefore leads to three eigenvalues and three corresponding eigenvectors. The eigenvalues (ρv^2) give the three phase velocities and the

eigenvectors give the corresponding mutually orthogonal polarization vectors $\boldsymbol{U}$ since Γ_{ik} is real and symmetric.

The solution to the Kelvin-Christoffel equation reveals that for every direction of propagation $\boldsymbol{n}$, there are three different wave types: a quasi-compressional wave (qP), a pure shear wave (S1) and a quasi-shear wave (S2). The term "quasi" is used to indicate that the eigenvectors (polarization vectors) are not exactly aligned parallel or normal to the propagation direction as would be expected in an isotropic medium. The fact that two S-waves are present with different velocities gives rise to shear wave splitting.

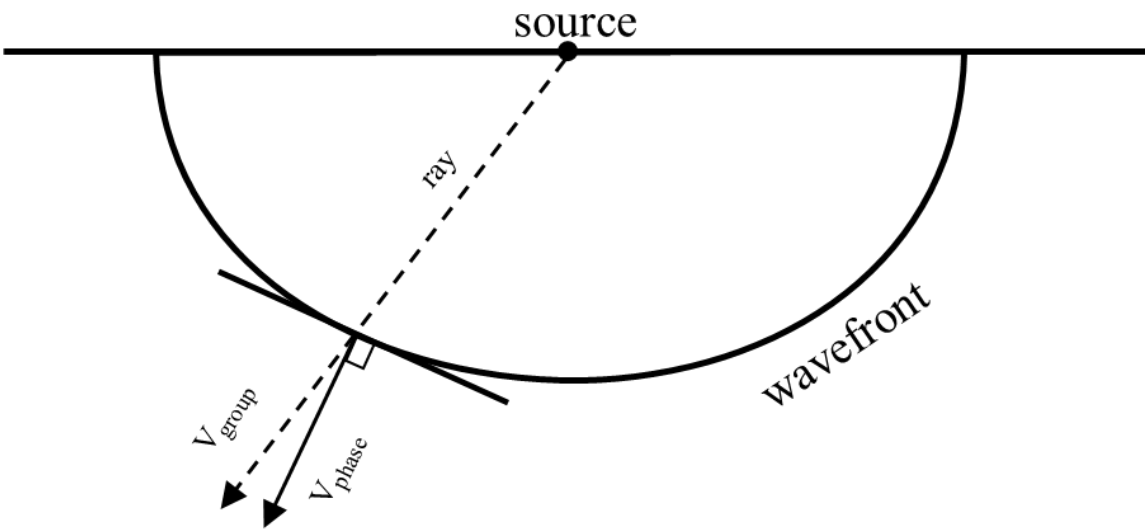

Figure 2.1: The relationship between group velocity V_{group} and phase velocity V_{phase}. V_{group} is in the source-receiver direction, while V_{phase} is normal to the wavefront.

In anisotropic media, phase and group velocity are not identical. When seismic waves propagate in an isotropic, elastic, homogeneous medium the phase and group velocities coincide (Mavko et al., 2009) but this is not the case in an anisotropic medium. The concept of phase and group velocities and phase velocities in an anisotropic medium is illustrated in Figure 2.1. The phase velocity is always normal to the wavefront and is the velocity at which a point of constant phase travels in the direction normal to the wavefront, while the group velocity is the velocity at which the wave energy propagates along a ray (Thomsen, 2002). The relationship between group and phase velocity (v) is given by (Berryman, 1979)

$$V_g = grad^k(kv) = \frac{\partial(kv)}{\partial(k_1)} i_1 + \frac{\partial(kv)}{\partial(k_2)} i_2 + \frac{\partial(kv)}{\partial(k_3)} i_3 , \qquad (2.15)$$

where k is the wave vector which is parallel to the phase velocity vector, and $i_{1,2,3}$ are unit vectors aligned with the coordinate system. It can be further derived that the projection of the group velocity vector onto the phase or slowness direction is equal to the phase velocity

$$v = V_g . \boldsymbol{n} . \tag{2.16}$$

2.3.1 Symmetry classes

The symmetry of the stiffness tensor C_{ijkl} and its number of independent components determine the symmetry of a medium, which in turn controls the anisotropic behaviour of the elastic waves travelling through the medium. As pointed out above, the maximum number of independent elastic constants of the stiffness tensor is 21. Further restrictions imposed by symmetry considerations reduce the number of independent elastic constants.

Isotropic symmetry represents the highest possible symmetry class and hence is the simplest type of symmetry. Here, only two independent elastic constants are needed to describe the medium, namely the Lamé parameters λ and μ. Triclinic symmetry represents the lowest possible symmetry class and contains no symmetry planes (Crampin, 1989). Here, all 21 independent stiffness components are required to describe the elastic properties of the medium. Other symmetry classes that are important for seismic applications include hexagonal, orthorhombic and monoclinic symmetry classes, requiring 5, 9 and 13 independent stiffness constants respectively. This thesis only considers materials with hexagonal symmetry because making synthetic rocks with lower symmetries is not possible at the moment.

2.3.1.1 Hexagonal Symmetry (Transverse Isotropy)

A medium possessing hexagonal symmetry has a single axis of rotational symmetry and is described by 5 independent elastic constants. They are rotationally invariant about their symmetry axis and are also called transversely isotropic (TI). In a TI medium, two directions (in Cartesian coordinates) are equivalent to each other, with only one direction being different. Properties of elastic waves propagating through a TI medium depend on the angle between the direction of propagation and the axis of symmetry. For a TI medium having a

vertical axis of symmetry (VTI), the stiffness tensor has the following form (e.g. Thomsen, 2002):

$$\begin{bmatrix} C_{11} & C_{11}-2C_{66} & C_{13} & 0 & 0 & 0 \\ C_{11}-2C_{66} & C_{11} & C_{13} & 0 & 0 & 0 \\ C_{13} & C_{13} & C_{33} & 0 & 0 & 0 \\ 0 & 0 & 0 & C_{44} & 0 & 0 \\ 0 & 0 & 0 & 0 & C_{44} & 0 \\ 0 & 0 & 0 & 0 & 0 & C_{66} \end{bmatrix}.$$

In rocks, VTI symmetry can be caused by horizontal layering on a scale much smaller than the seismic wavelength (Backus, 1962, Thomsen, 1986, Winterstein, 1990). This can due to horizontal bedding or the preferential alignment of minerals. Shales are important seals and source rocks that exhibit preferential horizontal mineral alignment causing VTI anisotropy, and this has been well documented (e.g. White et al., 1983, Banik, 1984, Winterstein and Paulsson, 1990, Wang, 2002, Chesnokov et al., 2010, Sayers and Dasgupta, 2015). VTI anisotropy is also known as polar anisotropy due to the variation of seismic wave properties with polar angle (Thomsen, 2002).

TI media can also have a horizontal axis of symmetry (HTI), also requiring 5 independent elastic constants. Rotating the VTI system by 90° using the Bond transformation technique (Winterstein, 1990, Mavko et al., 2009) to make x_1 the axis of symmetry gives the stiffness tensor for the HTI medium, which is of the form (e.g. Rüger, 1997):

$$\begin{bmatrix} C_{11} & C_{13} & C_{13} & 0 & 0 & 0 \\ C_{13} & C_{33} & C_{33}-2C_{44} & 0 & 0 & 0 \\ C_{13} & C_{33}-2C_{44} & C_{33} & 0 & 0 & 0 \\ 0 & 0 & 0 & C_{44} & 0 & 0 \\ 0 & 0 & 0 & 0 & C_{66} & 0 \\ 0 & 0 & 0 & 0 & 0 & C_{66} \end{bmatrix}.$$

A medium containing vertically aligned cracks or fractures (on a scale much smaller than the seismic wavelength) that are rotationally invariant about the symmetry axis exhibits HTI symmetry. Therefore, seismic anisotropy in rocks containing such vertically aligned fractures are described using HTI symmetry. HTI anisotropy is also referred to as azimuthal anisotropy due to the variation of seismic properties with azimuth. Fractures that are open at depth in the subsurface are usually oriented normal to the direction of minimum in-situ stress (Crampin, 1987, Schoenberg and Sayers, 1995). Consequently, HTI anisotropy can be sensitive to stress as only open fractures would be expected to contribute to the anisotropy of the fractured rock.

2.4 Seismic fracture detection

As pointed out above, open (seismically visible) fractures in the subsurface generally tend to be oriented normal to the direction of minimum compressive stress (Schoenberg and Sayers, 1995). At reservoir depths, the largest compressional stress is the overburden pressure which is in the vertical direction and the smallest compressional stress is usually horizontal, therefore, open fractures in the subsurface tend to be aligned in the vertical direction (Crampin, 1987, Helbig and Thomsen, 2005).

The simplest model for representing fractured rocks is that of a material containing vertically aligned fractures with a horizontal axis of symmetry (HTI). In practice, HTI or azimuthal anisotropy is the most widely used for fracture detection from seismic anisotropy because analysis based on lower symmetries is often impractical due to, for example, the limited spatial coverage of field seismic data. I will restrict the discussion in this thesis to HTI symmetry.

The presence of fractures affects the travel times and amplitudes of seismic waves propagating through or reflecting from the fractured zone. In the case of shear waves, shear wave splitting also occurs. Therefore, the seismic attributes commonly used for fracture detection are shear wave splitting, the azimuthal variation of travel times or normal move-out (NMO) velocities, and the variation of reflected amplitudes with offset and azimuth.

When a shear wave enters an anisotropic medium, it splits into two approximately orthogonal polarizations that travel at different velocities (Crampin and Peacock, 2005). The velocity difference between the split shear waves results in a time delay between the two modes. This phenomenon is referred to as shear wave splitting (or seismic birefringence). The polarization of the leading shear wave is parallel to the fracture strike and the time delay is a measure of the magnitude of the anisotropy (the average crack density in the case of fractured rocks) (Crampin, 1981, Crampin and Peacock, 2005). Shear-wave splitting has been widely used for fractured rock characterisation since it was first positively identified above small earthquakes by Crampin et al. (1980a). However, widespread applications of shear-wave splitting only became possible when three-component digital recording became available (Crampin and Lovell, 1991). In exploration seismology, shear-wave splitting has gained wide application for fracture characterisation (e.g. Alford, 1986, Crampin et al., 1986, Lynn and Thomsen, 1990, Queen and Rizer, 1990, Mueller, 1991, Shuck, 1991, Lynn et al.,

1999, Winterstein et al., 2001, Sil et al., 2010). In the absence of shear sources (e.g. in marine environments), shear-wave splitting analysis on PS converted-wave data from surface seismic or VSP can be used for fracture characterisation (e.g. Gaiser, 2000, Horne, 2003, Olofsson et al., 2003).

The NMO velocity method measures the azimuthal variation of NMO velocity of the reflection from the base of the fractured zone (Thomsen, 1988, Tsvankin, 1997, Grechka and Tsvankin, 1998, Li, 1999, Lynn et al., 1999). The direction with the fastest NMO velocity is taken to be parallel to the fracture strike, and the difference between the fastest and slowest NMO velocities is an indication of the magnitude of the anisotropy. Instead of using azimuthal variation of NMO velocities, another approach is to use the residual travel times after applying NMO correction to the seismic gathers with isotropic velocities (Li, 1999, Thomsen, 2002). The residual travel time versus azimuth is of elliptical form and yields the symmetry of the fractured medium, with the smallest residual time corresponding to the fracture strike and the difference between the smallest and the largest residual an indicator of the magnitude of anisotropy. Although, the azimuthal variation of interval NMO velocity or travel time might be clearly present in the data, sometimes a more complicated interpretation in terms of fractures may be required. For example, this can be the case when vertical resolution is poor (much thicker than target zone) and observations from seismic data differ from those from other data (e.g. stress directions inferred from borehole data) (Thomsen, 2002).

Reflected seismic amplitudes have become important attributes for fractured rock characterization. Seismic reflection coefficients in azimuthally anisotropic media vary not only with angle of incidence but also with azimuth. This phenomenon has found many applications for fractured rock characterisation since earlier reports in the literature by Lynn and Thomsen (1986) (on land) and Lefeuvre (1994) (at sea) (Thomsen, 2002). If the incident angle is not too great, the reflection coefficient can be approximated and written in terms of an AVO gradient and an AVO intercept (Rüger, 1997, Rüger and Tsvankin, 1997, Thomsen, 2002). For a given angle of incidence, the variation of the AVO gradient with azimuth is elliptical in form. These attributes can then be inverted for the axis of symmetry and the magnitude of anisotropy of the fractured medium from multi-azimuth seismic reflection data. Many studies have applied this technique for fractured rock characterisation (e.g. Mallick et al., 1998, Lynn et al., 1999, Gray and Head, 2000); however, the azimuthal variation of amplitudes can be

ambiguous as it might not always be related to the presence of fractures. Other factors such as velocity variation in the overburden, geometric spreading, lateral heterogeneity of velocity or reflectivity could also lead to azimuthal amplitude variation (e.g. Thomsen, 2002). Attenuation in fractured rock due to wave induced fluid flow can also significantly affect the azimuthal variation of amplitudes by strengthening, diminishing, or reversing variations that are solely due to the reflectivity (MacBeth, 1999). These limitations should be taken into account when interpreting azimuthal variations of amplitudes in terms of fracture properties.

2.5 Effective medium representation of fractured media

Seismic characterisation of fractured rocks are usually done using equivalent or effective medium theories (the long-wavelength approximation). Equivalent medium theories replace a medium containing heterogeneities much smaller than the seismic wavelength with an equivalent homogeneous medium having the same effective properties as the heterogeneous medium. If the heterogeneities have a preferred orientation, then the resulting equivalent medium is anisotropic. Rocks containing aligned fractures are modelled as equivalent media. Such models can be used to relate the measured seismic anisotropy to the fracture properties such as the fracture orientation, density and filling material. The common equivalent medium theories either model the fractures or cracks as penny-shaped (oblate spheroids) voids embedded in an isotropic solid (e.g. Hudson, 1981) or as planes of weakness with linear slip (non-welded) boundary conditions (e.g. Schoenberg, 1980).

Since the pioneering work of Eshelby (1957), many theoretical models treating fractures as isolated ellipsoidal inclusions in an infinitely homogeneous elastic medium have been developed (Garbin and Knopoff, 1973, O'Connell and Budiansky, 1974, Garbin and Knopoff, 1975, Hudson, 1981, Nishizawa, 1982). One such fractured rock model commonly used for seismic characterisation of fractured rocks is the model of Hudson (1981) which gives the effective moduli for the cracked solid as

$$C_{ijkl} = C^0_{ijkl} + \varepsilon_f C^1_{ijkl} + \varepsilon_f^2 C^2_{ijkl}\,, \tag{2.17}$$

where C^0_{ijkl} is the isotropic background stiffness tensor, C^1_{ijkl} and C^2_{ijkl} are the first and second order corrections respectively. C^1_{ijkl} accounts for the presence of fractures reacting independent of the others and C^2_{ijkl} accounts for crack-crack interaction (Hudson, 1986). ε_f is the fracture (or crack) density given as the number of cracks *N* of radius *a* per unit volume V given as (e.g. Crampin, 1981, Hudson, 1981, Mavko et al., 2009):

$$\varepsilon_f = \frac{Na^3}{V}. \tag{2.18}$$

The model of Hudson is used to estimate fracture density from seismic anisotropy measurements. It can be seen from Equation 2.18, that the fracture density parameter could be ambiguous as a material with many small fractures could have the same fracture density as one with a few large fractures.

The linear slip model (Schoenberg, 1980, 1983, Schoenberg and Douma, 1988) is another commonly used equivalent medium model for fractured rocks. Here, fractures are treated as planes of weakness with linear-slip boundary conditions regardless of the microstructural details of the fractures. In this approach, the effective compliance (inverse of stiffness) tensor is obtained by adding an excess compliance tensor due to the presence of fractures to the compliance tensor of the host medium as follows:

$$S_{ijkl} = S^b_{ijkl} + S^f_{ijkl}\,, \tag{2.19}$$

where S^b_{ijkl} and S^f_{ijkl} are compliance tensors for the host medium and the fractures, respectively. The effective stiffness tensor of the medium can then be obtained by

$$C_{ijkl} = S^{-1}_{ijkl}\,. \tag{2.20}$$

This approach works well for one or more sets of parallel fractures and as such can be very useful for materials with lower symmetry than hexagonal symmetry (e.g. Schoenberg and Muir, 1989, Schoenberg and Protazio, 1992, Sayers, 2009). For a medium with a single set of parallel fractures the effective elastic tensor has the same structure as the effective elastic tensors of microstructural models such as the models of Hudson (1981) and Thomsen (1995). The linear slip model can be written in terms of microstructural parameters such as fracture density and crack geometry (Schoenberg and Douma, 1988, Hudson et al., 1996, Bakulin et al., 2000). Many studies have derived such expressions and concluded that that

these models cannot distinguish between various fracture properties (e.g. Schoenberg and Douma, 1988, Liu et al., 2000).

2.6 Frequency-dependent seismic anisotropy

In the Section 2.1.1, the importance of wave induced fluid flow on the elastic response of fluid (liquid) saturated rocks was discussed. When a fluid-filled rock contains compliant (thin) fractures connected to the stiffer pore space (so-called equant porosity), a passing seismic wave compresses the fractures to a greater extent than the stiffer regions causing fluid exchange between the fractures and the pore space. If the wave frequency is low enough for the fluid to flow from the fracture to the pore space, the weakness as a result of the presence of the fracture is felt by the compressive wave. However, when the wave frequency is so high that there is not enough time for the fluid to flow out of the fracture, the fracture appears stiffer and hence, the rock appears stiffer. It is straightforward to see that this can cause frequency-dependent anisotropy in rocks containing aligned fractures. These two scenarios represent the low and high frequency limits respectively. At intermediate frequencies, significant dispersion and attenuation are expected and a number of dispersive equivalent medium theories have been developed to quantify these effects. The idea of frequency-dependent anisotropy has been applied to field data to model fluid effects in fractured rocks (e.g., Van Der Kolk et al., 2001, Maultzsch et al., 2007, Qian et al., 2007).

The model of Hudson (1981) did not consider fluid flow between fractures and equant porosity and in that sense represents the high frequency limit where the fractures are in essence isolated with respect to fluid flow. However, Hudson et al. (1996) considered fluid flow between cracks and equant porosity and flow between interconnected cracks. The expressions for the effective stiffness constants for the cracked solid retain the same form as that of Hudson (1981). However, the parameter that governs the response of a crack to normal stress entering the first order corrections becomes frequency-dependent, while the crack response to a shear stress remains unaffected since the shear stress applied to a crack face does not produce a volume change (Hudson et al., 1996, Pointer et al., 2000). The equant porosity model takes account of diffusion into the porous matrix and has a single expression for a whole range of frequencies. The resulting expression for the high frequency limit is equivalent to the original ‘isolated crack’ expression of Hudson (1981). At very low frequencies the equations give a response equivalent to that of dry cracks, however, the flow

associated with independent cracks will begin to interfere at relatively low frequencies and the model does not take this into account (Hudson et al., 2001).The low frequency limit of the model does not correspond to the equations of Gassmann (1951) and Brown and Korringa (1975), where the material should behave as if static and undrained (Hudson et al., 2001). Therefore, the model is not valid for the entire frequency range. Hudson et al. (2001) gave an expression for the frequency below which the model becomes unreliable. Significant dispersion and attenuation anisotropy is expected from the equant porosity model of Hudson et al. (1996) (e.g. Pointer et al., 2000, Maultzsch et al., 2003b). For flow between interconnected cracks, the model assumes that otherwise isolated cracks are connected by mechanically (or seismically) invisible fluid pathways; meaning, the fluid pathways have no effect on the overall properties of the material if the fluid is a compressible non-viscous gas (Hudson et al., 1996). It is not clear what limitations this places on the model as it does not seem very realistic to expect fluid pathways that could be on the order of centimetres to metres to be seismically invisible. For fluid flow between aligned cracks, pressure gradients occur at the wavelength scale and there is no local flow at the microstructural scale (Hudson et al., 1996, Pointer et al., 2000). At seismic frequencies (and wavelengths), Hudson et al. (1996) showed that velocity dispersion and attenuation from this mechanism are not expected to be important as the mechanism becomes important in practice at high values of permeability (> 1 D).

Van Der Kolk et al. (2001) developed an equivalent medium theory to model velocity dispersion and attenuation in rocks containing aligned fractures. The effective medium model was developed by combining three different ideas. Firstly, randomly oriented fractures are introduced into an isotropic background using the theory of O'Connell and Budiansky (1977). The fractures are then aligned along a single plane using the formulation of Sayers and Kachanov (1991). The Schoenberg and Muir (1989) scheme is finally used to stack media with different fracture orientations and fracture densities. This combination of different theories was referred to collectively as the BOSK theory. The theory was used to explain shear wave anisotropy anomaly and attenuation which was interpreted to be a result of wave-induced squirt flow from the fractures. However, as pointed out by Hudson and Crampin (2003), the model of Sayers and Kachanov (1991) treated isolated cracks whose behaviour is not affected by fluid communication with other neighbouring cracks. Also the model of O'Connell and Budiansky (1977) only considers effects due to squirt flow between cracks with

different orientations. Therefore, it is not clear what the physical interpretation is for the wave induced fluid flow mechanism causing dispersion and attenuation in the BOSK model since the cracks have a preferred orientation.

Chapman (2003) developed a model for the frequency-dependence of the stiffness tensor for a medium containing so called equant porosity and fractures larger than the grain scale but much smaller than the seismic wavelength (mesoscale) by extending the poroelastic model of Chapman et al. (2002). The model explicitly considers two different pore scales; the grain scale where squirt flow takes place between microcracks and equant pores and between cracks with different orientations, and a larger scale where squirt flow takes place between the fractures and the surrounding matrix porosity. The theory predicts that dispersion as a result of wave induced fluid flow (and hence frequency-dependent anisotropy) can be significant at seismic frequencies. An attractive feature of the model of Chapman (2003) is that it has the correct frequency limits. The high frequency limit of the model is equivalent to the effective medium theory of Hudson (1981) for isolated fluid filled cracks. The low frequency limit of the theory is consistent with the anisotropic Gassmann equations of Brown and Korringa (1975) (Chapman et al., 2003). Also, in the absence of fractures, the model returns to the poroelastic theory of Chapman et al. (2002) which has a low frequency limit equivalent to the isotropic Gassmann theory. The ideas of Chapman (2003) was extended by Chapman (2009) to account for mesoscopic fracture sets with different orientations and connectivities.

Jakobsen et al. (2003), Jakobsen and Hudson (2003), and Jakobsen (2004) developed an effective medium theory to model the frequency-dependence due to wave induced fluid flow in fluid saturated heterogeneous media using the T-matrix approach. This approach can take into account non-dilute concentrations of pores and fractures of any size and aspect ratio. Their inclusion-based approach considered a homogeneous matrix material with embedded inclusions representing the communicating cavities (e.g. pores and cracks) and other unconnected particles (e.g. clays found in sandstones) (Jakobsen, 2004). The model takes into account squirt and/or global flow due to local and/or global pressure gradients induced by a passing seismic wave. This wave induced fluid flow subsequently leads to velocity dispersion and attenuation. Agersborg et al. (2007) showed that the squirt flow models of Chapman et al. (2002) and Chapman (2003) can be reproduced as a special case of the T-matrix approach. The low frequency limit of this model is consistent with the Brown and Korringa

(1975) relations for the static case (Jakobsen, 2004). Jakobsen and Chapman (2009) produced a unified theory of global flow and squirt flow where they rectified an error related to the coupling between the processes of squirt flow and global flow in cracked porous media. They showed that depending on the nature (e.g. porosity, statistical distribution of shapes and orientation) and content (e.g. fluid saturation) of the pores and cracks, either fluid flow mechanisms (global or squirt) could be important. They however concluded that global flow would still be associated with negative velocity dispersion (e.g. Hudson et al., 1996) and squirt flow would be associated with positive velocity dispersion. Although it is believed squirt flow would dominate global flow in real rocks, the coupled nature of both mechanisms should be considered as even though the velocity dispersion might be positive, the actual numerical values might be significantly affected by global flow processes (Jakobsen and Chapman, 2009).

2.7 Synthetic rocks and fractured rock experiments

Controlled experiments are needed to validate, calibrate and test the range of applicability of theoretical models. Controlled laboratory experiments can also be used to make observations even when a theory does not exist and could help inform the development of suitable theories. Equivalent medium theories for fractured rocks are no exception and need to be tested for their validity and applicability. Fractures in the subsurface do not usually occur at laboratory scales and neither are their distributions and orientations ideal for laboratory experiments. Therefore, controlled laboratory experiments require the use of artificial rocks. Artificially fractured natural rocks have also been used (e.g., Peacock et al., 1994a, 1994b), however, this presents difficulties in controlling and obtaining the required fracture properties.

Oda et al. (1984) presented results from experimental determination of elastic compliance for rock-like materials with random cracks. The synthetic rock-like sample was made using water-gypsum mixture (2:3 by weight) poured into a rectangular prismatic mould. Strips made of greased picture postcards were inserted into the mixture at predetermined positions and orientations to simulate cracks. The hardened gypsum was taking out of the mould after about an hour and trimmed to make a rectangular prism (for unconfined compressional test) and an equilateral polygon (for ultrasonic velocity tests). The samples were then

cured for about three weeks in a constant temperature and humidity room. The greased postcards were expected to act as cracks because they are very soft in comparison with the hardened gypsum plaster and would respond as open cracks when stress is applied. This point was later confirmed experimentally by pulling out the greased plaster leaving the voids open, after which they observed no distinction in mechanical response. To determine the complete two-dimensional strain tensor, uniaxial stresses where applied to the rectangular prism and at least three extensional strains were measured by a contact gauge with accuracy of 1/1000 mm. For the ultrasonic velocity test, three equilateral polygon samples were chosen: A) with randomly oriented cracks; B) with completely aligned parallel cracks; and C) with intermediate crack orientations between A and B. Velocity measurements were taken in eight directions using a pulse generator and receiver tightly pressed to the sample at diagonal positions. The samples were highly attenuating and could not transmit shear waves; hence, only compressional wave velocities were measured. Velocity in sample A was found to be almost independent of measured direction with velocity anisotropy increasing with alignment of cracks, as such, sample B had the maximum velocity anisotropy. Despite establishing important relationships between cracks and their corresponding effects on elastic compliance, limitations of the study on velocity anisotropy are evident. Limitations include unrealistic rock samples (devoid of properties such as grains, porosity, permeability), no emphasis on fluid effects, and shear waves were not measured. As a result, velocity anisotropy relationships established using this method cannot be reliably extended to real world applications.

Ass'ad et al. (1992) presented results from experimental investigations using a model consisting a solid matrix of epoxy resin with thin rubber disc inclusions representing aligned fractures. A total of seven models were produced, including two models containing no inclusions that were used to test the construction method of the samples while the remaining five models contained different amounts of inclusions to give different fracture densities. The experiments were carried out using an ultrasonic (30 – 60 kHz) pulse transmission method to measure velocity anisotropy. The properties of the matrix and the inclusions were known so they were able to measure relationships between fracture density and velocity anisotropy in their samples. The transducers were rotated in order to measure the fast and slow shear waves from which shear wave splitting was calculated. Their observations were then compared to the theory of Hudson (1981), with good agreement achieved

between experiments and theoretical predictions. Despite the success of the study, there were some drawbacks including unrealistic rock samples and measurements were only made on dry samples.

Rathore et al. (1995) produced synthetic porous sandstone samples by mixing washed Danish beach sand and epoxy as a cement. Cracks with known geometry were introduced by embedding thin metallic discs in successive layers during the manufacturing process, later leached out by chemical percolation. A sample was left free of cracks in order to measure background anisotropy introduced by the manufacturing process. Ultrasonic velocity measurements were carried out using a bench-top assembly with transducers (with a central frequency of 100 kHz) attached to opposite sides of the samples. Nine traces were taken from an angle of 11.25° to the fracture normal and subsequently increased by intervals of 22.5°. The results were compared to the theories of Hudson (1981) and Thomsen (1995). It was found that the dry measurements showed better agreement with the predictions from Hudson's model while the water saturated results showed better agreement with Thomsen's model. Despite the success of the laboratory study in verifying some important aspects of the theory, limitations are evident, such as unrealistic rock cement (epoxy), and limited investigation of fluid effects.

Peacock et al. (1994a), (1994b) presented results for attenuation and velocity measurements in fractured Carrara marble. Carrara marble, a naturally occurring low porosity (0.7%) calcium carbonate rock with very low intrinsic anisotropy was subjected to axial stresses of up to 376 MPa under a confining pressure of 65 MPa in a Hoek cell in a servo-hydraulic loading actuator to induce a permanent strain on the sample. This was done to introduce fractures in the rock sample. Measurements were taken on fractured and unfractured samples to study the effect of fractures on attenuation and velocity using the ultrasonic pulse-echo method. Fracture properties were calculated from magnified images of the fracture samples. Relationships between attenuation and crack density were observed and compared to theory. The results of the velocity and crack density relationships were also compared to Hudson's theory. Limitations observed include uncontrollable fracture geometry resulting from the fracturing method which in turn introduced errors in estimated fracture properties (e.g. density, orientation and distribution).

Chau and Wong (1997) initially conducted experiments on natural rocks containing cracks to measure effective moduli of microcracked rocks by

interpreting changes in ultrasonic wave speeds. The problem of controlling the crack density in the natural rocks in order to establish relationships between wave speed changes and crack density, led to the production of artificial samples. Artificial samples were made using a method similar to that used by Oda et al. (1984) as described above. However, this time, the samples were made with dental plaster and greased penny-shaped papers were used to simulate cracks. Two samples were produced: one cracked and the other left blank. They pointed out that it was extremely difficult to fix the position for parallel cracks; thus, satisfactory results were only obtained for the isotropic case. Clearly, similar limitations to those encountered in Oda et al. (1984) are evident regarding investigation of fracture induced anisotropy.

Wei and Di (2008) presented a fracture model study using an epoxy resin background with low velocity thin penny-shaped inclusions of silicon rubber to simulate fractures. Fracture models with different fracture radii and thicknesses (aperture) but the same fracture densities were constructed for the study. Fractured rock anisotropy studies are usually done as a function of crack density but this study was done to distinguish between fracture properties (radius and thickness) in samples having the same fracture densities. Velocity and attenuation measurements were taken using the ultrasonic pulse transmission method. The study showed that samples with the same fracture density can cause different amounts of velocity anisotropy and attenuation. Despite the success of this study, it suffers from similar limitations to the study by Ass'ad et al. (1992) as pointed out above. Limitations include unrealistic matrix (epoxy resin) and inclusions (rubber discs), measurements in one direction only, and measurements were made on only dry samples.

Tillotson et al. (2012) modified the fractured rock preparation method of Rathore et al. (1995) to create synthetic silica-cemented sandstones containing aligned penny-shape fractures. The rock making process was adopted from foundry casting in the metal casting industry where aqueous sodium silicate is mixed with sand to give moulds with a degree of strength suitable for use in the metal casting industry. To produce synthetic rocks strong enough to withstand high measurement pressures without altering the rock properties, they found a way to increase the rock strength by adding kaolinitic clays as a setting agent. Penny-shaped voids were created by spreading aluminium discs on each 4 mm layers and then placing the samples in acid after the rock solidifies in order to leach out the aluminium discs to leave blank voids. Two blocks were made

simultaneously: one containing fractures and the other left blank to measure background anisotropy. The rock matrix properties and the fracture properties (fracture density, radius and aspect ratio) were obtained using helium porosimetry, nitrogen permeametry, X-ray diffraction and SEM imaging. The ultrasonic pulse-reflection system was used with a broadband frequency range of 500 – 800 kHz. Samples were cored at 0°, 45° and 90° to the fracture normal in order to make measurements at different directions to the fracture normal. Velocity and attenuation measurements were made on air dry, water (1 cP) saturated and glycerine (100 cP) saturated samples to investigate the effect of saturating fluids with different viscosities on fractured rock anisotropy. Shear wave splitting as a function of fluid viscosity was observed in the laboratory, consolidating field observations using multicomponent seismic data for oil-water discrimination by Qian et al. (2007). This is something that was not done in previous studies mentioned above, as saturated measurements were taken with only one fluid viscosity. Also, there was valuable emphasis on attenuation in this study. However, the heterogeneous distribution of grains at the pore scale meant that each sample had a different effective background material and as such, all three directions could not be taken as representative of a single anisotropic fractured medium. This limitation meant that samples cored at different directions had to be evaluated individually. This drawback was rectified by Tillotson et al. (2014) where a single sample was made and then ground into an octagonal prism to enable measurements to be taken at different directions to the fracture normal and hence the full elastic tensor could be obtained. The drawbacks to this approach were: a reduction in measurement accuracy, and measurements could not be carried out under confining pressure.

Other methods of making synthetic rocks including CIPS (Calcite In-situ Precipitation System) and Silica-lock have been reported, however, they have not been used to investigate fracture-induced anisotropy but are worth mentioning.

The Calcite In-situ Precipitation System (CIPS) was developed at the Commonwealth Scientific and Industrial Research Organisation (CSIRO) in Australia by Ed Kucharski and Graham Price (Sherlock and Siggins, 2004, Onishi et al., 2006). CIPS is a method of cementing sand grains through the injection of aqueous solutions and the precipitation of calcite cement around the grains and their contacts in a manner that mimics the cementation process in naturally occurring limestones. Sherlock and Siggins (2004) showed that artificial rocks can be fabricated with systematic, controllable and reproducible variations of a single

parameter, while keeping all other parameters constant. Rocks made using this method have been used in laboratory studies such as velocity-saturation relation (Lebedev et al., 2008), analog reservoir modelling for seismic and reservoir engineering (Sherlock et al., 2007), and elastic wave properties of methane hydrate rocks (Onishi et al., 2006). Although a promising method for synthetic rock manufacturing, a way would have to be found to embed penny shaped cracks of known distributions. Previous methods of achieving predetermined crack properties in sandstone rocks has been to emplace aluminium discs in the manufacturing stage and etching them out with acid once the cement has cured. This method would not be suitable for rocks made using CIPS because of calcite dissolution in acid.

Silica-lock was a method used by Visser (1988) to produce synthetic sandstones with silica cement, to study acoustic behaviours of real and synthetic rocks. This method uses silicon-tetrachloride to precipitate silica cement at grains and their contacts in the presence of water by reacting with the water to form silica cement, thereby consolidating the sand grains. This method is similar to CIPS since both methods involve cement precipitation at grain contacts; however, the silica-lock method produces toxic by-products discouraging the use of this method. Visser (1988) reported a well consolidated sample with homogeneous distribution of cement, porosity and permeability but another drawback of the method was crack-like irregularities in the samples.

Tien and Tsao (2000) prepared synthetic rocks to simulate mechanical properties of transversely isotropic rock samples. Although this approach was used in civil engineering studies, the synthetic rock manufacturing process could be extended to rock physics studies. They set out to manufacture synthetic rocks similar in mechanical behaviour to natural rocks by using three model materials (A, B and C) to prepare two blocks of artificial transversely isotropic rocks. Model material A was composed of cement, Ottawa sand, and microsilica in ratios 6:5:1, material B was composed of cement and kaolinite in a ratio of 4:1 and model material C was composed of cement and kaolinite in a ratio of 4.5:1 in weight. Compaction of stratified materials A and B were used to make an inter-layered material (block I) to represent anisotropic behaviour of sandstone-shale inter-bedded rock masses. Material C was used to make a stratified material (bock II) to simulate anisotropic behaviour of rocks such as shale and slate. The cured blocks were then cored at 0°, 15°, 30°, 45°, 60°, 75°, and 90° relative to the plane of the

layers to produce cylindrical samples of 48 mm diameter and 100 mm length for the mechanical tests.

2.8 Theoretical models used in this thesis

2.8.1 White's model

White (1975) quantified the effects of heterogeneous saturation distribution by deriving approximate solutions for the frequency-dependent seismic response of a homogeneous porous medium containing gas and liquid in different regions of the pore space. He considered spherical gas-filled regions of radius a located periodically at the centre of a liquid-filled cubic array.

An elementary cube with its enclosed spherical gas pocket (Figure 2.2a) is considered to be a typical volume having the same average properties as the average properties of the bulk composite. To simplify the calculations, the liquid-filled cube was replaced with a liquid-filled sphere of radius b chosen to have the same volume as the cube. So the model considers two concentric spheres (Figure 2.2b), where the outer liquid-filled sphere has a radius of b and the inner gas-filled sphere has a radius of a so that the gas saturation is given as $S_g = (a/b)^3$. White only considered patch sizes much smaller than the seismic wavelength but larger than the pore size.

The representative volume was then subjected to oscillatory forcing and the effective bulk modulus is estimated from the ratio of the imposed pressure amplitude and the fractional change in volume (White, 1975). The resulting effective bulk modulus is complex due to wave-induced fluid flow considerations, implying dispersion and attenuation. Dutta and Seriff (1979) corrected an error in White's analysis, where a P-wave modulus was used instead of a bulk modulus. Dutta and Odé (1979b), (1979a) gave a more rigorous derivation of White's model using Biot's theory of poroelasticity. Their results showed that the solutions from White's approach are in good agreement with their more rigorous approach.

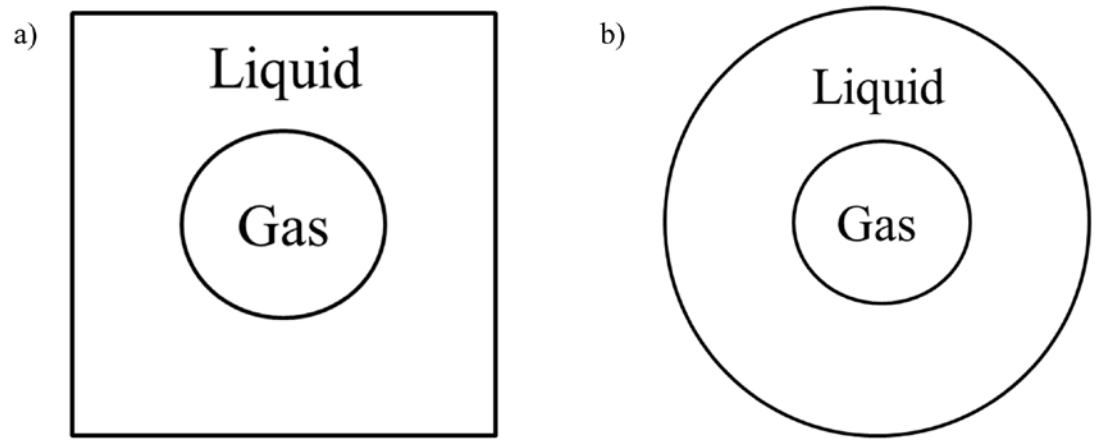

Figure 2.2: 2-D representation of the typical volume (a) gas sphere encased in a liquid cube; (b) concentric spheres of liquid and gas.

When the representative unit volume is compressed by a compressional wave, pressure gradients occur at the gas-liquid boundary and the liquid pressure will try to equilibrate with the gas phase by compressing the gas pocket (Gist, 1994b). In both the high and low frequency limits, there is no attenuation predicted because there is no fluid flow between the liquid and gas patches. In the low frequency (or static) limit, there is enough time for pore pressure equilibration so that the elementary volume is in equilibrium locally (White, 1975). This long wavelength (or period) response is identical to the equations of Gassmann with a Reuss averaged fluid modulus, which is the low frequency limit of White's model.

In the high frequency limit, there is not enough time for fluid to flow to equilibrate any pressure gradient; however, the gas pocket appears stiffer, leading to a higher effective rock bulk modulus than the relaxed case. At intermediate frequencies, wave induced fluid flow occurs, causing velocity dispersion and attenuation quantified by the equations of White (1975). White's model predicts significant dispersion and attenuation which spans a wide frequency range depending on wave frequency, porosity, permeability, viscosity and patch size. These are the only additional parameters needed for White's model in addition to those required for Gassmann's equations except for porosity which already exists in Gassmann's equations. All these parameters can be measured in the laboratory except for the patch size which is often a free parameter. At full water saturation, White's model is consistent with Gassmann's predictions. In this thesis I have used White's model corrected by Dutta and Seriff (1979) (see Mavko et al., 2009, p. 327 for explicit equations).

White's model is an idealised representation of patchy saturation and as such may fail to explain the observed velocity dispersion and attenuation in nature as the spatial distribution of heterogeneities in real rocks is random. However, the predictions are qualitatively correct and the simplicity of the model provides an intuitive understanding of the wave induced fluid flow mechanism due to mesoscopic heterogeneities. For example, the smaller the patch size compared to the seismic wavelength, the closer the behaviour approaches the Reuss averaged fluid modulus case and the characteristic frequency (where the transition from relaxed to unrelaxed case occurs) moves to higher frequencies. Examples of model predictions of White's model is shown in chapters 3 and 4 (Figures 3.2 and 4.5).

2.8.2 The model of Chapman (2003)

Chapman (2003) developed a theory to model the frequency-dependent effects due to wave induced fluid flow in rocks containing fractures, and fully saturated with a single fluid phase. The poroelastic equivalent medium model of Chapman (2003) considers an isotropic background medium containing spherical pores with a random distribution of randomly oriented ellipsoidal microcracks and aligned ellipsoidal fractures. The size of the spherical pores (equant porosity) and the ellipsoidal microcracks are on the scale of the grain size (microscopic scale), while the aligned ellipsoidal fractures are allowed to be larger as long as their size and spacing remain much smaller than the seismic wavelength (mesoscopic scale). The ellipsoidal fractures are aligned along a preferred direction and are rotationally invariant about the fracture normal so that the medium is transversely isotropic with hexagonal symmetry. A schematic illustration of the network of inclusions considered in this model is given in Figure 2.3.

Fluid exchange takes place between adjacent elements of pore space due to wave-induced pressure gradients according to Darcy's law. It should be pointed out that an element of pore space refers to any void (crack, pore or fracture). Fluid mass exchange between adjacent voids a and b is given by

$$\partial_t m_a = \frac{\rho_o \kappa \varsigma}{\eta}(p_a - p_b) \ , \tag{2.21}$$

where m_a is the fluid mass in element a, ρ_o is the fluid density, η is the fluid viscosity, κ is the permeability, ς is the grain size and p_i is the pressure in the ith element. It was assumed that each void was connected to six other elements. The fractures are larger than the microcracks and pores, and should therefore be connected to more elements. Each pore and microcrack was also assumed to be connected to at most one fracture, and that there is no connection between fractures which is ensured by making sure the number of microcracks and pores vastly exceeds the number of fractures.

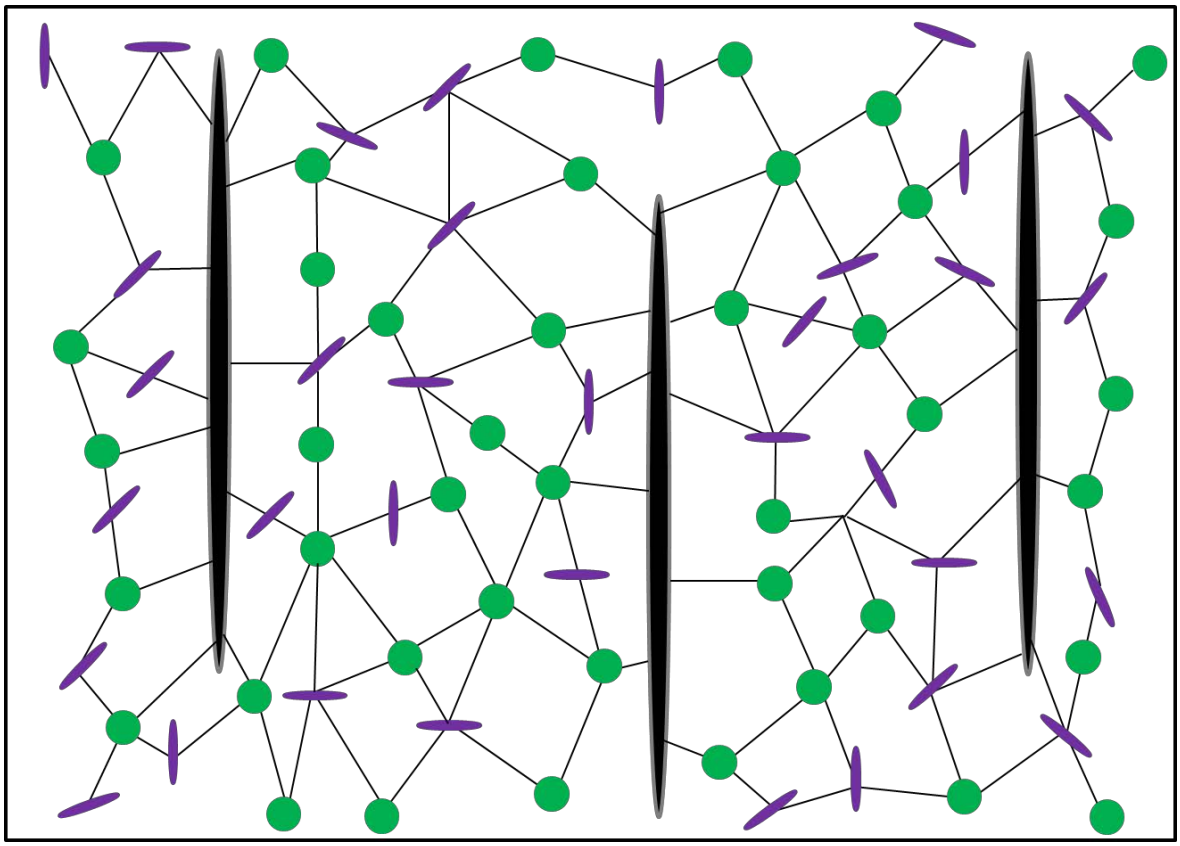

Figure 2.3: A schematic illustration of the network of spherical pores (green), randomly oriented ellipsoidal microcracks (purple), and fractures (black) considered in the model of Chapman (2003). Adapted from Liu and Martinez (2013).

Ensuring mass conservation throughout the pore space, Chapman (2003) then derived expressions for the expected fluid mass flow out of individual elements of pore space in terms of the inclusion pressure and applied stress. The time-dependent pressure in each type of void was then solved in terms of the applied stress field. The effective elastic constants were then calculated using the interaction energy approach of Eshelby (1957) for a material with embedded inclusions, where the stress and strain inside the inclusions were calculated from

the time-dependent pressures. The effective elastic constants of the model are of the form:

$$C_{ijkl} = C^0_{ijkl} - \Phi_p C^1_{ijkl} - \varepsilon_c C^2_{ijkl} - \varepsilon_f C^3_{ijkl}\,, \tag{2.22}$$

where ϕ_p is the porosity, ε_c is the microcrack density, ε_f is the fracture density. C^0_{ijkl} is the isotropic elastic tensor of the rock mineral, C^1_{ijkl}, C^2_{ijkl}, and C^3_{ijkl} are the contributions from the pores (with porosity Φ_p), the microcracks (with crack density ε_c), and fractures (with fracture density ε_f), respectively. These contributions depend on the Lamé parameters, fracture and fluid properties, wave frequency and relaxation times associated with the wave induced fluid flow.

Two relaxation timescales emerge due to the fact that fluid exchange is considered at two different scales of the pore space. Fluid flow between pores and microcracks is associated with the traditional squirt-flow frequency (τ_m), while a lower characteristic frequency (τ_f) also emerges, which depends on the size of the fractures. Both timescales are related by (Chapman, 2003)

$$\tau_f = \left(\frac{a_f}{\varsigma}\right)\tau_m\,, \tag{2.23}$$

where a_f is the fracture radius and ς is the grain size. The time scale parameter τ_m is given by

$$\tau_m = \frac{c_v \eta (1 + K_c)}{\sigma_c \kappa \varsigma c_1}, \tag{2.24}$$

where c_v is the volume of individual cracks, c_1 is the number of connections to other voids, $\sigma_c = \frac{\pi \mu r}{[2(1-\upsilon)]}$, is the critical stress with r being the aspect ratio of the cracks, υ the poisson ratio, and $K_c = \sigma_c / k_f$, where k_f is the fluid bulk modulus. The traditional squirt-flow frequency (τ_m) has been estimated to lie between the sonic and ultrasonic range (e.g. Murphy, 1985, Winkler, 1986), however, it is the larger relaxation timescale (τ_f) that can lead to velocity dispersion and attenuation in the seismic frequency range (Chapman et al., 2003).

The effective elastic tensor of the model of Chapman (2003) was derived using the interaction energy approach of Eshelby (1957), and as such is only valid for dilute concentrations of inclusions (i.e. low porosity). As shown above, the effective elastic tensor of the model depends on the Lamé parameters λ and μ of the mineral grains, the porosity Φ_p, the microcrack density ε_c, the fracture density ε_f, the density of the rock ρ, the aspect ratio r of the fractures and cracks (which

are taken to be the same for simplicity), the fracture radius a_f, the fluid bulk modulus k_f, and the relaxation time τ_m. To reduce the number of free parameters, it is desirable to be able to constrain as many of these parameters as possible through direct measurements from physical properties of the rock or through inversion from data.

The dependence of the model on the Lamé parameters of the mineral grains meant that the reference moduli should be obtained from the velocities of rock without pores or cracks. Due to the restriction to low porosities, in practice, this would mean the moduli λ and μ would themselves have to be fitted to achieve agreement with the background velocities which could result in substantial errors in calculating the effect of fractures (Chapman et al., 2003). To get around this limitation, Chapman et al. (2003) proposed a slightly modified approach similar to the self-consistent scheme (Zimmerman, 1991), where the effect of the inclusions is approximated by replacing the background medium with the as-yet-unknown effective medium (Zimmerman, 1991, Mavko et al., 2009). Chapman et al. (2003) suggested using Lamé parameters λ^o and μ^o obtained at some frequency from the velocities V_p^o and V_s^o, and density ρ of the saturated unfractured rock. For the isotropic unfractured rock, the model takes the form (Chapman et al., 2003):

$$\lambda_{eff} = \lambda - \Phi_{c,p}[\lambda, \mu, \omega_0] , \tag{2.25}$$

$$\mu_{eff} = \mu - \Phi_{c,p}[\lambda, \mu, \omega_0] , \tag{2.26}$$

where the functions $\Phi_{c,p}$ are perturbations due to the presence of microcracks and pores. It should be ensured that at a frequency ω_0 and in the absence of fractures:

$$\lambda_{eff} = \lambda^o , \tag{2.27}$$

$$\mu_{eff} = \mu^o . \tag{2.28}$$

In order to avoid choosing non-physical λ and μ to ensure this condition holds, which would also lead to non-physical velocities, Chapman et al. (2003) insisted that the corrections are calculated with the physical values λ^o and μ^o so that we must have:

$$\lambda^o = \Lambda - \Phi_{c,p}[\lambda^o, \mu^o, \omega_0] , \tag{2.29}$$

$$\mu^o = M - \Phi_{c,p}[\lambda^o, \mu^o, \omega_0] , \tag{2.30}$$

Λ and M are frequency independent reference constants with no direct physical meaning, although they can be calculated from measureable values V_p^o and V_s^o. The frequency-dependent, anisotropic, effective elastic tensor can then be calculated as (Chapman et al., 2003):

$$C_{ijkl}(\omega) = C^0_{ijkl}(\Lambda, M) - \Phi_p C^1_{ijkl}(\lambda^o, \mu^o, \omega_0) - \varepsilon_c C^2_{ijkl}(\lambda^o, \mu^o, \omega_0) - \varepsilon_f C^3_{ijkl}(\lambda^o, \mu^o, \omega_0)\,, \tag{2.31}$$

where $C^0_{ijkl}(\Lambda, M)$ is the isotropic elastic tensor with Lamé parameters Λ and M. In this form, the corrections for the pores, microcracks and fractures can be calculated with physical properties obtained from laboratory measurements on the unfractured rock.

Chapman et al. (2003) then showed the model could be simplified further by setting the microcrack density ε_c to zero for high porosity rocks as its influence to the overall result is negligible if the equant porosity is significantly greater than the microcrack porosity. This assumption holds true for most clastic sedimentary rocks, but it may not hold for fractured carbonate reservoir rocks or fractured tight unconventional reservoir rocks. This assumption reduces the number of unknown parameters to be specified in the model to two. One parameter that is usually unknown is the aspect ratio r of microcracks and fractures, which enters the calculations through the parameter $K_c = \frac{\pi\mu r}{[2k_f(1-\upsilon)]}$. It can be seen that for small aspect ratios $K_c \ll 1$, and as a result, the effective elastic constants will be insensitive to the exact value of r provided it is small enough (Maultzsch et al., 2003a). A small value of r is reasonable since the cracks and fractures represent the flat (or thin) compliant part of the pore space (Maultzsch, 2005). The parameter that is most difficult to determine is the relaxation time τ_m. This can be estimated by calibrating the model against laboratory data (e.g., Maultzsch et al., 2003a, Tillotson et al., 2011, Tillotson et al., 2014).

In the Chapters 4 and 5, I present a modelling approach that combines the models of Chapman (2003) and White (1975) to explain the effects of partial saturation on fracture-induced seismic anisotropy. The approach can be visualised as a periodic distribution of gas patches (White's model) in an otherwise liquid-filled porous rock, with aligned penny-shaped mesoscopic fractures (from Chapman's model). A schematic diagram is given in Figure 2.4. Details of the modelling approach are given in Chapters 4 and 5.

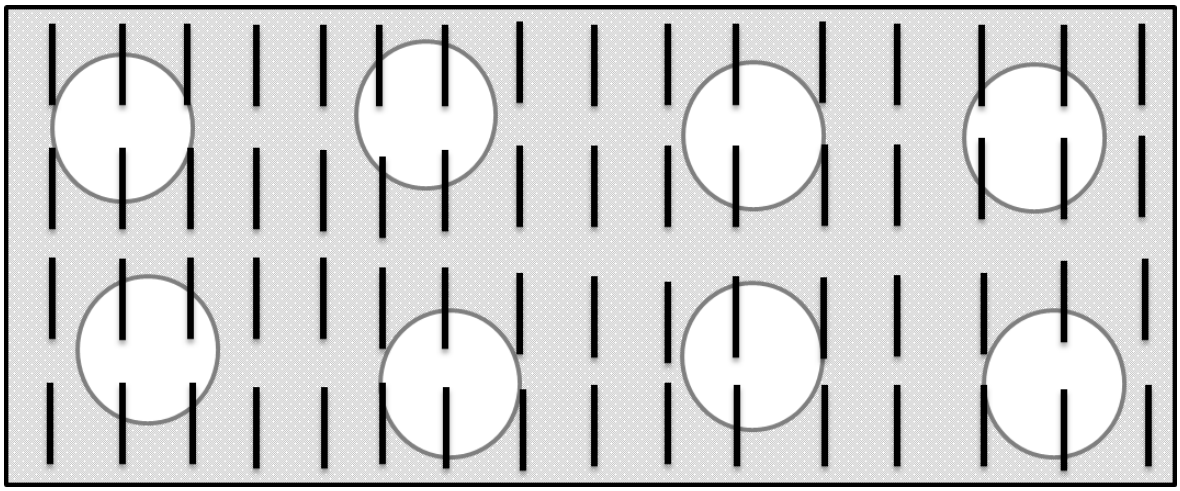

Figure 2.4: Schematic illustration of combining White's gas pocket model with the fractured model of Chapman (2003).

Chapter 3: Water saturation effects on elastic wave attenuation in porous rocks with aligned fractures.

This chapter forms a paper published in Geophysical journal international as an express letter: Amalokwu, K., A. I. Best, J. Sothcott, M. Chapman, T. Minshull, and X.-Y. Li. 2014, Water saturation effects on elastic wave attenuation in porous rocks with aligned fractures. Geophysical Journal International, 197, no. 2,943-947. doi: 10.1093/gji/ggu076.

Abstract: Elastic wave attenuation anisotropy in porous rocks with aligned fractures is of interest to seismic remote sensing of the Earth's structure and to hydrocarbon reservoir characterisation in particular. We investigated the effect of partial water saturation on attenuation in fractured rocks in the laboratory by conducting ultrasonic pulse-echo measurements on synthetic, silica-cemented, sandstones with aligned penny-shaped voids (fracture density of 0.0298 ± 0.0077), chosen to simulate the effect of natural fractures in the Earth according to theoretical models. Our results show, for the first time, contrasting variations in the attenuation (Q^{-1}) of P- and S-waves with water saturation in samples with and without fractures. The observed Q_s/Q_p ratios are indicative of saturation state and the presence or absence of fractures, offering an important new possibility for remote fluid detection and characterisation.

3.1 Introduction

Velocity and attenuation of compressional (P) and shear (S) waves are known to vary with fluid type and saturation in the Earth's crust, a fact that is currently exploited for seismic exploration of hydrocarbons. Recent advances in multicomponent seismology have led to improved methods for characterising rocks with aligned fractures. The combined effects of fluid type and aligned fractures have also been studied theoretically and experimentally, and have revealed useful relationships for interpreting reservoir quality from remote seismic data. However, the seismic response to partial gas saturation in fractured rocks is poorly understood at present, even though such conditions are commonly encountered in hydrocarbon reservoirs. The ability to discriminate between zones of high and low gas content in the subsurface, as well as between less or more densely fractured zones, would offer important economic advantages, for example, for the characterisation of tight gas, shale gas and geothermal steam reservoirs that all rely on fracture networks for their viability; this know-how would also benefit geological CO_2 storage and monitoring, needed for climate change mitigation.

Rocks containing aligned fractures are frequently encountered in the Earth; they exhibit seismic anisotropy and give rise to shear wave splitting (Crampin, 1981), resulting in two orthogonally polarized shear waves with velocity and attenuation (inverse quality factor Q^{-1}) expressed as V_{s1}, Q_{s1}^{-1} for the fast S-wave, and V_{s2}, Q_{s2}^{-1} for the slow S-wave. Studies have shown Q^{-1} to be more sensitive to changes in the physical state of rocks than velocity; for example, to changes in fluid saturation (Murphy, 1982, Yin et al., 1992) and the presence of fractures (Zhu et al., 2007, Chichinina et al., 2009). Experimental studies have shown the ratio of P- to S-wave attenuation (Q_s/Q_p ratio) to be more sensitive to gas saturation than the ratio of P- to S-wave velocity (V_p/V_s) (e.g., Winkler and Nur, 1982). Chichinina et al. (2009) used stacks of Plexiglas sheets as a physical model for fractured rock and showed anisotropic variation of Q_s/Q_p ratios as a possible indicator for gas; however, partial gas saturation was not considered. Seismic attenuation in particular remains poorly understood and underutilized in field seismology. However, advances have been made in the qualitative use of attenuation for fractured rock characterisation (Liu et al., 2003, Maultzsch et al., 2007) and saturation discrimination (Klimentos, 1995). Although fluid effects (100% gas or liquid saturation) in fractured rocks have received experimental and

theoretical evaluation (e.g., Rathore et al., 1995, Chapman, 2003), the effect of partial saturation on the seismic properties of fractured rocks is still unknown.

A major challenge to experimentalists seeking to validate theoretical seismic models is the idealised fracture geometries (e.g., penny shaped cracks) often used in theoretical models as a mathematical approximation to natural fractures. Such geometries are not readily available in natural rocks which has led researchers to use synthetic materials to construct physical models, such as an epoxy matrix with embedded rubber discs to represent fractures (e.g., Ass'ad et al., 1992, de Figueiredo et al., 2013). These studies provided very useful results on elastic wave behaviour in fractured rocks, but they did not capture important wave attenuation mechanisms associated with viscous fluid flow (e.g., squirt flow; see Thomsen, 1995, Chapman, 2003). Recently, Tillotson et al. (2012) produced novel synthetic silica cemented sandstones with controlled fracture geometry. These synthetic samples offer new possibilities for the validation and calibration of various aspects of theoretical models for fractured, porous rocks. In particular, the prediction of partial liquid/gas saturation effects is a complex problem; hence, we seek to guide the development of a suitable model through primary experimental observations.

Here, we present new laboratory experimental measurements of Q_p^{-1}, Q_{s1}^{-1} and Q_{s2}^{-1} as functions of water/air saturation in a synthetic, silica-cemented sandstone containing vertically aligned fractures and compare the results to those of a blank (unfractured) sample of the same material. The results show that the presence of aligned fractures changes the relationship between Q_s/Q_p ratio and water saturation in porous rocks, an observation that could have a significant impact on remote seismic characterisation.

3.2 Methods

3.2.1 Synthetic rocks

We used the same synthetic silica cemented sandstone samples as Tillotson et al. (2012), who give details of the manufacturing process. Samples were made from a mixture of sand, kaolinite and aqueous sodium silicate gel using a similar approach to Rathore et al. (1995), by arranging a predetermined number of 2 mm diameter aluminium discs of 0.2 mm thickness on successive 4 mm layers of sand mixture. Image analysis of X-ray CT scans (Figure 3.1a) was used to obtain

the fracture density, ε_f = 0.0298 ± 0.0077 and an average fracture aspect ratio of 0.088 ± 0.001. As pointed out by Tillotson et al. (2012), this value includes voids created as a result of overlapping discs as well as discrete penny-shaped voids.

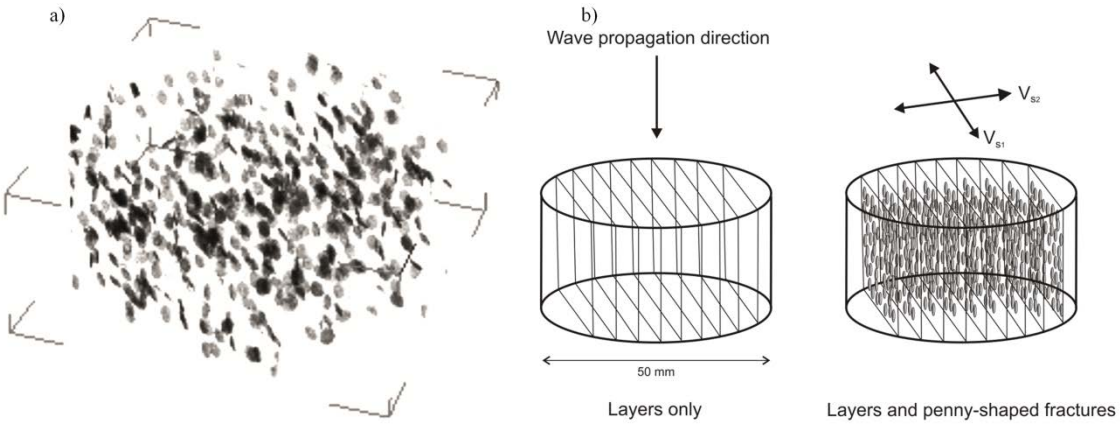

Figure 3.1: a) X-ray CT images of the 90° fractured sample showing size, density and distribution of penny-shaped fractures. b) orientation of layering and fracture planes within the rocks relative to the direction of wave propagation in our experiments. After Tillotson (2012).

The petrophysical properties of the synthetic sandstones are given in Table 1 (see supporting information). The porosity and permeability of both samples are 30.43% and 40.7 mD for the blank sample, and 31.68% and 18.1 mD for the fractured sample, respectively. Note the relatively large difference in permeability, seemingly unrelated to the presence of discrete penny-shaped voids, and more probably due to small differences in silica cement.

3.2.2 Ultrasound Experiments

We measured ultrasonic wave attenuation coefficient to an accuracy of ± 0.2 dB/cm using the same pulse-echo (reflection) method as Tillotson et al. (2012) (see McCann and Sothcott, 1992 for detailed equipment description). Shear-wave splitting was measured by rotating the piezoelectric shear-wave transducer (while the sample was under elevated pressure) and observing the minimum and maximum signal amplitudes (maximum and minimum Q^{-1}, respectively) corresponding to shear wave polarization at 0° and 90° to the fracture normal, respectively (see Best et al., 2007).

Ultrasonic wave measurements were then taken at different partial saturation states of air/water (see supporting information for details on saturation methods used), quantified by water saturation S_w.

3.3 Results

3.3.1 Saturation dependence of Q_p^{-1} and Q_s^{-1}

We present all results at an effective pressure of 40 Mpa and a single frequency of 650 kHz obtained from Fourier analysis of broadband signals. The results in Figure 3.2 are expressed in terms of the inverse quality factors Q_p^{-1}, Q_{s1}^{-1} and Q_{s2}^{-1} as functions of water saturation S_w; subscripts P, S1 and S2 refer to the compressional wave, the fast shear wave with polarization along the bedding planes and co-incident fractures, and the slow shear wave with polarization perpendicular to the bedding and fractures, respectively.

In the blank sample (Figure 3.2a), Q_{s1}^{-1} and Q_{s2}^{-1} have similar values for all S_w, showing the attenuation anisotropy induced by layering is negligibly small. Between S_w of 0 – 0.8, P-wave attenuation increases steadily to a maximum at about S_w = 0.4 and then decreases, and is higher than S- wave attenuation, which is not as sensitive to changing S_w except for a sharp increase at $S_w \sim 0.1$, after which it steadily increases until full water saturation. Both P- and S-wave attenuations are comparable between S_w = 0.8 – 0.9; as S_w approaches 1.0, P-wave attenuation drops to a minimum value while S-wave attenuation continues to increase slightly. The results show that Q_p^{-1} is more sensitive to S_w than Q_s^{-1}. These results are broadly in agreement with previously published experimental observations for non-fractured rocks (Murphy, 1982, Bourbie and Zinszner, 1985).

By contrast, the fractured sample (Figure 3.2b) shows completely different behaviour to the blank sample. Firstly, Q_p^{-1} is much lower and, except at S_w = 0.4, smaller or only slightly larger than Q_{s1}^{-1} and Q_{s2}^{-1} (a sharp maximum is seen at about S_w = 0.4). Secondly, as expected, the rock shows significant shear wave (Q^{-1}) splitting. Q_{s1}^{-1} and Q_{s2}^{-1} increase slightly from S_w = 0 – 0.1, then stay reasonably constant between S_w = 0.1 – 0.7, then increase slightly as S_w approaches 1.0.

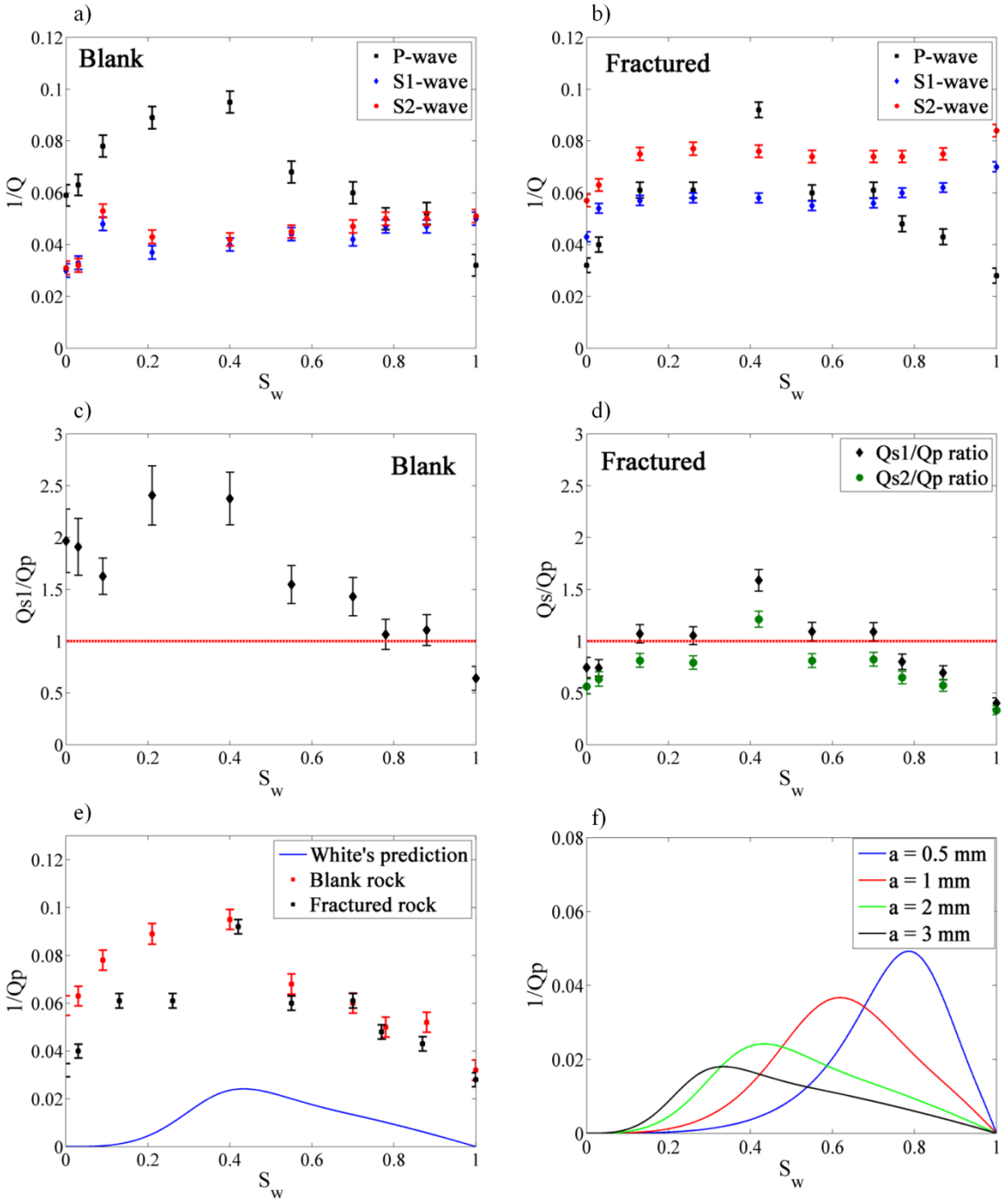

Figure 3.2: a) and b) (top row) show measured Q^{-1} versus Sw for the blank and fractured rocks (direction of wave propagation is 90° to the fracture normal), respectively. c) and d) (middle row) show Q_s/Q_p ratios versus S_w for both samples (only Q_{s1} is used both shear attenuations are similar in the blank rock); the dashed line is for a ratio of 1. e) Observed Q_p^{-1} versus S_w for both rocks and White's (1975) model predictions for a gas pocket radius "a" = 2 mm and frequency of 650 kHz (blank rock only). f) White's (1975) model predictions using different gas patch radii (a = 0.5 to 3 mm) at 650 kHz for the blank rock sample.

3.3.2 Q_s/Q_p Ratios

Previous studies have shown that the ratio of Q_p^{-1} to Q_s^{-1} gives a clear distinction between full and partial saturation along with a better estimate of gas saturation than V_p/V_s ratios (Winkler and Nur, 1982). Hence, Q_s/Q_p could be potentially useful for the determination of water saturation in reservoir rocks from remote seismic measurements, provided that Q_p^{-1} and Q_s^{-1} can be determined with sufficient accuracy. When used together with V_p/V_s ratios, which are only sensitive to small amounts of gas, Q_s/Q_p ratios could provide more reliable subsurface S_w estimates (Klimentos, 1995, Dvorkin and Mavko, 2006). For approximately isotropic rocks, the Q_s/Q_p ratio is greater than unity for $S_w < 0.9$ and less than unity at higher saturations (e.g., Murphy, 1982), which is also in good agreement with our observations for the blank rock (Figure 3.2c).

However, our results show markedly different behaviour in the fractured rock. For rocks with aligned fractures, Q_s/Q_p is only significantly greater than 1 at intermediate saturations of about $S_w = 0.45$ for fast S-waves only (S1). Otherwise, Q_s/Q_p is about unity (± 0.2) except at low saturations ($S_w < 0.1$) and high saturations ($S_w > 0.8$) for both fast (S1) and slow (S2) shear waves.

Crucially, these observations show that the presence of aligned fractures can significantly change the Q_s/Q_p relationships previously established for approximately isotropic rocks.

3.4 Attenuation Mechanisms

3.4.1 Scattering versus viscous losses

Attenuation can be caused by several mechanisms broadly divided into elastic processes (scattering attenuation, geometric spreading) and inelastic dissipation (viscous losses), of particular interest to exploration geophysics (Müller et al., 2010). We present evidence that our observations in the fractured rock sample are dominated by inelastic dissipation and not scattering attenuation. We also discuss some possible viscous loss mechanisms and implications from our observations.

The presence of fractures in rocks is known to increase dispersion and attenuation from two main mechanisms, namely wave induced flow and scattering

(Liu et al., 2003). Both mechanisms occur at different scales (as fractures can range from microscopic to macroscopic scales), but scattering attenuation becomes significant as the size of the heterogeneity becomes comparable to the elastic wavelength (Johnston et al., 1979, Blair, 1990, Liu et al., 2003). In the 90˚ fractured sample, we measure Q_p^{-1}, Q_{s1}^{-1} parallel to the fractures and Q_{s2}^{-1} perpendicular to the fractures. Experimental studies using synthetic materials as physical models for fractured rocks have shown that the amplitudes of the P- and S1-waves propagating parallel to the fractures depends mainly on the fracture aperture (thickness) and not the diameter of the fractures (Wei and Di, 2008, de Figueiredo et al., 2013). Wei and Di (2008) showed that increasing the fracture diameter does not have any significant effect on the amplitude or velocity of the P- and S1- waves; however, significant increases in the fracture aperture reduces both amplitude and velocity.

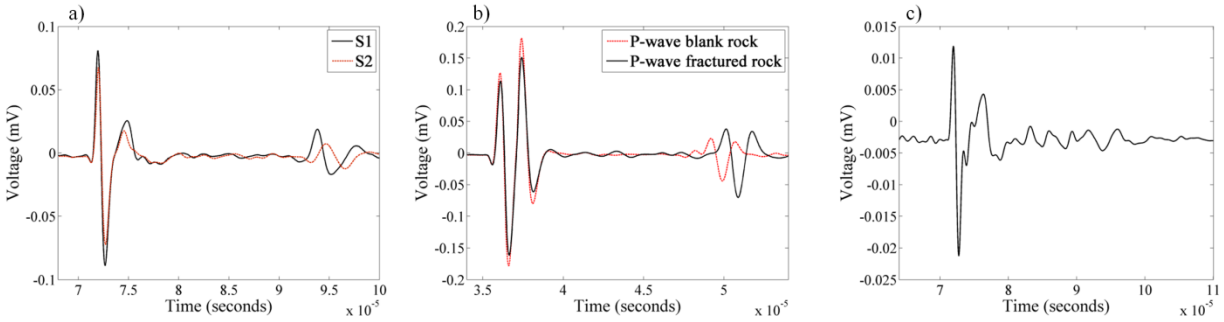

Figure 3.3: a) S1 and S2 waveforms for the fractured sample with S-wave propagation direction at 90˚ to the fracture normal. b) P waveforms for blank sample (red line) and 90˚ fractured sample (black line), respectively. c) Pulse-echo shear waveform for the fractured sample with S-wave propagation direction parallel to the fracture normal (note that the disc-like fractures are about one wavelength in diameter, giving rise to significant scattering attenuation and no apparent sample base reflection). Notice the clean pulse-echo waveforms for a) and b) compared to the scattering evident multiples in c).

In our ultrasonic pulse-echo experiments, the wavelength is approximately 5 mm and 3 mm for P- and S1-waves, respectively, and the ratio of wavelength to fracture aperture (0.2 mm) is ~ 25 and 16, respectively, suggesting that the presence of fractures does not contribute significantly to scattering attenuation for wave propagation at 90˚ to the fracture normal. However, for waves propagating parallel to the fracture normal, the pulse reflection method is sensitive to the presence of the aligned fractures which are on the order of one wavelength, leading to multiple reflections before the desired sample base

reflection (Figure 3.3c); in fact, scattering is so intense that there is insufficient energy to generate an observable sample base reflection.

Wei and Di (2008) and de Figueiredo et al. (2013) show that Q_{s2}^{-1} also depends more on the fracture aperture than the fracture diameter, although increasing the fracture diameter (compared to the wavelength) does increase the scattering attenuation. Again, our wavelength to aperture ratio for the S2-wave is ~ 15. The scattering contribution to Q_{s2}^{-1} is unknown in our experiments and there are no similar experiments in the literature for comparison. However, experiments and theory show that Q_{s2}^{-1} is always higher than Q_{s1}^{-1} for wave propagation parallel to the fractures (90° to fracture normal) (e.g., Chapman, 2003, Chichinina et al., 2009). Consequently, comparing Q_{s1}^{-1} and Q_{s2}^{-1}, the scattering attenuation contribution has to be less than 1% to keep $Q_{s2}^{-1} > Q_{s1}^{-1}$. Hence, we conclude that scattering attenuation as a result of the fractures does not compromise the validity of our results.

3.4.2 Viscous Losses

Quantitative interpretation of seismic attenuation anisotropy remains problematic as the underlying physics remains poorly understood (Maultzsch et al., 2007). It is now generally agreed that the dominant cause of attenuation in fluid saturated crustal rocks is the viscous fluid-solid interaction (Winkler and Nur, 1979, Murphy, 1982, Winkler and Nur, 1982, Murphy, 1984, Müller et al., 2010). Although no satisfactory model exists at present to quantitatively interpret attenuation experiments, existing theoretical mechanisms can qualitatively explain the observed saturation effects remarkably well.

Q^{-1} variation with saturation is known to depend on the rock and fluid properties. White (1975) modelled attenuation in rocks with partial saturation as a function of gas pocket size, wave frequency, permeability and porosity of rocks; it has been shown that the Q_p^{-1} behaviour depends on these parameters (e.g., Carcione et al., 2003, Nakagawa et al., 2013). Using a gas patch radius (a) of 2 mm in White's model, we see qualitative agreement with the observed Q_p^{-1} versus S_w trend but an underestimation of the magnitude of attenuation (Figure 3.2e). This is as a result of additional dissipation mechanisms not considered in White's model (Carcione et al., 2003, Nakagawa et al., 2013), such as local (or "squirt") flow (see Mavko and Nur, 1979, Winkler and Nur, 1982, Dvorkin et al., 1994), which has been shown to give higher attenuation values (Winkler and Nur, 1979, Dvorkin and Nur, 1993, Carcione et al., 2003). Figure 3.2f shows White's model

prediction for a range of patch sizes. The gas patch radius that fits our observed saturation trend falls within the range observed by Nakagawa et al. (2013) and inferred by Lei and Xue (2009).

Q_s^{-1} is not very sensitive to partial saturation where it is lower than Q_p^{-1} but increases at full saturation where it is larger than Q_p^{-1}, consistent with observations in the literature (Murphy, 1982, Winkler and Nur, 1982). This observation is interpreted using a mechanism which involves "squirt" flow between cracks at different orientations which results in higher Q_s^{-1} than Q_p^{-1} as predicted by O'Connell and Budiansky (1977) and observed by Winkler and Nur (1979).

More importantly, our results show markedly different behaviour in the fractured sample (Figs. 2b & d). Wave propagation at 90° to the fracture normal leads to three waves propagating in different planes relative to the fractures. P-wave attenuation is not significantly increased by the presence of fractures as long as the fracture aperture is much less than the wavelength (e.g., Wei and Di, 2008); however, the presence of fractures appears to increase both Q_{s1}^{-1} and Q_{s2}^{-1} (the effect being greater on Q_{s2}^{-1}). This produces a striking difference in the Q_s/Q_p versus saturation relationship from that seen in the blank sample.

Another interesting observation from Figure 3.2e is that the fluid effect on Q_p^{-1} is greater in the fractured rock where Q_p^{-1} begins from a lower dry ($S_w = 0$) value and still peaks at a value similar to that of the blank rock. This can be interpreted as additional wave induced fluid flow as a result of the presence of fractures (Kong et al., 2013). Note that it is difficult to interpret differences in absolute attenuation between the blank and fractured sample because of small microstructural differences associated with the manufacturing process. We instead focus on comparing the relative changes in attenuation with saturation in each rock sample.

Partial gas saturation and fractures are known to increase Q_p^{-1} because of large compressibility contrasts between liquid and gas, and between relatively stiff rock matrix and compliant fractures, respectively. With sufficient azimuthal coverage, Q_p^{-1} can be used to detect and characterise fractures (e.g., Maultzsch et al., 2007). Partial gas saturation effects could be detected using Q_s/Q_p ratios even in the presence of increased attenuation from fractures, reducing the ambiguity. Chichinina et al. (2009) showed that fractures oriented perpendicular to the direction of wave propagation would follow similar Q_s/Q_p trends to those for

isotropic rocks (Q_s/Q_p >>1 for full and partial gas and $Q_s/Q_p \leq 1$ for water saturated rocks). However, our experiments show that for wave propagation parallel to the fracture strike, there is a contrasting difference in Q_s-Q_p relationships. Q_{s1}/Q_{s2} and Q_{s1}/Q_p could indicate degree of fracturing and saturation respectively. This observation highlights the importance of careful interpretation of seismic data for gas reservoirs containing fractures and could be useful during data acquisition design stages in terms of desired attributes from the survey.

Although our observations are in the ultrasonic frequency range, it has been shown theoretically (e.g., Chapman, 2009, Rubino et al., 2013) and experimentally (e.g., Batzle et al., 2006) that these viscous loss mechanisms are expected over a wide frequency range, including seismic frequencies. These observations could be extended to different frequencies using a suitable frequency-dependent model.

3.5 Conclusions

We present novel experimental observations of the effect of liquid/gas saturation on elastic wave attenuation in sandstones with aligned fractures. The results not only support the potential of Q_s/Q_p ratios for fluid saturation discrimination but, more importantly, they show the contrasting behaviour of isotropic rocks and rocks with fractures aligned in the direction of wave propagation. Also, the fluid saturation effect on Q_p^{-1} is higher in the fractured rock than in the isotropic rock.

Advances in theoretical and experimental seismic studies of fractured rocks are important for the interpretation of multi-component, azimuthal seismic reflection data. These relationships are particularly important for interpreting sonic well logs and cross well data for horizontally fractured reservoirs. Further experimental and modelling studies are needed for extension to non-zero angles (between wave propagation and fracture orientation), and for generalization to a range of parameters such as wave frequency, fracture properties (e.g., diameter, aperture and density), porosity and permeability.

Chapter 4: Experimental observation of water saturation effects on shear wave splitting in synthetic rock with fractures aligned at oblique angles

This chapter forms a paper published in Geophysical journal international: Amalokwu, K., M. Chapman, A. I. Best, J. Sothcott, T. A. Minshull, and X.-Y. Li. 2015, Experimental observation of water saturation effects on shear wave splitting in synthetic rock with fractures aligned at oblique angles. Geophysical Journal International, 200, no. 1,17-24. doi: 10.1093/gji/ggu368.

Abstract: Fractured rocks are known to exhibit seismic anisotropy and shear wave splitting (SWS). SWS is commonly used for fractured rock characterisation and has been shown to be sensitive to fluid type. The presence of partial liquid/gas saturation is also known to affect the elastic properties of rocks. The combined effect of both fractures and partial liquid/gas saturation is still unknown. Using synthetic, silica-cemented sandstones with aligned penny-shaped voids, we conducted laboratory ultrasonic experiments to investigate the effect fractures aligned at an oblique angle to wave propagation would have on SWS under partial liquid/gas saturation conditions. The result for the fractured rock shows a saturation dependence which can be explained by combining a fractured rock model and a partial saturation model. At high to full water saturation values, shear wave splitting decreases as a result of the fluid bulk modulus effect on the quasi-shear wave. This bulk modulus effect is frequency dependent as a result of wave-induced fluid flow mechanisms, which would in turn lead to frequency dependent SWS. This result suggests the possible use of SWS for discriminating between full liquid saturation and partial liquid/gas saturation.

4.1 Introduction

Elastic wave propagation is strongly affected by the presence of partial liquid/gas saturation and by the presence of fractures. The combined effect of both is still poorly understood as little work has been done on saturation effects in fractured rocks. Aligned fractures are widespread in crustal rocks, causing seismic anisotropy (Crampin, 1981, Winterstein, 1992). The sensitivity of seismic waves to the presence of aligned fractures in the form of seismic anisotropy makes it possible to obtain fracture information from seismic data. A commonly used method is shear-wave splitting (SWS), given as the time delay between the fast and slow shear-waves, which is usually related to the fracture density (Crampin, 1985, Marson-Pidgeon and Savage, 1997, Liu et al., 2003, Verdon and Kendall, 2011). This splitting results in two orthogonally polarized shear waves with velocities V_{s1} and V_{s2} for the pure shear and quasi-shear waves respectively. For isotropic rocks, Gassmann's formula predicts that the shear modulus of the rock is insensitive to saturation. However, in the anisotropic case fluid compressibility can affect shear wave propagation (Brown and Korringa, 1975), causing fluid-dependent shear wave splitting. This fluid-dependent shear wave splitting could be used as a diagnostic tool to infer the saturation properties of fractured reservoirs (e.g., Qian et al., 2007).

Fluid-dependent shear wave splitting has been observed both in field data (Van Der Kolk et al., 2001, Qian et al., 2007) and laboratory experiments (Tillotson et al., 2011). This fluid dependent SWS is indeed frequency dependent as shown by theoretical studies and field studies (Marson-Pidgeon and Savage, 1997, Chapman, 2003, Liu et al., 2003, Al-Harrasi et al., 2011). Theoretical models are needed to interpret seismic data in terms of fracture properties and fluid properties. The combined effect of fluids (100% gas or liquid saturation) and aligned fractures have been studied theoretically and experimentally (e.g., Hudson, 1981, Ass'ad et al., 1992, Rathore et al., 1995, Thomsen, 1995, Hudson et al., 2001, Chapman, 2003). The fluid independent relationship between fracture density and shear wave splitting for wave propagation at 90° to the fracture normal has been observed in laboratory experiments (e.g., Rathore et al., 1995, Tillotson et al., 2012) in line with theoretical predictions (e.g., Hudson, 1981). Theoretical predictions of fluid sensitivity of the slow shear-wave propagating at oblique angles to the fracture normal was observed in laboratory experiments by Tillotson et al. (2011) using a synthetic fractured sample cored at

45° to the fracture normal and saturated with single fluid phases of different viscosities. However, the seismic response to partial gas saturation in fractured rocks is still poorly understood at present, even though such conditions are commonly encountered in the Earth's crust.

Experimental investigation of water saturation effects have been limited to approximately isotropic rocks, most likely because of experimental limitations associated with fractured rock studies. A major limitation is that idealised fracture geometries (e.g., penny shaped cracks) often used in theoretical models as a mathematical approximation do not resemble natural fractures in rock, and it is difficult to control the introduction of aligned natural fractures in laboratory samples. Controlled fractured rock experiments have therefore required the use of synthetic rocks, leading to the use of synthetic materials to construct physical models, such as an epoxy matrix with embedded rubber discs to represent fractures (e.g., Ass'ad et al., 1992, de Figueiredo et al., 2013). These studies provided very useful results on elastic wave behaviour in fractured rocks, but they did not capture important wave-induced flow mechanisms (e.g., squirt flow; see Thomsen, 1995, Chapman, 2003). Recently, Tillotson et al. (2012) produced novel synthetic silica cemented sandstones with controlled fracture geometry. These synthetic samples offer new possibilities for the validation and calibration of various aspects of theoretical models for fractured, porous rocks. In particular, the prediction of partial liquid/gas saturation effects is a complex problem; hence, we seek to guide the development of a suitable model through primary experimental observations.

Here, we present new laboratory experimental measurements of V_{s1} and V_{s2} as functions of water/air saturation in synthetic, silica-cemented sandstone containing fractures aligned at 45° to the fracture normal. The results show an interesting saturation dependence of SWS. We find that combining the corrected White (1975) model for partial saturation (sometimes referred to as the White and Dutta-Ode model – see Mavko et al. (2009)) with the fractured rock model of Chapman (2003) could give insight into the mechanisms controlling our experimental observations.

4.2 Methods

4.2.1 Synthetic rock samples

The samples used in this study (Figure 4.1a) were made by Tillotson (2012) as part of the same batch used by Tillotson et al. (2012), who give more details of the manufacturing process. The fractures are just visible on the surface of the sample in Figure 4.1a but Figure 4.1b shows the idealised distribution throughout the sample volume. The synthetic rock samples were made from a mixture of sand, kaolinite and aqueous sodium silicate gel using a similar approach to Rathore et al. (1995). A predetermined number of 2 mm diameter aluminium discs of 0.2 mm thickness were arranged on successive 4 mm layers of sand mixture. The blank sample (rock sample without fractures) was cored parallel to the layering and the fractured sample used in this study was cored at 45° to the fracture normal using a diamond drill bit. Each sample had a diameter of 50 mm and a length of 20-25 mm. Image analysis of X-ray CT scans was used to obtain the fracture density, $\varepsilon_f = 0.0298 \pm 0.0077$, and the average fracture aspect ratio of 0.088 ± 0.001, for a sample cored at 90° to the fracture normal (that was not used in this study). As pointed out by Tillotson et al. (2012), this value includes voids created as a result of overlapping discs as well as discrete penny-shaped voids. Although the above fracture parameters were for a different sample to the one used in our experiments, both samples were made as part of the same batch, so are expected to have very similar fracture parameters.

The porosity and Klinkenberg corrected permeability were measured using Helium porosimetry and Nitrogen permeametry respectively. Permeability was measured in the direction of the core axis. The porosity and permeability are 30.43% and 40.7 mD for the blank sample, and 31.8% and 2.66 mD for the fractured sample, respectively. Note the difference in permeability between both samples, attributed to differences in grain packing during rock manufacturing stage and the direction in which the rocks were cored.

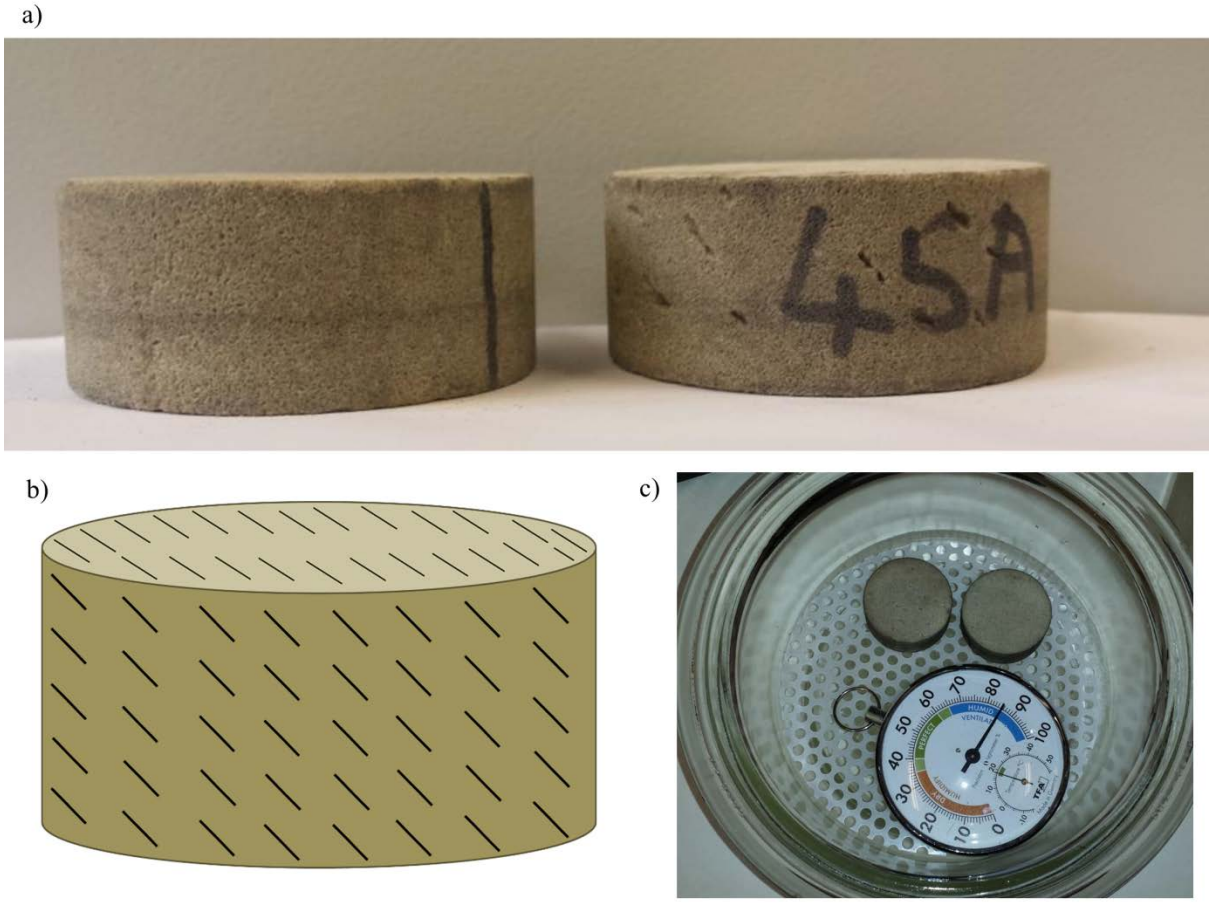

Figure 4.1: a) blank rock (left) and fractured rock (right). b) A schematic of the synthetic rock containing aligned fractures c) rock samples in vacuum desiccator containing saturated salt solution, and a hygrometer to verify the relative humidity.

4.2.2 Saturation methods

Partial saturation was achieved using the method described by Amalokwu et al. (2014). The rock samples were oven dried at 40°C for 48 hours and then placed under a vacuum until a pressure of 10^{-4} Pa was achieved, ensuring the rock was completely dry. Ultrasonic wave measurements were then taken on the dry samples. Partial water saturation (S_w) was achieved by placing the samples in an atmosphere of known and controlled relative humidity (RH) for between ten days to two weeks, until they had reached equilibrium. This method is known to give homogeneous S_w distributions for the lower S_w values (compared to imbibition and drainage); similar methods have been used elsewhere (Schmitt et al., 1994, Papamichos et al., 1997, King et al., 2000). Equilibration was monitored by weighing the samples at two-day intervals until the sample mass reached a constant value. The weighing scale used was an A&D GR-200-EC with accuracy up to 10^{-4} g; Sw can then be determined from rock porosity and dry weight. The

temperature and relative humidity in the laboratory was controlled at 20°C and 55% respectively; as such, the samples were also weighed after the measurements to ensure no change in S_w had occurred as a result of exposure to a different RH atmosphere. There was hardly any loss of S_w, which was expected because of the much longer time for samples to absorb moisture and equilibrate compared to the relatively short time taken to make the ultrasonic measurements (< 2 hours in most cases). Also, measurements were not made with the sample directly exposed to the atmosphere as it was placed inside a high pressure rig (see McCann and Sothcott, 1992 for detailed equipment setup)

Controlled relative humidity (RH) was achieved using aqueous saturated salt solutions. Greenspan (1977) gave a range of salt solutions that would maintain a given RH at a particular temperature. The salts used and their approximate RH values (at 20 °C laboratory temperature) were Magnesium Nitrate (54%), Ammonium Sulphate (82%), Sodium Carbonate Decahydrate (92%), and Potassium Sulphate (98%) respectively, giving four different S_w values. A saturated aqueous salt solution was placed at the base of a vacuum desiccator, over which a wire gauze held the rocks in suspension (Figure 4.1c). A hygrometer was also placed on the wire gauze to monitor relative humidity. The desiccator was then placed under a vacuum for about two minutes and left to stand. This procedure was repeated whenever the rocks were taken out to be weighed. The maximum S_w achieved using this method was about 0.4 for the blank rock and 0.2 for the fractured rock.

The rocks were dried using the process described above, fully saturated in a vacuum with distilled, deionised and de-aired water and then pressurised to 7 MPa for at least 24 hours see (see McCann and Sothcott, 1992). Ultrasonic wave measurements were taken on the fully saturated samples. To achieve intermediate S_w values, we used a modified air/water drainage technique. In order to minimise effects of heterogeneous saturation distribution caused by drainage (Cadoret et al., 1995, Knight et al., 1998), the samples were wrapped in plastic ("cling") film after each drainage process. The wrapped samples were then placed in a desiccator containing the 98% RH solution, sealed (not vacuum sealed) and left for a minimum of 48 hours. The plastic film (and also the high RH atmosphere) prevents further air/water drainage, thus allowing capillary re-distribution over the length of time left to equilibrate (≥ 48 hours). Although steps were taken to avoid/minimize heterogeneous saturation, it should be pointed out that the objective was to observe differences between the fractured

rock and the blank rock response as a function of saturation using identical saturation and measurement methods.

4.2.3 Ultrasound experiments

We measured ultrasonic wave velocity to an accuracy of ± 0.3% using the same pulse-echo (reflection) method as Tillotson et al. (2011) (see McCann and Sothcott, 1992 for detailed equipment description). Shear-wave splitting was measured by rotating the piezoelectric shear-wave transducer (while the sample was under elevated pressure) and observing the maximum and minimum signal amplitudes corresponding to S1 and S2 waves, respectively (see Best et al., 2007).

The numerical modelling experiment of wave propagation in anisotropic media by Dellinger and Vernik (1994) showed that if the wavefront is propagating parallel or perpendicular to the layering (or in this case fractures), a true phase velocity is measured in laboratory ultrasonic experiments. However, for wave propagation at 45° to the fracture normal, the wavefront can suffer a lateral translation dependent on the length of the sample and the strength of the anisotropy. If the lateral translation suffered by the wave is greater than the radius of the receiving transducer, then a group velocity is measured, not a phase velocity. Using equations (1) and (2) from Dellinger and Vernik (1994) to calculate the lateral translations, we get conservative estimates of 2 mm for the S1-waves and -0.16 mm for the S2-waves. We used estimates because measurements at other directions to the fracture normal are not available. We can conclude we measure phase velocity in our experimental setup as our transducer radius of 12.7 mm is much larger than the lateral translations suffered by the wavefronts. A similar conclusion was reached by Tillotson et al. (2011) using the same experimental setup as that used in this study.

Ultrasonic wave measurements were then taken at different partial saturation states of air/water, quantified by water saturation S_w.

4.3 Results

We present all results at an effective pressure of 40 MPa and a single frequency of 650 kHz obtained from Fourier analysis of broadband signals. Shear-wave splitting (SWS) is expressed as SWS (%) = 100 × (S1 − S2)/S1, where S1 and

S2 are the parallel and perpendicular shear-wave velocities relative to the fracture direction, respectively. Figure 4.2 shows sample waveforms from the pulse-echo method; the waveforms are for dry and full water saturated cases for the fractured rock.

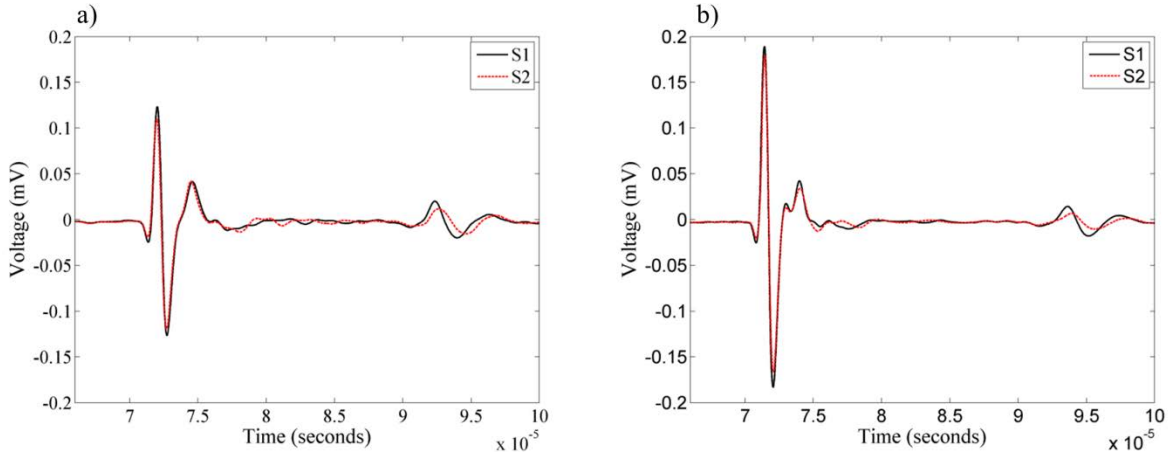

Figure 4.2: a) S1 and S2 waveforms for the dry fractured sample with S-wave propagation direction at 45˚ to the fracture normal. b) S1 and S2 waveforms for the water saturated fractured sample with S-wave propagation direction at 45˚ to the fracture normal. In both images, the first pulse is the reflection from the top of the rock while the second pulse is the reflection from the base of the rock.

In the blank sample, V_{s1} and V_{s2} have similar values for all S_w (Figure 4.3a), showing the shear-wave splitting induced by layering is negligibly small (~ 0.4 ± 0.6%) as shown in Figure 4.4a. The general trend of both shear velocities is a decrease with increasing water saturation, with the decline being more pronounced at intermediate S_w (between 0.2 – 0.7). For both shear waves, velocity is highest at $S_w = 0$ (dry) and lowest at $S_w = 1.0$ (full water saturation).

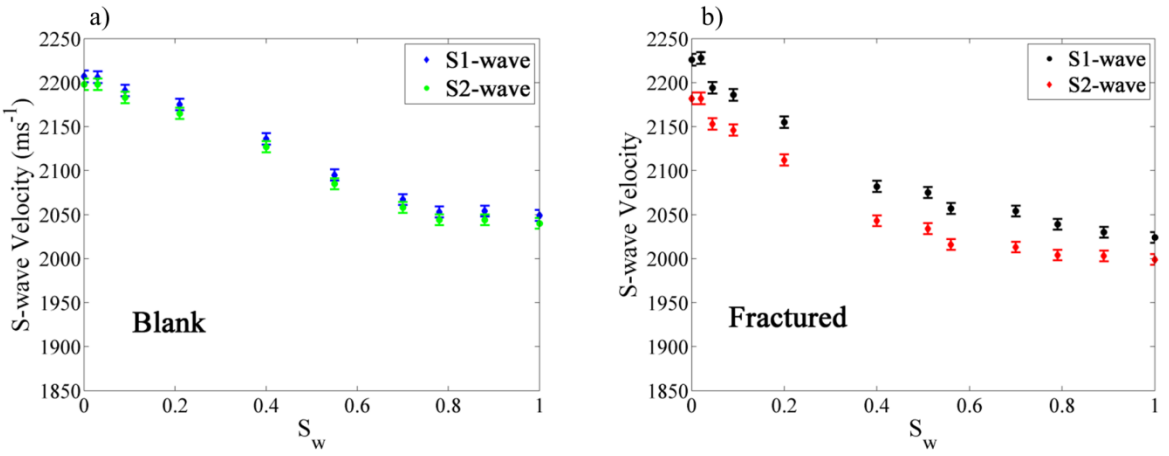

Figure 4.3: a) shows measured shear wave velocities versus S_w for the blank sample b) shows measured shear wave velocities versus S_w for the fractured sample.

In the fractured sample, there is significant shear wave splitting as expected (Figure 4.3b), the general trend of both shear-wave velocities is a decrease with increasing water saturation similar to the blank sample. Shear-wave splitting in the fractured rock (Figure 4.4b) begins at ~ 2 ± 0.6% at S_w = 0 (dry), remaining fairly constant until $S_w \approx 0.7$ followed by a steady decrease between $S_w \approx 0.8 - 1.0$, SWS being lowest at full water saturation.

Figures 4.4c and 4.4d show plots of the shear wave velocities at the different S_w values normalised by their individual dry velocities (S_w = 0). When both shear velocities are changing at the same rate, the data points overlap, however, in the fractured sample the S2-wave velocity appears to increase compared to the S1-wave velocity (Figure 4.4d), hence does not decrease at the same rate as the S1-wave velocity between $S_w \approx 0.8 - 1.0$. The SWS error bars show the minimum and maximum possible values of SWS. These were calculated from the maximum and minimum of velocity range based on absolute velocity errors of ±0.3%.

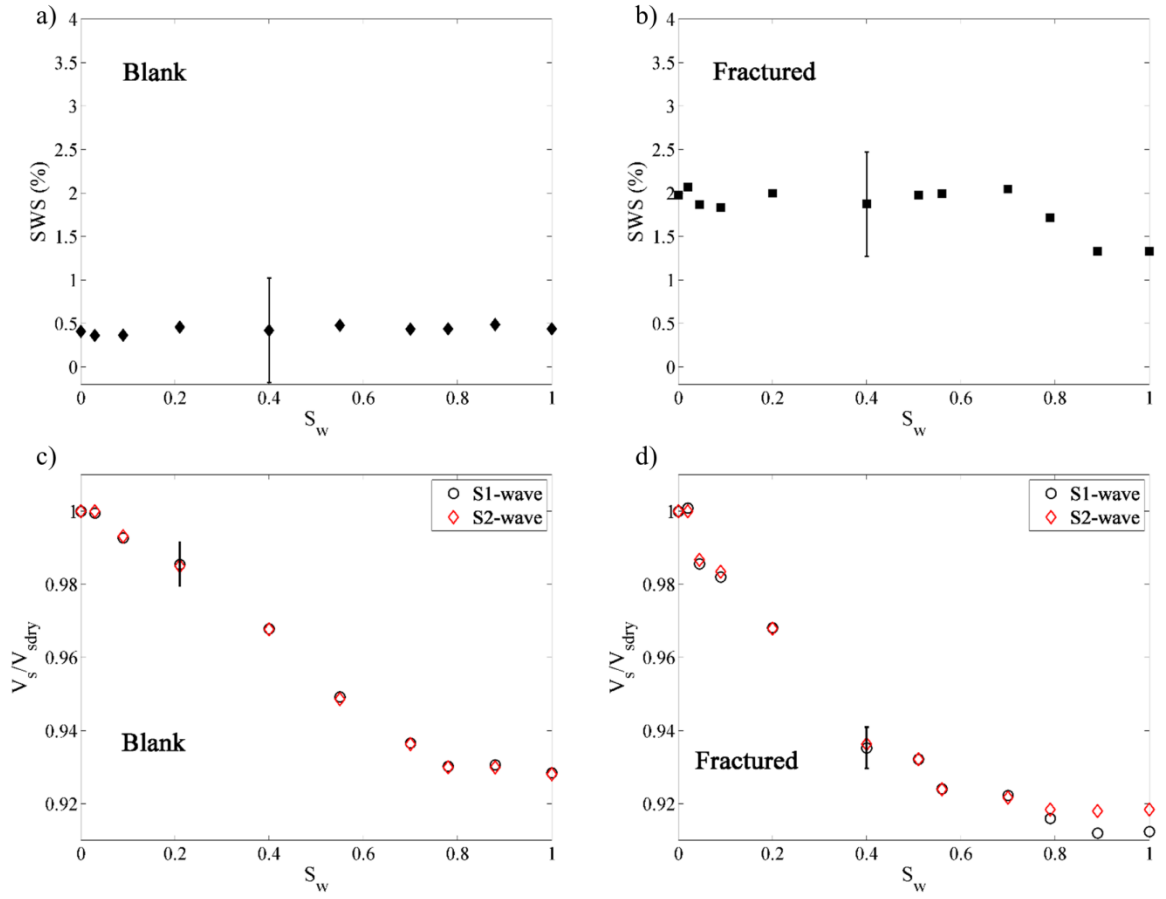

Figure 4.4: a) shows measured SWS versus S_w for the blank sample. b) shows measured SWS versus S_w for the fractured sample. c) shows ratios of the shear wave velocities to the dry shear wave velocity versus S_w for the blank sample. d) shows ratios of the shear wave velocities to the dry shear wave velocity versus S_w for the fractured sample. Error estimates are represented by the black vertical error bars.

4.4 Insight from modelling study and discussion

There is a lack of frequency dependent theoretical models for elastic wave velocities in partially saturated fractured rocks. Here, we combine two models to give some insight into the viscous mechanisms at play in our experiments. We combine the fractured rock model of Chapman (2003) (later modified by Chapman et al. (2003) to enable better practical applicability) and the partial saturation model of White (1975). The stiffness tensor, C_{ijkl}, given by Chapman (2003) relating the contributions from the isotropic elastic tensor (C^0, with Lamé parameters, λ and μ), C^1 (pores), C^2 (microcracks) and C^3 (fractures) multiplied by the porosity (Φ_p), microcrack density (ε_c) and fracture density (ε_f) is of the form:

$$C_{ijkl} = C^{o}_{ijkl} - \Phi_p C^{1}_{ijkl} - \varepsilon_c C^{2}_{ijlk} - \varepsilon_f C^{3}_{ijkl}\,. \tag{4.1}$$

This model is not designed for partial saturation, so in the expressions for the elastic tensor, we replace all terms apart from the fracture correction, with the Lamé parameters λ^o and μ^o obtained from the model of White (1975) for each water saturation value. The Lamé parameters λ^o and μ^o from White's model already contain pore corrections, and as shown by Chapman et al. (2003) ε_c can be set to zero in high porosity rocks which would make C^2 zero. We now have an equation of the form:

$$C_{ijkl} = C^{iso}_{ijkl}(\lambda^o, \mu^o) - \varepsilon_f C^{3}_{ijkl}\,, \tag{4.2}$$

where the term C^{iso}_{ijkl} is obtained from the Lamé parameters λ^o and μ^o calculated using the model of White (1975), after which the fracture correction C^3 from the model of Chapman et al. (2003) is applied. It should be pointed out here that the Lamé parameter, μ^o is the rock shear modulus which is assumed to be unaffected by saturation in White's model. Here the dispersion as a result of partial saturation is obtained from the model of White (1975) while anisotropy and dispersion at full water saturation are obtained from the model of Chapman (2003). The dispersion obtained from the model of Chapman (2003) is at full water saturation because the model was not developed for partial saturation. As we did not measure the full elastic tensor of the fractured rock, we only look to propose an explanation for our observations using a simple modelling exercise. It should be pointed out that since the fractured rock model of Chapman (2003) only predicts dispersion at full saturation, we needed to include dispersion as a result of partial saturation. We do this by using White's model because it is a simple frequency-dependent saturation model. However, we do not restrict the cause of the dispersion in the partially saturated case to patchy saturation. White's model could be replaced with any other model that incorporates a frequency-dependent loss mechanism (e.g. viscous squirt flow).

Figure 4.5a shows White's model predictions of bulk modulus versus S_w at different frequencies. Figure 4.5b shows the corresponding predictions at 45° to the fracture normal after applying the fracture correction but without dispersion from the fractured rock model. This was achieved by setting the frequency in the model of Chapman (2003) to zero. The frequency dependence as a result of partial liquid/gas saturation can be seen. However, White's model is consistent with Gassmann's predictions at full water saturation because there are no saturation patches at full saturation and as such no dispersion is observed. As a

result, the SWS at the different frequencies are the same at full water saturation (Figure 4.5b).

These predictions were calculated using the blank rock properties as input into White's model and an arbitrary fractured rock fracture density, ε_f = 0.023 as input into the model of Chapman (2003). The gas patch size in White's model was kept constant (0.5 mm) and the frequency was varied, however, similar plots can be reproduced by varying the gas patch size and keeping the frequency constant. Setting the frequency in the model of Chapman (2003) to the same value as that used in White's model, the SWS becomes frequency dependent at full water saturation (Figure 4.5c). Figure 4.5d shows an enlarged portion of Figure 4.5c at higher S_w values to enable better visualisation of the results at different frequencies. It can be seen that the SWS versus S_w trend we observe can be reproduced qualitatively by applying a fracture correction to a partial saturation model. It then follows that if the S2 wave is sensitive to the bulk modulus of the saturating fluid, and the bulk modulus is frequency dependent, the SWS would also be frequency dependent.

We realise this is a rather simplistic approach of combining both models but our purpose here is simply to suggest an explanation for prediction of partial liquid/gas saturation effects. This is already a complex problem and the presence of fractures complicates it further. The actual mechanisms in an experiment like this, and their interactions would be very complex, however, using this simple approach we can at least gain some valuable insight into possible mechanisms causing the observed trend.

The presence of partial gas saturation is known to cause dispersion believed to be as a result of wave induced fluid flow (e.g., mesoscopic and microscopic "squirt" flow) (see Müller et al., 2010). White's model considers only one dispersion mechanism (mesoscopic flow) and this could lead to an under-prediction of the amount of dispersion as a result of partial saturation (e.g., Carcione et al., 2003). An additional mechanism not considered by White's model, but believed to be responsible for the additional dispersion (at partial gas and full water saturation) observed at high frequencies, is squirt or local fluid flow (see Mavko and Nur, 1979, Winkler, 1985, Dvorkin et al., 1994, Carcione et al., 2003).

The presence of fractures is also known to cause dispersion in saturated rocks through the squirt flow mechanism (see Chapman, 2003, Gurevich et al., 2009). This squirt flow mechanism as a result of the presence of fractures is

incorporated in the model of Chapman (2003). Although our modelling exercise only incorporates the squirt mechanism at full water saturation, using the simple modelling approach we adopted, it is straightforward to see that in the presence of squirt flow at partial liquid/gas saturation the fluid effect on the S2 wave would be even greater (increasing V_{s2} further), hence reducing the SWS. Dedicated partial saturation models could be introduced to make the modelling more rigorous in future (e.g., Kong et al., 2013).

Although our observations are in the ultrasonic frequency range, it is reasonable to expect that these laboratory observations will be applicable to, or at least give guidance on, anisotropic saturation effects at the lower frequencies used in seismic field studies. Previous ultrasonic experiments on synthetic fractured rocks already demonstrated the validity of frequency-dependent seismic anisotropy theory in response to different (fully saturated) fluid viscosities (Tillotson et al., 2011, Tillotson, 2012). This implies that the geometric relationship between the meso-scale, penny-shaped fractures and the surrounding macro-porosity gives rise to viscous fluid flow losses that are representative of much lower frequencies through model scaling considerations (fracture size v. grain size v. wavelength). Hence, we would expect to observe representative wave-induced fluid flow losses associated with partial saturation effects, although there is no adequate model to describe these effects at present and thus make the link to seismic frequency behaviour. Although strictly speaking this experiment does not fall into the equivalent medium regime as the size of the fractures is comparable to the ultrasonic wavelength, we still observe important saturation dependence of SWS that we found could be explained using equivalent medium theory.

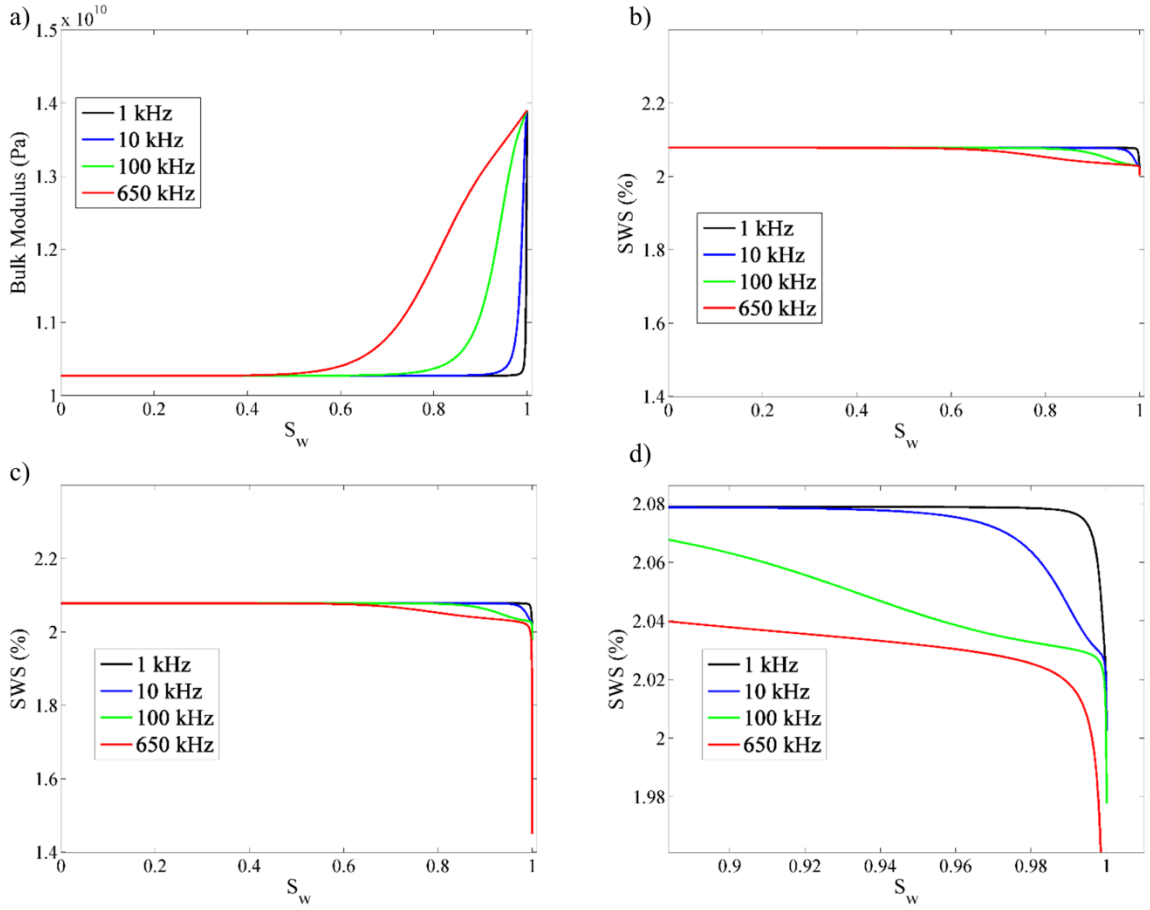

Figure 4.5: a) shows White's model predictions of bulk modulus versus S_w at different frequencies (using a constant patch size of 0.5 mm). b) shows SWS versus S_w obtained after applying fracture corrections to the bulk moduli obtained from Figure 4.5a. c) shows SWS versus S_w with squirt flow added to the results obtained in Figure 4.5b. d) shows an enlarged image of Figure 4.5c at higher S_w values to enable better visualisation of the model prediction at different frequencies. In Figures 4.5c and 4.5d, SWS at $S_w = 1$ for the different frequencies are 2.0, 2.0, 1.97 and 1.45 for 1, 10, 100 and 650 kHz respectively.

Our results show that SWS can be indicative of the presence of gas saturation in fractured reservoirs and could be useful in both exploration and production. The dispersion could also be exploited for gas saturation estimate. SWS information can be obtained from various types of seismic surveys such as passive monitoring of microseismicity, conventional seismic surveys, well logs, and vertical seismic profiles. These methods span different frequency ranges, which makes dispersion important. Knowledge of saturation effects on SWS could be important for the characterization of fractured reservoirs containing gas during exploration, production and monitoring. For example, it may give the ability to discriminate between gas and water saturated zones, as well as between less or more densely fractured zones. It may also be useful for the monitoring of

reservoirs during gas injection such as for steam flooding, gas-driven reservoirs, injection of CO_2 for geological CO_2 storage and monitoring needed for climate change mitigation.

4.5 Conclusions

Novel synthetic sandstones containing aligned fractures were used to investigate the effect of liquid/gas saturation on SWS. The synthetic rock samples provide realistic analogues of naturally occurring sandstones. Within experimental errors, the results show evidence for saturation dependent SWS in the rock with fractures aligned at 45° to the fracture normal. This is because in rocks with fractures aligned at oblique angles, the quasi-shear wave is sensitive to the bulk modulus of the saturating fluid, and hence to the effective bulk modulus of the rock-fluid mixture. This effective modulus is frequency dependent as a result of wave-induced fluid flow mechanisms which could be due to the presence of partial liquid/gas saturation, the presence of fractures or both. This acts to stiffen the rock leading to a higher effective bulk modulus, thus increasing the quasi-shear wave velocity and reducing the SWS, as the pure shear wave is not sensitive to the bulk modulus of the saturating fluid. By applying a fracture correction to a partial saturation model, we were able to explain our observations qualitatively. The results show that shear wave splitting in rocks with fractures aligned at oblique angles to wave propagation could potentially be used to distinguish between partial gas saturation and full liquid saturation.

Chapter 5: Water saturation effects on P-wave anisotropy in synthetic sandstone with aligned fractures

This chapter forms a paper published in Geophysical journal international: Amalokwu, K., M. Chapman, A. I. Best, T. A. Minshull, and X.-Y. Li. 2015, Water saturation effects on P-wave anisotropy in synthetic sandstone with aligned fractures. Geophysical Journal International, 202, no. 2,1088-1095. doi: 10.1093/gji/ggv192.

Abstract: The seismic properties of rocks are known to be sensitive to partial liquid or gas saturation, and to aligned fractures. P-wave anisotropy is widely used for fracture characterisation and is known to be sensitive to the saturating fluid. However, studies combining the effect of multiphase saturation and aligned fractures are limited even though such conditions are common in the subsurface. An understanding of the effects of partial liquid or gas saturation on P-wave anisotropy could help improve seismic characterisation of fractured, gas bearing reservoirs. Using octagonal-shaped synthetic sandstone samples, one containing aligned penny-shaped fractures and the other without fractures, we examined the influence of water saturation on P-wave anisotropy in fractured rocks. In the fractured rock, the saturation related stiffening effect at higher water saturation values is larger in the direction across the fractures than along the fractures. Consequently, the anisotropy parameter "ε" decreases as a result of this fluid stiffening effect. These effects are frequency dependent as a result of wave-induced fluid flow mechanisms. Our observations can be explained by combining a frequency-dependent fractured rock model and a frequency-dependent partial saturation model.

5.1 Introduction

Experimental and theoretical studies have long shown that seismic waves are strongly affected by the presence of partial gas saturation and by the presence of aligned fractures, the latter causing seismic anisotropy. Shear waves are considered to be more reliable indicators of fracture properties (e.g., fracture orientation and density) than P-waves. However, the use of P-waves for fracture characterisation has received considerable attention since P-waves form the basis of most commercial seismic surveys (Sayers and Rickett, 1997). Consequently P-wave anisotropy has been extensively studied and is widely used for fracture characterisation (e.g., Winterstein, 1986, Lynn et al., 1996, Rüger, 1997, Li, 1999). P-waves have the potential not only to characterise fractures but also of discriminating between saturating fluids (Rüger and Tsvankin, 1997, Bakulin et al., 2000). Liquid (brine, oil) and gas usually share the available pore space in reservoirs containing gas (Gregory, 1976), making it necessary to understand the combined effects of multiphase saturation and fractures on seismic wave propagation for improved reservoir characterisation. However, multiphase saturation effects on seismic anisotropy of fractured rock are still poorly understood even though such conditions are common. Such know-how would be useful for characterisation of fractured hydrocarbon reservoirs containing gas and geothermal steam reservoirs. Important applications could also be found in seismic time-lapse monitoring of gas injection into hydrocarbon reservoirs for enhanced oil recovery; and for the geologic storage of carbon dioxide (CO_2) where fractures can serve as leakage pathways (Carcione et al., 2013).

P-wave velocity anisotropy in fractured rocks is known to depend on saturating fluid and is frequency-dependent due to wave-induced fluid flow (Chapman et al., 2003, Gurevich et al., 2009, Tillotson et al., 2014). The presence of partial gas saturation is also known to affect P-wave velocities in a frequency-dependent way (White, 1975, Murphy, 1984, Cadoret et al., 1995, Carcione et al., 2003). Fracture and fluid properties are inferred from seismic data using theoretical models. As such, there is a desire to validate theoretical models using controlled experiments. Experimental studies of partial liquid/gas saturation effects on P-wave velocities have been presented for isotropic rocks (Murphy, 1984, Bourbie and Zinszner, 1985, Cadoret et al., 1995, King et al., 2000), however, the effect of partial liquid/gas saturation on P-wave velocity (and hence P-wave anisotropy) in fractured rocks remains unknown. Also, a handful of

controlled fractured rock experiments have been carried out (e.g., Rathore et al., 1995, Tillotson et al., 2011, Tillotson et al., 2014) and results have been compared to theoretical models such as the models of Hudson (1981), Thomsen (1995) and Chapman et al. (2003). However, theoretical and experimental studies of fluid effects on P-wave anisotropy have focused primarily on single fluid phases (100% gas or liquid saturation). To date, no experimental study has been carried out to observe the effects of water saturation on P-wave anisotropy in fractured rocks.

This work examines the influence of two-phase (liquid-gas) saturations (which would be referred to here as partial saturation) on P-wave anisotropy in fractured rocks. Using an octagonal-shaped synthetic sandstone sample containing aligned penny-shaped fractures, we present laboratory measurements of water saturation effects on P-wave anisotropy. These novel results show an interesting sensitivity of P-wave anisotropy to changing water saturation. Qualitative agreement with theory was found by combining the corrected White (1975) model for partial saturation (sometimes referred to as the White and Dutta-Ode model - see Mavko et al. (2009)) with the fractured rock model of Chapman (2003) using similar ideas presented by Amalokwu et al. (2015b). As pointed out by Tillotson et al. (2014), the ultrasonic wavelengths used were close to the size (diameter) of the penny-shaped voids (fractures), in common with previously reported experimental results of this nature. Nevertheless, Tillotson et al. (2014) found several useful correlations between the data and the model of Chapman (2003), which suggest that the model predictions are reasonably unaffected by scattering (Tillotson et al., 2014). Our experiments appear also to be little affected by scattering because we were able to explain saturation effects using equivalent medium modelling.

5.2 Methods

5.2.1 Synthetic rock samples

A detailed description of the synthetic rock samples used in this study can be found in the paper by Tillotson et al. (2014). Two octagonal samples (Figure 5.1) were used in this study – one fractured sample and a blank sample (rock sample without fractures). The rock samples were made from a mixture of sand,

kaolinite and aqueous sodium silicate gel and then the mixture was packed into a mould in successive layers. A predetermined number aluminium discs were distributed on top of each layer of sand mixture for the creation of penny-shaped voids. After the sandstone was formed by heating and drying, the aluminium discs were leached out using hydrochloric acid, leaving blank penny-shaped voids. Image analysis of X-ray CT scans was used to obtain the fracture density, ε_f = 0.0314 ± 0.0059, mean fracture radius of 2.91 ± 0.06 mm, and mean fracture aspect ratio of 0.0429 ± 0.0008. Porosity is 30% and 33% for the blank and fractured sample respectively, and permeability for both samples is 21 mD (see Tillotson et al., 2014). As pointed out by Tillotson et al. (2014), the advantage of these octagonal samples is that we can measure the full elastic wave tensor on single sandstone samples and thus gain an unambiguous dataset for comparison with theoretical models.

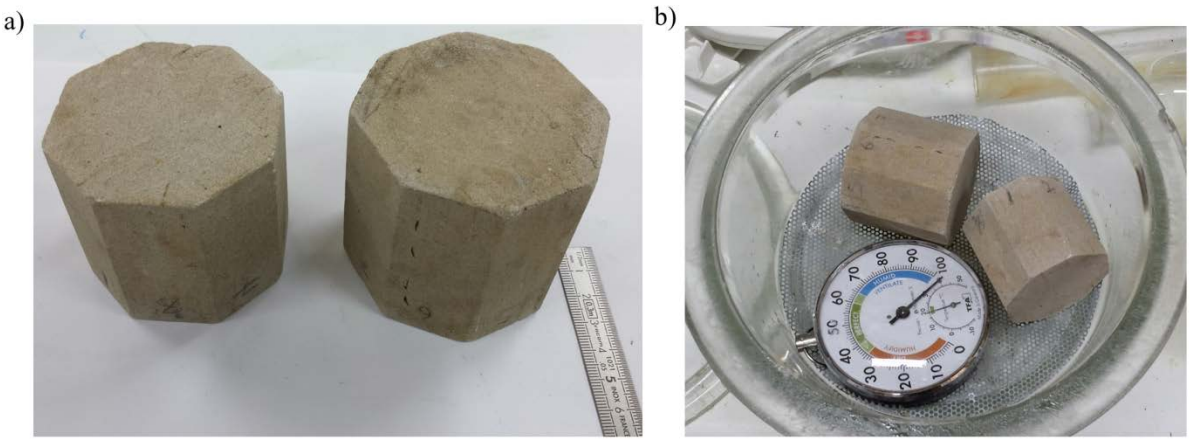

Figure 5.1: a) rock samples used in this study (blank sample on the left and fractured sample on the right) b) relative humidity method used to achieve partial saturation.

5.2.2 Ultrasonic measurements

We measured ultrasonic P-wave velocity using a laboratory bench-top pulse transmission system with one inch-diameter broadband ultrasonic transducers with a central frequency of 500 kHz placed on each of four sets of opposing sides of the octagonal samples, thus allowing measurement of velocity at different angles. A more detailed description of the technique is given by Tillotson et al. (2014). To ensure consistent coupling between experiments, a pneumatic ram applied a pressure of 60 psi to the transducer faces in contact with the samples, and couplant was carefully reapplied to the transducer faces between

experiments. P-wave velocity was measured for wave propagation at 0°, 45°, and 90° to the fracture/bedding normal.

Velocity was calculated by comparing the broadband signals from the rock samples with those of a duralumin reference sample (with known elastic properties). Velocity was calculated by comparing the Fourier phase angle spectra of the rock and reference wavelets using

$$V_1(f) = \frac{x_1}{\Delta t(f) + \frac{x_2}{V_2}}, \tag{5.1}$$

where $V_1(f)$ is the velocity of the rock sample, x_1 is the wave propagation distance in the rock sample, $\Delta t(f)$ is the difference in travel time calculated from the Fourier phase angle spectra of the rock $\varphi_{sample}(f)$ and reference $\varphi_{reference}(f)$ sample according to $\Delta t = t_{sample} - t_{reference} = \frac{(\varphi_{sample}(f) - \varphi_{reference}(f))}{2\pi f}$, x_2 is the wave propagation distance in the reference sample, and V_2 is the velocity of duralumin (taken to be 6398 m/s for P-waves for all frequencies as duralumin is non-dispersive). The velocity measurements were corrected for frequency-dependent diffraction effects as a result of beam spreading from the transducer face (Best, 1992). We used isotropic diffraction corrections only.

Ultrasonic wave measurements were then taken at different partial saturation states of air/water (see the Supporting Information for details of saturation methods used), quantified by water saturation S_w. Velocity was measured to an accuracy of ± 0.6% and results are presented at a single frequency of 500 kHz (see Tillotson et al., 2014).

The numerical modelling experiment of wave propagation in anisotropic media by Dellinger and Vernik (1994) showed that if the wavefront is propagating parallel or perpendicular to the layering (or in this case fractures), a true phase velocity is measured in laboratory ultrasonic experiments. However, for wave propagation at 45° to the fracture normal, the wavefront can suffer a lateral displacement dependent on the length of the sample and the strength of the anisotropy. If the lateral translation suffered by the wave is greater than the radius of the receiving transducer, then a group velocity is measured, not a phase velocity. Using equation (1) from Dellinger and Vernik (1994) to calculate the lateral translations, we get a value of 2.9 mm for the P-wave. We can conclude we measure phase velocity in our experimental setup as our transducer radius of 12.7 mm is much larger than the lateral translations suffered by the wavefronts.

A similar conclusion was reached by Tillotson et al. (2014) using the same experimental setup as that used in this study.

5.3 Results

The blank rock velocity results (Figure 5.2a) show minimal velocity anisotropy due to layering from the manufacturing process. P-wave velocity is at a maximum at 90° and a minimum at 0° to the bedding/layer normal. The velocity versus S_w trend is similar in the three directions. The general trend for each propagation direction is an increase in P-wave velocity with increasing S_w apart from a decrease at $S_w \approx 0.40$, the highest velocity occurring at $S_w = 1.0$. These results are in agreement with published ultrasonic data (e.g., Gregory, 1976, Murphy, 1984, Bourbie and Zinszner, 1985).

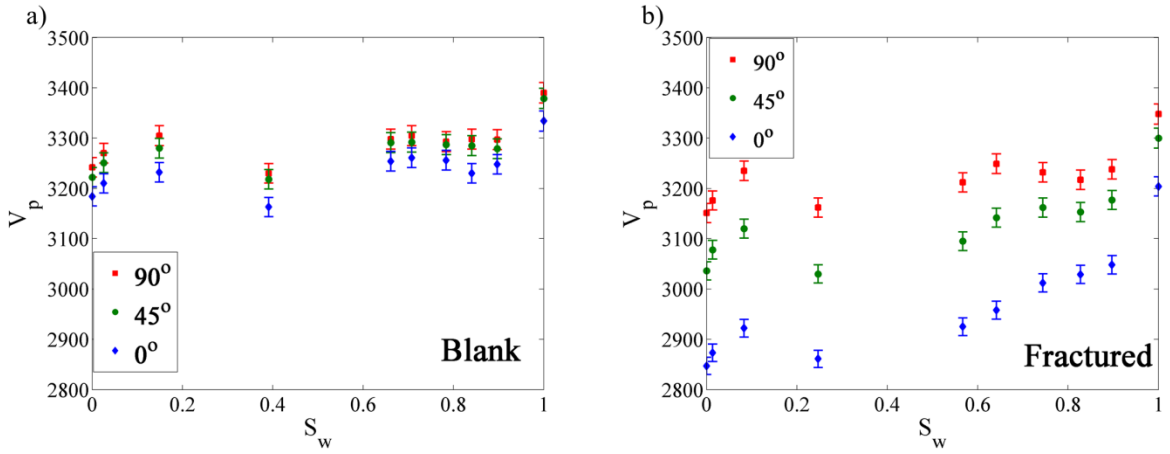

Figure 5.2: P-wave velocity versus S_w at 0° (blue diamond), 45° (green circle), and 90° (red square) for the a) blank sample b) fractured sample. Vertical error bars show error estimates.

Figure 5.2b shows P-wave velocity versus S_w relationship at 0°, 45°, and 90° to the fracture normal. Here we see significant angular variation in velocity as expected. Similar to the blank sample, the velocity versus S_w trend is similar in all three directions and is similar to that observed in the blank rock. The data trend suggests evidence of frequency dispersion (attributed to wave-induced fluid flow), which can be seen in the data from the steady increase in velocity from dry to full water saturation in contrast to Gassmann's low frequency predictions (see Murphy, 1982, Mavko and Nolen-Hoeksema, 1994). There is considerable literature on saturation related dispersion resulting from wave induced fluid flow (see Müller et al., 2010). In this paper we will focus mainly on the differences

between the blank and the fractured sample response to changing water saturation.

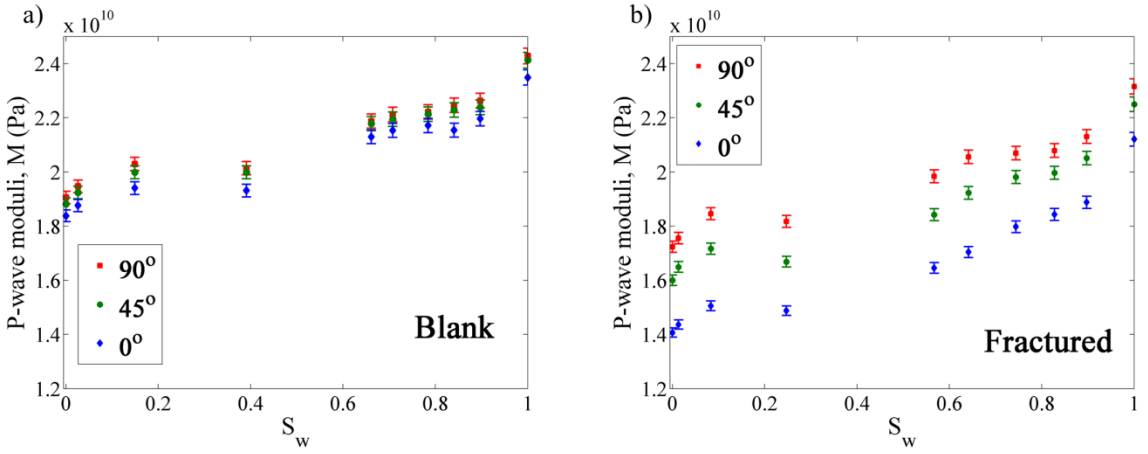

Figure 5.3: P-wave modulus versus S_w at 0°, 45°, and 90° for the a) blank sample and b) fractured sample. Vertical error bars show error estimates.

In order to remove any ambiguity caused by the effect of fluid saturation on bulk density, we calculated the P-wave moduli, $M = \rho V^2$, (Figure 5.3) in all three directions (equivalent to stiffness components C_{11} and C_{33} for the 90° and 0° directions respectively). In the blank sample (Figure 5.3a), all three directions show similar M versus S_w trends, with M increasing from $S_w = 0$ to $S_w \approx 0.15$, staying fairly constant between $S_w \approx 0.15$ to $S_w \approx 0.40$, after which there is a steady increase until $S_w = 1.0$. The fractured sample (Figure 5.3b) shows a similar trend to that observed in the blank sample, with M increasing from $S_w = 0$ to $S_w \approx 0.10$, staying fairly constant between $S_w \approx 0.10$ to $S_w \approx 0.25$, after which there is a steady increase until $S_w = 1.0$.

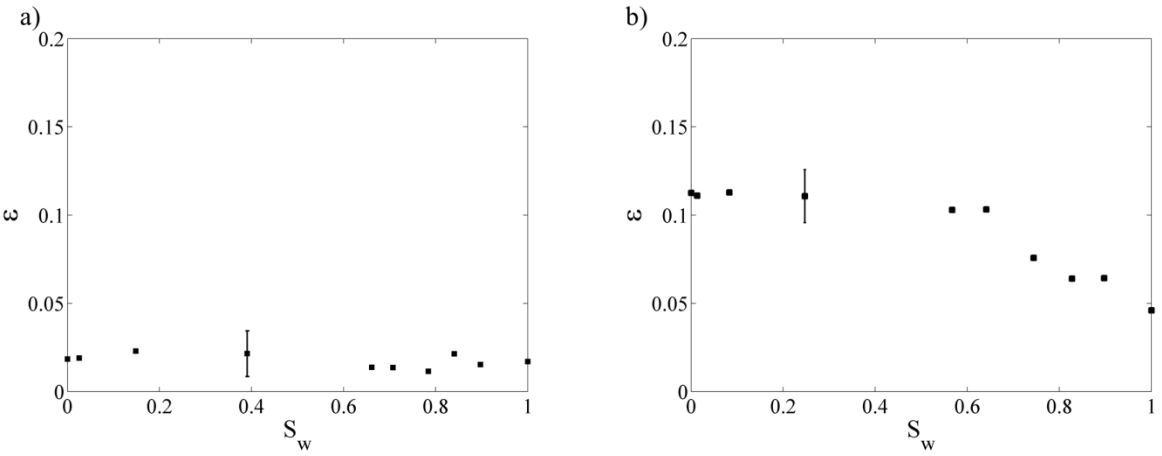

Figure 5.4: Measured P-wave anisotropy parameter (ε) versus S_w for the a) blank sample and b) for the fractured sample.

Figure 5.4 shows plots of Thomsen-style P-wave anisotropy parameter (see Thomsen, 1986), "epsilon" (ε) versus S_w. The parameter (ε) represents the difference in P-wave velocity between the vertical (90˚) and horizontal (0˚) directions and is given by $\varepsilon = \frac{C_{11} - C_{33}}{2C_{33}}$. The blank sample shows a fairly constant value of ε (Figure 5.4a) while a decrease in ε can be seen in the fractured sample at higher values of S_w (Figure 5.4b).

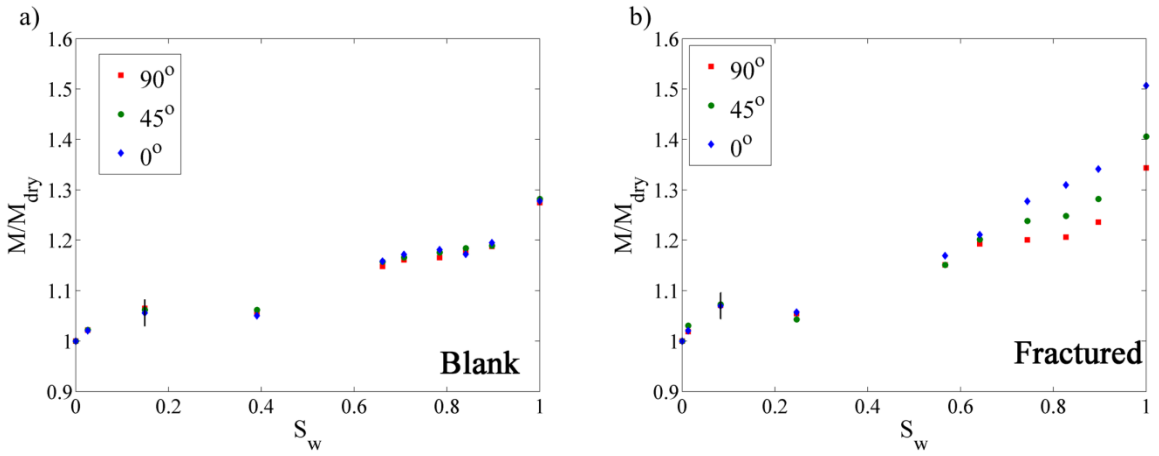

Figure 5.5: Ratios of the P-wave modulus to the dry P-wave modulus versus S_w at 0°, 45°, and 90° for the a) blank rock and b) for the fractured rock. Vertical error bars show error estimates.

Figure 5.5 shows plots of the P-wave moduli from Figure 5.3 at the different S_w values normalised by their individual dry values ($S_w = 0$). The data points almost overlap in the blank sample (Figure 5.5a), however, in the fractured sample the fluid effect appears to be maximum at 0°, intermediate at 45° and minimum at 90° to the fracture normal at higher S_w values (~ 0.75 - 1.0) (Figure 5.5b).

5.4 Modelling insights and Discussions

Analysis here will focus on the effect of water saturation on the P-wave moduli (anisotropic) and on the P-wave anisotropy parameter, ε. There is a lack of suitable frequency-dependent theoretical models for elastic wave velocities in partially saturated fractured rocks. Using the same method as Amalokwu et al. (2015b) we combine two models to give some insight into the possible mechanisms in our experiments. We combine the fractured rock model of Chapman (2003) and the partial saturation model of White (1975). The stiffness tensor, C_{ijkl}, given by Chapman (2003) relating the contributions from the

isotropic elastic tensor (C^0, with Lamé parameters, λ and μ), C^1 (pores), C^2 (microcracks) and C^3 (fractures) scaled by the porosity (Φ_p), microcrack density (ε_c) and fracture density (ε_f) is of the form:

$$C_{ijkl} = C^o_{ijkl} - \Phi_p C^1_{ijkl} - \varepsilon_c C^2_{ijlk} - \varepsilon_f C^3_{ijkl}\,. \tag{5.2}$$

This model is not designed for partial saturation, so in the elastic tensors, we replace all terms apart from the fracture correction, with the Lamé parameters λ^o and μ^o obtained from the model of White (1975) for each water saturation value. The Lamé parameters λ^o and μ^o from White's model already contain porosity effects, and as shown by Chapman et al. (2003), ε_c can be set to zero in high porosity rocks which would make the contribution from C^2 zero. We now have an equation of the form:

$$C_{ijkl} = C^{iso}_{ijkl}(\lambda^o, \mu^o) - \varepsilon_f C^3_{ijkl}\,, \tag{5.3}$$

where the term C^{iso}_{ijkl} is obtained from the Lamé parameters λ^o and μ^o calculated using the model of White (1975) (see Mavko et al., 2009, p. 327), after which the fracture correction C^3 from the model of Chapman et al. (2003) is applied. It should be pointed out here that the Lamé parameter, μ^o is the rock shear modulus which is assumed to be unaffected by saturation in White's model.

In our modelling approach, the dispersion as a result of partial saturation is obtained from the model of White (1975) while anisotropy and dispersion from the fractures are obtained from the model of Chapman (2003). We do not seek to model directly our experimental results but rather propose an explanation for our observations using a simple modelling exercise. We point out that dispersion as a result of partial saturation had to be included since the fractured rock model of Chapman (2003) was not developed for multi-phase saturations. White's model was used to model this dispersion because it is a simple frequency-dependent saturation model; however, the cause of the dispersion in the partially saturated case is not restricted to patchy saturation. The idea here is to achieve frequency-dependent bulk moduli caused by stiffening of the frame due to the presence of partial saturation. White's model could be replaced with any other model that incorporates a frequency-dependent stiffening mechanism (e.g. viscous squirt flow).

Model predictions were calculated using the same blank rock properties as those used by Amalokwu et al. (2015b) as input into White's model and a fracture density, ε_f = 0.0314 for the model of Chapman et al. (2003). The gas patch size in

White's model was kept constant (0.5 mm) and the frequency was varied, however, similar plots can be reproduced by varying the gas patch size and keeping the frequency constant. The model of Chapman (2003) was developed for single-phase saturation, therefore, in order to adapt this model for multi-phase saturation, we require an effective fluid bulk modulus as input for the fluid bulk modulus in the model of Chapman (2003). Taking the effective fluid modulus as the Reuss average (see Mavko et al., 2009) of air and water bulk moduli, no additional dispersion is obtained at partial saturation from the fractured rock model as shown by Amalokwu et al. (2015b). The Reuss average corresponds to the low frequency case where the gas and liquid are mixed uniformly, so the wave-induced pore pressures have enough time to equilibrate during a seismic period (Mavko and Mukerji, 1998). The Reuss average of the bulk moduli of air and water gives an effective fluid bulk modulus which is equivalent to the bulk modulus of air from full air (gas) saturation to very close to full water saturation (~ 2% air saturation). Consequently, the fractured model does not show any dispersion at partial saturation and this might not be the case at higher frequencies.

The Reuss average is known to under-predict the effective fluid moduli when the wave-induced pore pressures do not have enough time to equilibrate during a seismic period and in this case other mixing laws (see Mavko et al., 2009) should be used to calculate the effective fluid moduli. However, instead of using fluid mixing laws (e.g., Brie et al., 1995) or explicitly calculating the dynamic fluid modulus (e.g., Yao et al., 2013) (which could achieve similar effects we are attempting to show), we will take an effective fluid modulus equivalent to the fluid stiffening effect from White's model (compared to Gassmann's low-frequency predictions). We do this by taking the real part of the frequency-dependent bulk modulus obtained from White's model as the saturated rock bulk modulus and then by re-arranging Gassmann's equation, we can obtain the fluid bulk modulus. We then take this fluid bulk modulus as the bulk modulus for input into the fractured rock model. Our purpose here is to illustrate the potential effect of additional dispersion at partial saturation from the fractured rock model, which we require to achieve a better agreement with our experimental results. However, we can only obtain this additional dispersion by assuming an effective fluid modulus which is not the Reuss average of air and water, suggesting we need to consider the case where the fluid mixture within the cracks is not the Reuss average of air and water (hence unrelaxed) as this could play an important role in the effective stiffness of the fractures. This effective fluid modulus would

be frequency-dependent, similar to the case in isotropic rocks. Using the approach we have adopted, the fluid bulk modulus effect would be consistent in both the background isotropic rock model and the fractured rock model at each frequency (although this might not be the case in reality). We take the microcrack relaxation timescale (see Chapman, 2003, Chapman et al., 2003) to be the same (τ_m = 2.4 x 10^{-8} s) as that used for the same rock sample by Tillotson et al. (2014).

Figure 5.6a shows the frequency-dependent bulk modulus obtained from the model of White (1975) and Figure 5.6b shows the corresponding effective fluid moduli which is used as an input into the fractured rock model. A fracture correction using the model of Chapman (2003) was then applied and "ε" calculated for all frequencies corresponding to those used in White's model (Figure 5.6c). Initially, we consider dispersion solely from White's model. As a result of White's model being consistent with Gassmann's predictions at full water saturation because no patches exist at full water saturation, no dispersion occurs at full water saturation ("ε" is the same at all frequencies). To include dispersion from the fractured model, we set the frequency in the model of Chapman (2003) equal to that used in White's model. It can be seen that "ε" becomes frequency dependent both at partial saturation (higher S_w values) and full water saturation, with "ε" decreasing as frequency increases. In order to compare the observed experimental trend to our modelling results (Figure 5.6d), we used a fracture density of 0.034 (within the uncertainty range for the fracture density, ε_f = 0.0314 ± 0.0059) in order to fit the dry value for "ε", leaving other parameters the same as given above. We see better agreement with the trend when additional dispersion from the fractured rock model is considered.

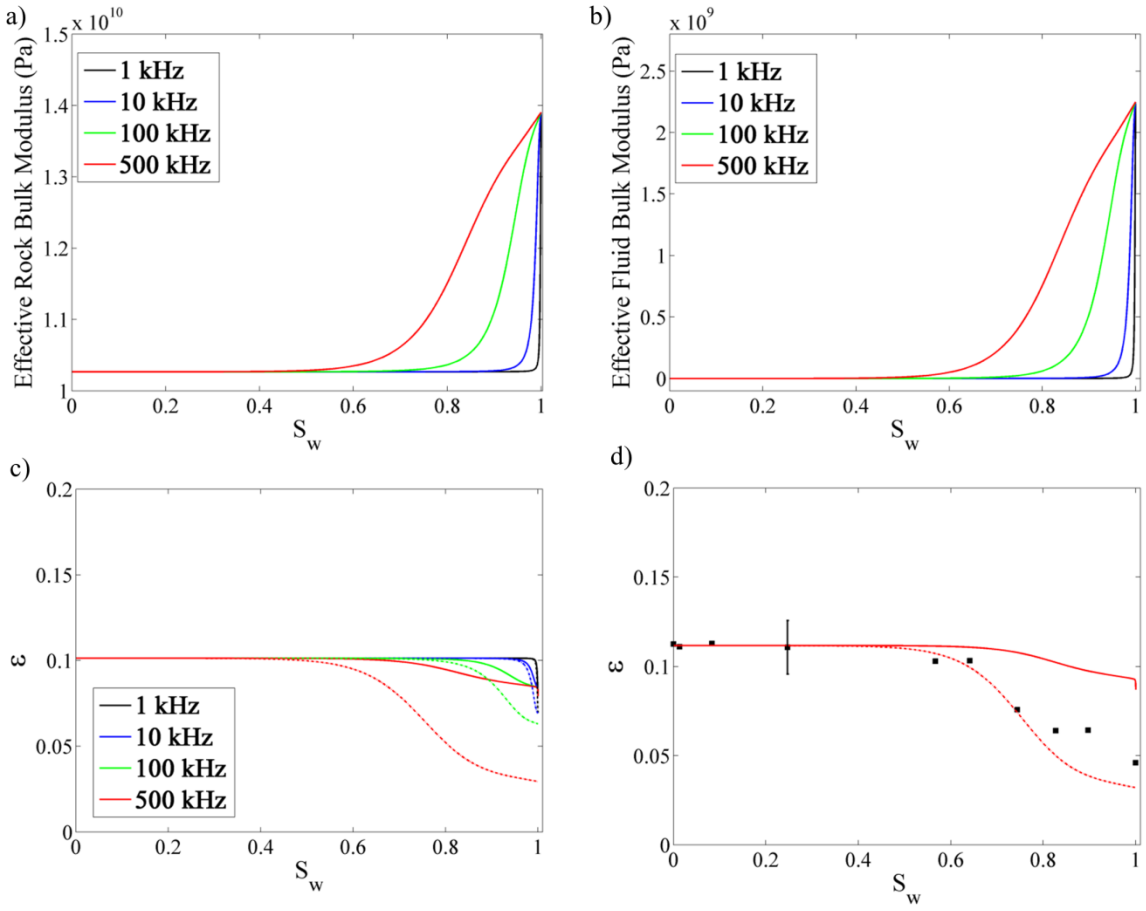

Figure 5.6: a) White's model predictions of bulk modulus versus S_w at different frequencies (using a constant patch size of 0.5 mm). b) Corresponding effective fluid bulk modulus calculated using Gassmann's equation. c) P-wave anisotropy parameter "ε" versus S_w without dispersion (solid lines) and with dispersion (dotted lines) from the fractured rock model, obtained after applying fracture corrections to the bulk moduli from Figure 5.6a. d) Comparing the experimentally observed trend for "ε" (black squares) to model predictions at 500 kHz without dispersion (solid line) and with dispersion (dotted line) from the fractured rock model.

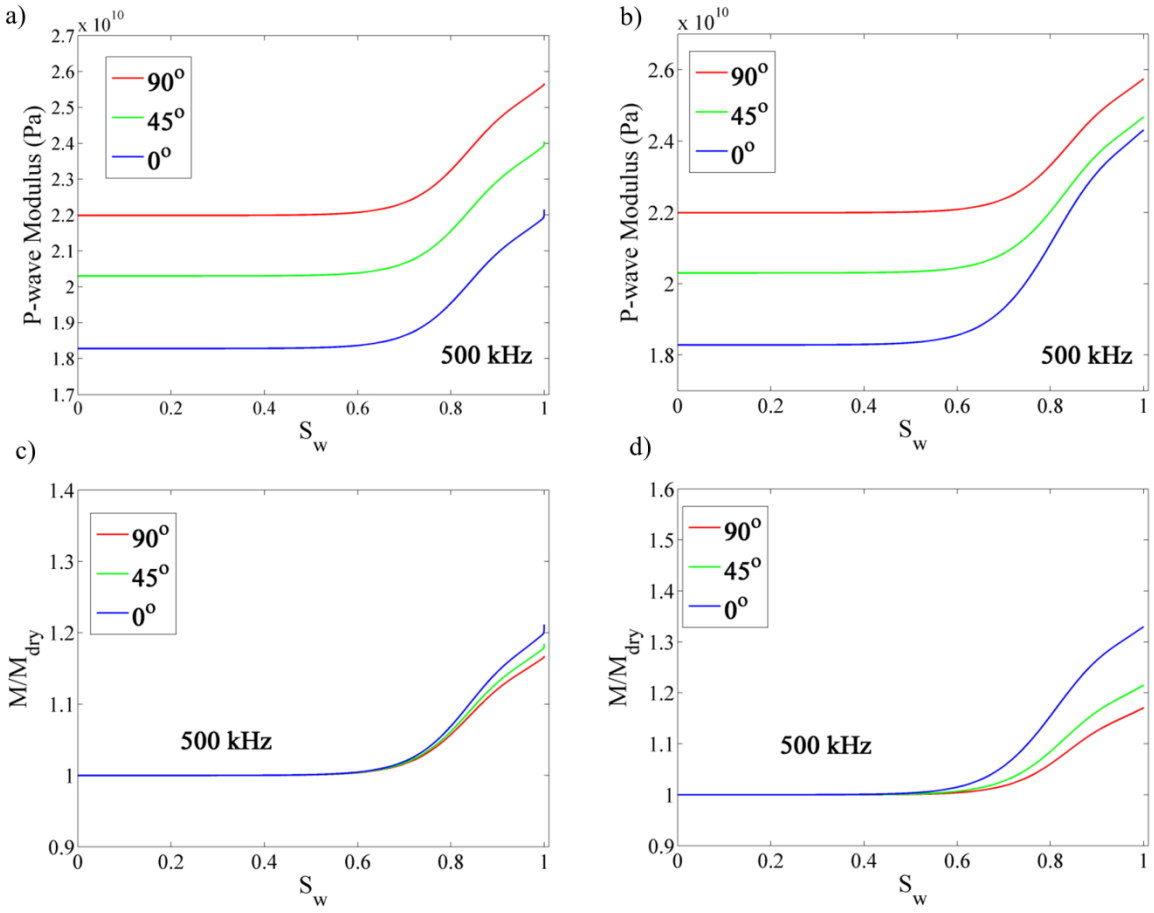

Figure 5.7: a) Model predictions of P-wave moduli versus S_w at 500 kHz without dispersion from the fractured rock model. b) Model predictions of P-wave moduli versus S_w at 500 kHz with dispersion included from the fractured rock model. c) Model predictions of ratios of P-wave moduli to the dry P-wave modulus without dispersion from the fractured rock model. d) Model predictions of ratios of P-wave moduli to the dry P-wave modulus with dispersion included from the fractured rock model.

Using the same results from the modelling above, we calculated the anisotropic P-wave moduli. We plot the P-wave anisotropic moduli at 500 kHz with dispersion from White's model alone (Figure 5.7a) and then with additional dispersion from the fractured rock model of Chapman (2003) (Figure 5.7b). We see that when dispersion from the fractured model is considered, the fluid effect at higher S_w values is greater in both the 0° and 45° directions, with a more pronounced effect at 0°. This is more obvious when the P-wave moduli are normalised with their dry values (S_w = 0) (Figures 5.7c & 5.7d). We see that at higher S_w values the maximum fluid effect is at 0° to the fracture normal while the minimum fluid effect is at 90° to the fracture normal with a greater fluid effect seen when dispersion is considered from the fracture rock model as well (Figure 5.7d) compared to dispersion considered from White's model alone (Figure 5.7c).

Therefore, the fluid effect increases as P-wave propagation goes from parallel (90^o) to perpendicular (0^o) to the fracture normal. The critical S_w where the fluid effect begins depends on the critical S_w when the P-wave modulus goes from relaxed to unrelaxed behaviour, which comes in from the frequency dependent model of White (1975) in this modelling approach.

The presence of partial liquid/gas saturation and the presence of fractures are both known to cause dispersion in rocks, believed to be as a result of wave-induced fluid flow (see Müller et al., 2010). It can be seen that as the effective isotropic background rock property (in this case as a result of changing water saturation) changes, this has an effect on the anisotropy of the fractured rock, a result which may not be obvious. A similar observation was made in the numerical study (although dispersion was not considered) by Sil et al. (2011) where they showed that changes in the isotropic background properties as a result of changes in water saturation and porosity had an effect on P-wave anisotropy of the fractured rock considered. It then follows that if the effective isotropic background property is frequency dependent, then the effect on P-wave anisotropy would be frequency dependent. Dispersion as a result of wave-induced fluid flow is also known to be caused by the presence of fractures (Chapman et al., 2003, Gurevich et al., 2009, Kong et al., 2013). It can be seen that a larger fluid effect on anisotropy is observed when dispersion is considered as a result of wave-induced fluid flow from the fractured rock model (Figure 5.6d).

For both "ε" and the P-wave modulus, we see good agreement with our experimental data when we consider dispersion from both the changing background rock and the fractured rock. This observation suggests that not only could the effect of saturation on the bulk property of the rock have an effect on P-wave anisotropy, but the effect of the fluid on the compliance of the fractures could also be important and both effects can be frequency dependent. We realise that we have taken a simplistic (but yet intuitive) approach to modelling our data. However, partial liquid/gas saturation effects on seismic properties of rocks already constitute a complex problem and the presence of fractures complicates it further as the actual mechanisms in an experiment like this and their interactions would be very complex. Therefore using this simple modelling approach we can gain some valuable insight into potential mechanisms causing the observed trend. Further advances in theoretical and experimental studies are needed to give a better understanding of the mechanisms involved and to isolate the dominant mechanisms at different conditions.

Our results show that water saturation affects the P-wave anisotropy of fractured rocks and this effect could be frequency dependent due to wave induced fluid flow mechanisms. This effect could be important for seismic characterisation of fractured reservoirs containing gas. The dispersion could be exploited for gas saturation estimates as dispersion has been shown to be sensitive to the amount of gas saturation (e.g., Wu et al., 2014). Understanding the effect of water saturation on P-wave anisotropy could help improve seismic characterisation of fractured reservoirs. The different frequencies at which elastic wave data are acquired makes understanding the frequency-dependence of these effects important.

5.5 Conclusion

We have presented experimental observations of two-phase saturation (water-air) effects on P-wave anisotropy in synthetic fractured sandstone. The results show a significant effect of water saturation on P-wave anisotropy of the fractured rock. We observed the fluid effect is greatest perpendicular to the fractures and lowest parallel to the fractures. As a result, the P-wave anisotropy parameter "ε" decreases as the effective modulus of the rock increases. The effective modulus of the rock is frequency-dependent due to wave-induced fluid flow mechanisms which act to stiffen the rock and the fractures. A larger effect is seen when dispersion due to wave-induced fluid flow is included from the fractured rock model. The frequency-dependence could be as a result of the presence of partial liquid/gas saturation or due to the presence of fractures or a combination of both. Our simple modelling approach shows good qualitative agreement with the experimental data. This frequency-dependent influence of water saturation on P-wave anisotropy could help improve fractured reservoir characterisation.

Chapter 6: An investigation into porosity effects on P-wave anisotropy in water saturated fractured rocks using synthetic sandstones.

Abstract: P-wave anisotropy is a commonly used method for characterization of fractured reservoir rocks. Fracture properties can be obtained, in principle, from seismic anisotropy using theoretical models that relate fracturing in rock to seismic anisotropy measurements. Reservoir rocks are generally located in the Earth's crust and as such have substantial background rock porosity (equant porosity) which usually contains saturating fluids. This fluid filled porosity has been shown to affect the amount of measured seismic anisotropy due to fluid exchange between the fractures and the pore space. This effect has been studied theoretically, however, the dependence on porosity and the expected coupled frequency-dependence of this mechanism has not been studied experimentally. Controlled laboratory experimental observations of the effect of porosity on fracture-induced seismic anisotropy do not exist at present due to experimental limitations associated with fractured rock experiments. A major limitation is the availability of samples with fractures of controlled and known geometry. Synthetic sandstones containing penny-shaped voids present an opportunity to study effects of porosity on fracture-induced P-wave anisotropy in a saturated porous rock. Hence, this work sought to address this by making fractured synthetic sandstones with different porosities but similar fracture properties, and by measuring P-wave anisotropy under both dry and water saturated states. The final results on the porosity effects on P-wave anisotropy were ambiguous due to limitations associated with the manufacturing process. However, the results do show that it is possible to vary the porosities of synthetic sandstones within a good range 17% - 27%. Also, an interesting fluid dependence was also observed in the non-fractured but anisotropic (due to layering) rocks; however, this would have to be investigated further.

6.1 Introduction

Fractures (natural and artificial) in reservoirs can significantly affect the flow characteristics of reservoirs and as such, the density and orientation of sets of fractures is of great interest for hydrocarbon exploration and production. Fractures that are open at depth usually show preferred orientations as they tend to be oriented normal to the direction of minimum stress, which may result in significant permeability anisotropy (Queen and Rizer, 1990, Sayers, 2002, 2009). Aligned fractures cause seismic anisotropy and as a result, there is a great deal of interest in the use of seismic waves for fractured rock characterization. P-waves form the basis of most commercial seismic surveys and have therefore received considerable attention for fractured rock characterization (Sayers and Rickett, 1997). P-waves are sensitive to fluids and therefore have the potential for saturation discrimination in fractured rocks (Rüger and Tsvankin, 1997, Bakulin et al., 2000). Consequently P-wave anisotropy has been extensively studied and is widely used for fracture characterization (e.g. Winterstein, 1986, Lynn et al., 1996, Rüger, 1997, Li, 1999).

Reservoir rocks have some porosity which usually contains fluids and these along with the rock matrix and grain properties control the seismic response of the rock. A crucial goal of seismic reservoir characterization is extracting information about rock saturants from the received seismic signals. The problem of predicting the effect of fluid properties on seismic properties is known as fluid substitution. Fluid substitution for isotropic porous rocks is commonly performed using the equations of Gassmann (1951) which relate the bulk modulus of a fluid-saturated rock to its porosity, bulk modulus of the dry skeleton, bulk modulus of the solid grain mineral and the bulk modulus of the pore fluid.

Aligned fractures are common in reservoirs and the isotropic expressions of Gassmann (1951) are not sufficient for describing the elastic properties of saturated rocks containing aligned fractures. Theoretical models that relate fracturing in rock to seismic anisotropy measurements are needed for fractured reservoir characterization. Earlier models developed to describe the effective elastic properties of saturated fractured porous rocks (e.g. Schoenberg, 1980, Hudson, 1981, Schoenberg and Douma, 1988) did not consider the importance of the background rock porosity (so-called equant porosity) on the anisotropy of the fractured medium. The importance of background rock porosity on the seismic

anisotropy of fluid-saturated fractured rocks has since been recognised in more recent studies (e.g. Thomsen, 1995, Hudson et al., 1996, Pointer et al., 2000). Thomsen (1995) showed that fluid exchange between the fractures and equant porosity is an important mechanism controlling the amount of seismic anisotropy produced by saturated rocks containing aligned fractures. Many subsequent models have incorporated these important wave-induced fluid flow mechanisms in describing the effective elastic properties of saturated fractured porous rocks (Hudson et al., 1996, Hudson et al., 2001, Chapman, 2003, Gurevich et al., 2009).

Although this dependence of fracture-induced seismic anisotropy on background rock porosity has long been established, it is yet to be studied experimentally. Gurevich (2003) showed the effect of background porosity on the elastic properties of fluid-saturated fractured rocks. The study gave explicit expressions for the low-frequency elastic constants by combining a linear-slip representation of fractures with equations of anisotropic poroelasticity, and showed that changing porosity can have an effect on fracture-induced anisotropy. The shear wave anisotropy parameter (γ) was shown to be insensitive to saturating fluid or porosity, but "ε" was shown to be sensitive to porosity and fluid saturation. It would be desirable to be able to experimentally observe (and validate) this effect of porosity on P-wave anisotropy and any coupled frequency-dependence which might alter these effects. Synthetic fractured sandstones (Tillotson et al., 2012) present a way to observe these effects if the porosity can be varied whilst keeping the fracture properties constant. The theory of communicating cavities (pores, cracks, fractures) by Jakobsen et al. (2003) can be used to model the effects equant porosity on the elastic properties of fluid-saturated fractured rocks in a manner consistent with the model of Gurevich (2003). The coupled frequency-dependence can also be taken into account in the model of Jakobsen et al. (2003).

This work investigates the possibility of varying the porosity of the synthetic sandstones with the aim of observing the effect of different porosities on fracture-induced P-wave anisotropy in water saturated sandstones. Previous synthetic sandstones containing aligned fractures have achieved a minimum porosity of 30% (e.g. Rathore et al., 1995, Tillotson et al., 2012, Tillotson et al., 2014) and although it is challenging to reduce the porosity further, this work attempts to achieve this. Fractured synthetic sandstones with different porosities were created and P-wave measurements were taken parallel and perpendicular to

the fracture normal at both dry and water saturated states. The limitations associated with the manufacturing process meant we were not able to draw any conclusions about the effect of the different rock porosities on the observed P-wave anisotropy. However, results show that it is possible to make different rock porosities within a good range 17% - 27%, and an interesting fluid dependence was also observed in the non-fractured but anisotropic (due to layering) rocks, which would have to be investigated further.

6.2 Methods

6.2.1 Synthetic rocks

The synthetic rock samples were made using the method presented by Tillotson et al. (2012). The samples were made from a mixture of sand, kaolinite and aqueous sodium silicate gel. Three fractured and three non-fractured (blank) rock samples were made. Porosity variation was achieved by using different ratios of cement for each fractured and blank pair. In order to achieve lower porosities than those achieved previously (see Tillotson et al., 2012, Tillotson et al., 2014), the cement volume had to be increased and the samples also had to be held under some confining pressure during the "cooking" period, which present some practical difficulties. Rectangular metal moulds (Figure 6.1a) capable of holding the mixture under confining pressure and also withstanding the required high temperatures were constructed to achieve this.

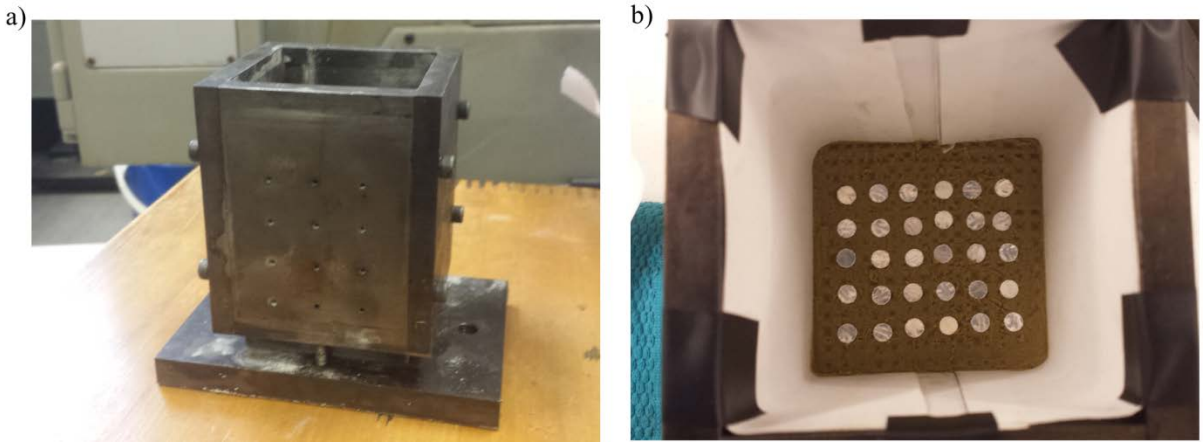

Figure 6.1: a) Rectangular mould designed to hold samples under pressure and high temperatures. b) Aluminium discs on sand layer inside rectangular metal mould. The paper lining prevents the sample sticking to the mould.

Initially, the voids for the fractured samples were created using a predetermined number of 5.5 mm diameter aluminium discs of 0.15 mm thickness chosen to give a fracture density of approximately 0.03. The discs were arranged on successive 4 mm thick layers of sand mixtures (Figure 6.1b). Each set (blank and fractured) was made from the same mixture but in different moulds. After assembling the samples in the moulds the samples were dried and heated, resulting in the production of solid silica cement around sand grains similar in morphology to that found in naturally occurring silica-cemented sandstones (Tillotson et al., 2014). The samples were then placed in hydrochloric acid to leach out the aluminium discs. The samples were left in acid for a total of at least 7 months; however, aluminium discs were still present in the samples after image analysis of X-ray computer tomography (CT) scans. This is a consequence of the additional confining pressure applied during the sample manufacturing process, leading to a much tighter rock (in terms of permeability). One way to improve the flow of acid into less permeable regions of the rock would be to pump the acid into the rock at elevated pressure, which would present significant health and safety challenges, and as such was not pursued in this study.

As a compromise, a decision was taken to create the voids in the fractured sample using a material that would not require leaching out with acid. The ideal material would have to be solid (and made into discs) at temperatures below at least 150°C (preferably 200°C) to prevent void closure before the rock solidifies, and then the material would sublime at higher temperatures (although < 400°C). However, such a material could not be found and any suitable material (as far as we know) would leave a residue. Many materials were tested, for example ash-less filter paper, starch paper, flash paper and Polyvinyl alcohol (PVA), but none produced the ideal situation described above. PVA which is a synthetic polymer was chosen as the most suitable compromise because it leaves behind a weakened residue and as such approximates a fracture (very weak inclusion in an otherwise stiff rock matrix (e.g. Liu et al., 2000).

Three fractured samples were made using the same method described above but this time the aluminium discs were replaced with 5.5 mm diameter and 0.086 mm thick PVA discs (Figure 6.2a). Note that the PVA discs were painted with a blue dye to enhance visibility in comparison with its normal transparent look. The final result after drying and cooking the samples is a set of transversely isotropic synthetic rock samples with fabric and physical properties analogous to

natural sandstones. The weakened PVA discs (Figure 6.2b) represent an approximation to the idealised geometry of penny-shaped voids assumed in theoretical models such as the models of Hudson (1981), Thomsen (1995) and Chapman (2003) and are not intended to represent natural fractures.

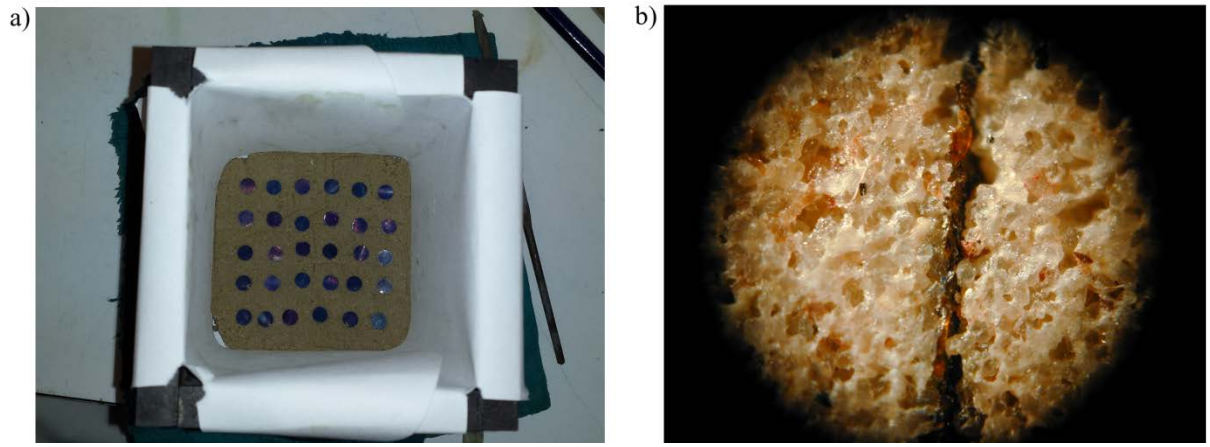

Figure 6.2: a) PVA discs arranged on sand layer inside a rectangular metal mould. b) Microscope image of a fracture showing PVA residue after cooking the rock sample.

The samples were then cut and ground into octagonal prisms with flat faces so that ultrasonic transducers could be directly pressed against them (Figure 6.3). The fracture density for the fractured rocks were taken to be the pre-determined value of approximately 0.03 since the discs remain in the samples and all samples were made using the same number of discs. The volumes of all samples were calculated using Archimedes' principle in a water filled beaker. The porosity of each sample was then calculated from the difference between the dry and water saturated sample mass and the density of the saturating water (assumed to be 1000 Kg/m^3). The porosities for the fractured samples were found to be 17%, 19% and 23%, while the blank samples had porosities of 22%, 25% and 27%.

Figure 6.3: Octagonal sandstone samples. First three from the left are blank samples and the other three samples contain PVA discs (fractured samples).

6.2.2 Measurement technique

I measured ultrasonic P-wave velocity parallel and perpendicular to the fracture (or layer for the blank samples) normal using a laboratory bench-top pulse transmission system (Figure 6.4). P-wave broadband ultrasonic transducers with a central frequency of 500 kHz were placed on opposing sides of the octagonal samples in the directions parallel and perpendicular to the fracture (or layer) normal. In order to ensure consistent coupling between experiments, a pneumatic ram applied a pressure of 60 psi to the transducer faces in contact with the samples. The samples were jacketed using a thin (10 μm thick) layer of aluminium foil to ensure retention of pore fluids.

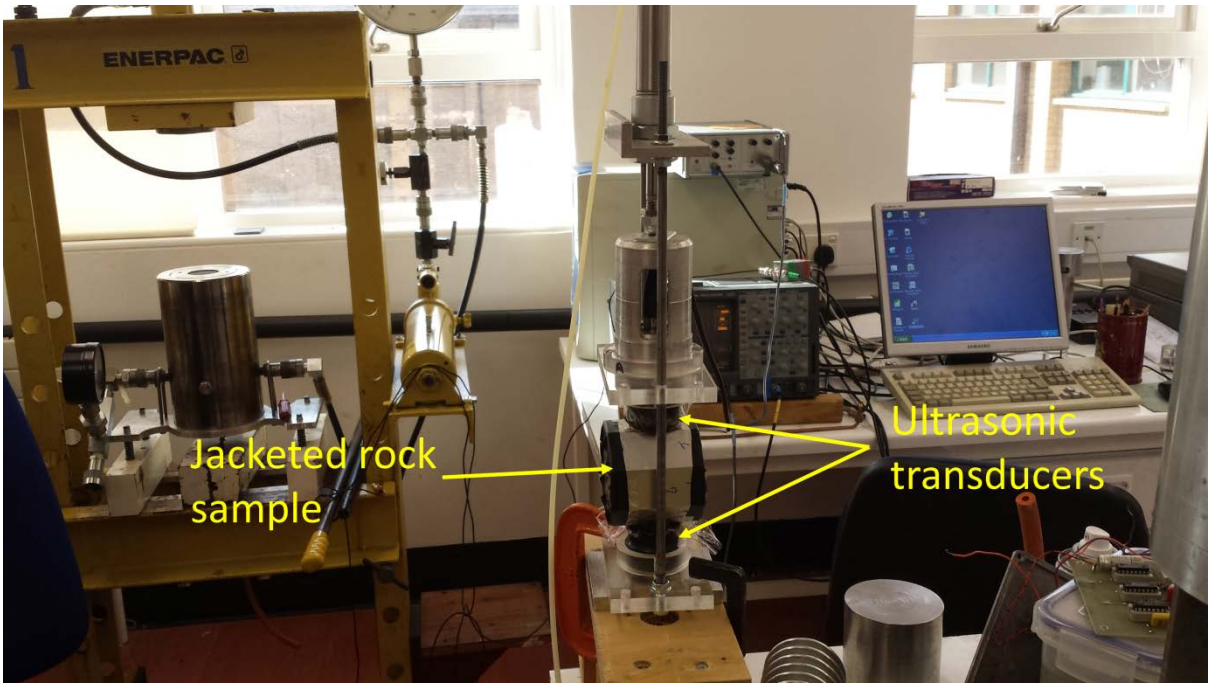

Figure 6.4: Pulse transmission experimental setup.

Velocity was calculated by comparing the Fourier phase angle spectra of the broadband signals from the rock samples with that of a duralumin reference sample (with known elastic properties) using

$$V_1(f) = \frac{x_1}{\Delta t(f) + \frac{x_2}{V_2}}, \tag{6.1}$$

where $V_1(f)$ is the velocity through the rock sample, x_1 is the wave propagation distance in the rock sample, $\Delta t(f)$ is the difference in travel time calculated from the Fourier phase angle spectra of the rock $\varphi_{sample}(f)$ and reference $\varphi_{reference}(f)$ sample. This difference is given by

$$\Delta t = t_{sample} - t_{reference} = \frac{\left(\varphi_{sample}(f) - \varphi_{reference}(f)\right)}{2\pi f}, \tag{6.2}$$

where x_2 is the wave propagation distance in the reference sample, and V_2 is the velocity of duralumin (taken to be 6398 m/s for P-waves for all frequencies as duralumin is non-dispersive). The velocity measurements were corrected for frequency-dependent diffraction effects as a result of beam spreading from the transducer face (Best, 1992). We used isotropic diffraction corrections only.

All six samples were measured dry and fully water saturated and were jacketed using a single layer of thin (10 μm thick) aluminium foil. Measurements

on the duralumin reference sample were also taken with a single layer of the same aluminium foil to account for the resulting increase in length in the velocity calculations.

6.3 Results

Velocity measurements are presented with an error estimate of ± 0.6% and at a single frequency of 500 kHz.

The blank samples show surprisingly considerable anisotropy which could be due to variable grain packing and layering. Figure 6.5 shows P-wave velocity vs. porosity at 0° and 90° to the bedding/layer normal for the dry (Figure 6.5a) and water saturated blank rocks (Figure 6.5b). Velocity is higher parallel to the layers in both dry and water saturated samples.

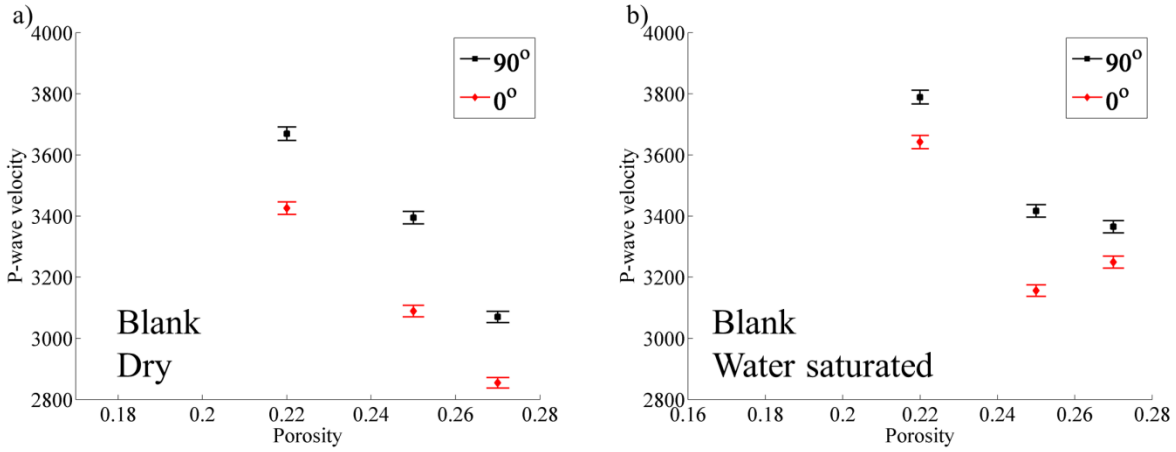

Figure 6.5: P-wave velocity versus porosity at 0° and 90° to the layer normal for a) dry and b) water saturated blank samples. Vertical error bars shown.

Figure 6.6 shows P-wave velocity vs. porosity at 0° and 90° to the fracture normal for the dry (Figure 6.6a) and water saturated fractured rocks (Figure 6.6b). Similar to the blank sample, P-wave velocity is higher in the direction parallel to the fractures in both dry and water saturated samples.

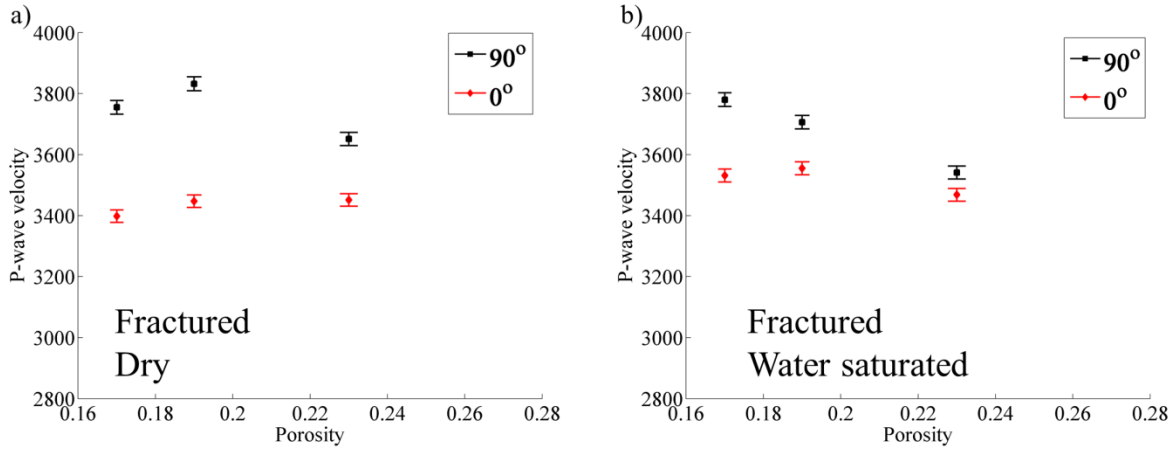

Figure 6.6: P-wave velocity versus porosity at 0° and 90° to the fracture normal for a) dry and b) water saturated fractured samples. Vertical error bars shown.

Figure 6.7 shows plots of the Thomsen-style P-wave anisotropy parameter (see Thomsen, 1986), "ε" versus porosity. The parameter (ε) represents the difference in P-wave velocity between the vertical (90˚) and horizontal (0˚) directions and is given by

$$\varepsilon = \frac{C_{11} - C_{33}}{2C_{33}}. \tag{6.3}$$

Figure 6.7a shows "ε" versus porosity for the dry and water saturated blank rocks and Figure 6.7b shows "ε" versus porosity for the dry and water saturated fractured rocks. "ε" can be seen to be higher in the dry state than when water saturated for both blank and fractured rock samples.

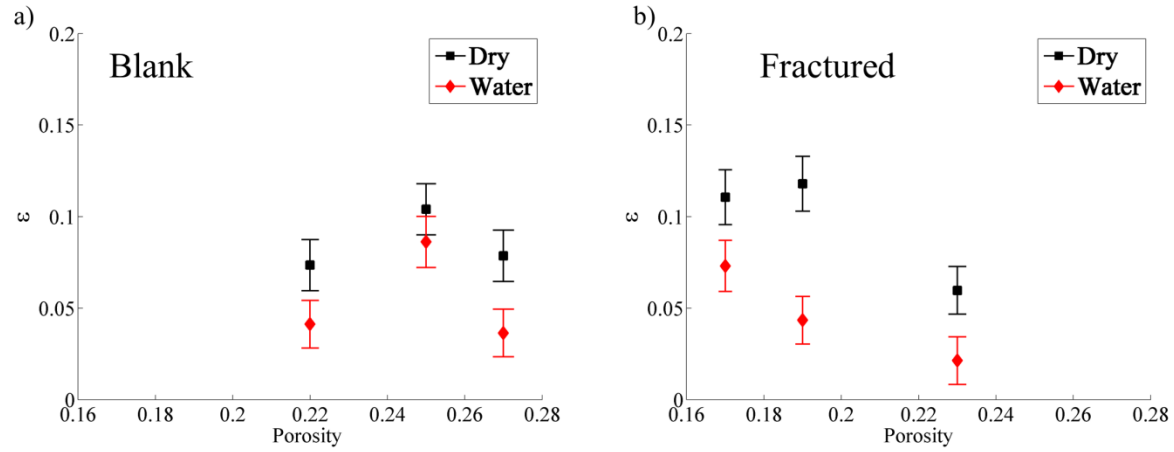

Figure 6.7: Measured P-wave anisotropy parameter "ε" versus porosity for a) blank sample and b) fractured sample.

6.4 Discussion

Theoretical works from many researchers have shown the importance of rock porosity on fracture-induced seismic anisotropy (e.g., Thomsen, 1995, Hudson et al., 2001, Chapman, 2003, Gurevich, 2003). This effect is due to background rock porosity (equant porosity) being stiffer than cracks which are compliant because of their 2D shape (Thomsen, 1995). Therefore, a saturating liquid can significantly stiffen an isolated crack because of the liquid incompressibility (bulk modulus), which reduces the amount of P-wave anisotropy. However, if the crack is connected to the pore space, then as the rock (and hence the crack) is compressed, the liquid will move into the stiffer pore space to equilibrate the fluid pressure. This leads to an increase in P-wave anisotropy as the rock is now weaker in the direction parallel to the fracture normal, due to this fluid pressure equilibration.

Not many studies have looked at how the amount of porosity affects P-wave anisotropy and how this relates to the frequency dependence. Gurevich (2003) studied the effect of porosity on anisotropy in the low frequency limit and showed that there is a characteristic porosity around which the sharpest increase of P-wave anisotropy occurs. This characteristic porosity was shown to be largely controlled by the dry fracture weakness or degree of fracture anisotropy. As the background porosity becomes significantly greater than the characteristic porosity, the P-wave anisotropy reduces gradually as a result of the isotropic nature of the pore fluid which acts to reduce the overall anisotropy of the rock (Gurevich, 2003). Therefore, the predicted porosity dependence for the porosity range of the fractured rocks (17% - 23%) in our experiment would be expected to be subtle because the characteristic porosity is small as shown by Gurevich (2003).

However, at higher frequencies velocity dispersion is expected as a result of wave-induced fluid flow, which occurs at different scales: macroscopic, mesoscopic, and microscopic (Pride et al., 2004, Carcione and Picotti, 2006, Müller et al., 2010). The frequency dependence is known to be a function of the rock (e.g. porosity and permeability) and fluid (e.g. bulk modulus, viscosity) properties (Carcione and Picotti, 2006, Mavko et al., 2009, Müller et al., 2010). The relationship between porosity and dispersion (or attenuation) is still poorly understood. Bourbie and Zinszner (1985) could not discern a conclusive trend between porosity and attenuation and concluded that the scatter observed from

their experiments was mostly related to differences in rock structure. Porosity effects on velocity has so far remained elusive.

Synthetic sandstones present an opportunity to observe the effect of porosity on P-wave anisotropy and any associated dispersion effects if the rock porosity can be varied whilst keeping the fracture properties constant. However, we did not envisage that the blank rocks would have significant and variable intrinsic anisotropy as a result of the manufacturing process. Also, the saturation dependence of the anisotropy in the blank rocks which also differs between the different samples was not expected. It appears that although the samples were made using the same process, the packing in the different moulds ended up being different. The significant amount of anisotropy measured in the blank samples appears to be due to the uniaxial pressure applied to help reduce the sample porosity. The uniaxial nature of the applied pressure appears to have increased the layer-induced anisotropy instead, due to more significant preferential stiffening of the layers perpendicular to the direction of applied pressure (i.e. parallel to layers). This inconsistency of layering effects between the different blank samples makes it impossible to correct the fractured samples for the layer induced anisotropy. This makes any observations of porosity effects on fracture-induced P-wave anisotropy from these set of experiments ambiguous at best, thus, drawing any conclusions would be impossible.

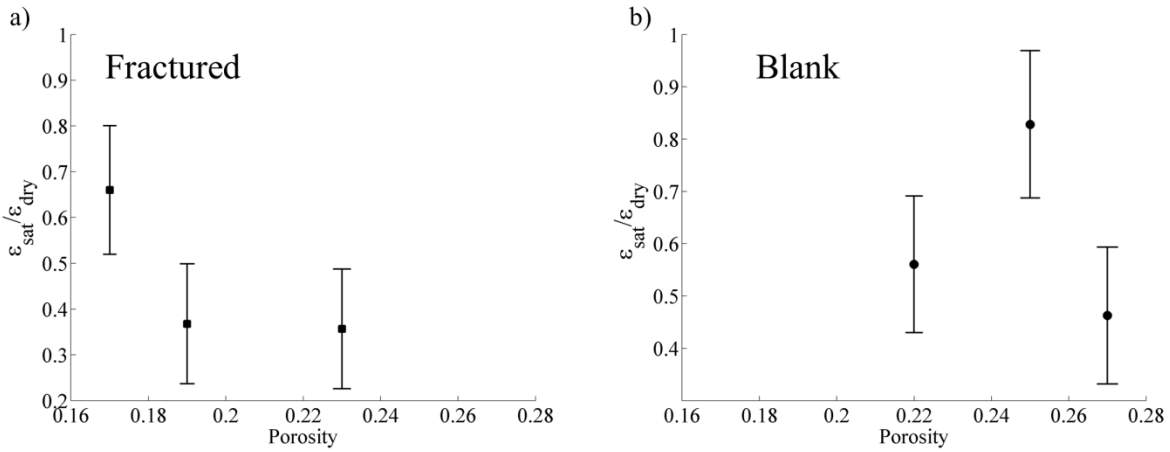

Figure 6.8: Ratio of water saturated to dry P-wave anisotropy parameter (ε) versus porosity for the a) fractured sample and b) for the blank sample.

For an ambitious look at the data, we could look at the ratio of the saturated to the dry P- wave anisotropy for the different porosities (Figure 6.8) to get around the different P-wave anisotropy measured for the dry fractured rocks due

to the rock manufacturing process. We could say that the trend in the fractured rocks agrees with the resulting effect being a decrease in P-wave anisotropy with increasing porosity (within our porosity range) as shown by Gurevich (2003). This is an ambitious statement due to the size of the associated errors and other limitations as discussed above.

Although we are not able to draw any conclusions regarding the relationships we set out to study, the experimental study does reveal some interesting observations. The study shows we can vary the porosity of the synthetic sandstones between 17% - 27% which is not trivial. Higher porosities (>27%) can be easily achieved, the challenge is lower porosities. Another interesting observation from the study is that the layer-induced P-wave anisotropy appears to be sensitive to water saturation, something that has not been observed before (e.g., Tillotson, 2012, Amalokwu et al., 2015a). This might be because in the previous studies (Tillotson, 2012, Amalokwu et al., 2015a), P-wave anisotropy due to layering was not significant and hence a saturation dependence could not be observed. However, it appears when the layer-induced anisotropy is significant, P-wave anisotropy could be saturation dependent – but this effect needs to be explored further.

For the purposes we set out to achieve (porosity effects on fracture-induced P-wave anisotropy), more stringent controls are needed during the rock manufacturing process. The effect of layering needs to be consistent between samples or preferably removed and this consistency is something that is missing in this experimental study. Such a result would require additional improvements to the sample manufacturing process which would require further research.

6.5 Conclusions

The porous nature of crustal rocks has been shown to affect the fracture-induced P-wave anisotropy when liquid saturated. This effect on P-wave anisotropy has been shown to be due to fluid exchange between the more compliant fractures and the background rock porosity. However, there has not been any reported laboratory experimental observation of the effect of porosity on fracture-induced P-wave anisotropy in saturated porous rocks. This study aimed to change this situation by creating synthetic fractured rocks with different porosities, along with non-fractured rocks as control samples to account for the effect of layering.

However, the final results for the porosity effects on P-wave anisotropy were ambiguous due to unexpected inconsistencies of the layering effects in the non-fractured (and hence the fractured) samples. However, some positives can be drawn from the study. The study showed that the porosity of the synthetic rocks can be varied within a decent range (17% - 27%) and the 'approximately' fractured rocks created behave as expected in terms of the anisotropic response to fluid saturation. Also, there was an interesting observation of saturation dependent layer-induced anisotropy which was unexpected and needs to be investigated further. If this turns out to be the case, then this could have important implications for seismic characterisation of layered rocks with similar layer material properties. Further work needs to be done to improve the procedure but this work could serve as a template for future similar works.

Chapter 7: Conclusions

7.1 Summary of main findings

In this thesis, controlled laboratory experiments using novel synthetic sandstones containing aligned penny-shaped fractures have allowed for observations of water saturation effects on fracture-induced anisotropy. Certain new phenomena are observed and I find that despite the violation of the equivalent medium criteria, mechanisms from frequency-dependent equivalent medium theories are able to explain the experimental observations. The main findings are summarised below.

In chapter 3, P- and S-wave attenuation measurements were taken at different values of water saturation on a blank sample, and one containing fractures aligned parallel to wave propagation direction using the ultrasonic pulse-reflection measurement system. Previous work showed that full/partial gas saturation can be distinguished from full liquid saturation using Q_s/Q_p ratios, with the later usually having values of $Q_s/Q_p \leq 1$ and the former having values of $Q_s/Q_p > 1$. This was shown to be consistent with observations for the blank rock, but the presence of fractures aligned parallel to wave propagation direction showed a different behaviour. There were two main differences due to the presence of vertically aligned fractures. Q_s/Q_p ratios are reduced in magnitude, and the separation between full/partial gas saturation and full liquid saturation is not as clear as in the case of the blank sample.

In chapter 4, experimental results of shear wave splitting due to fractures aligned at 45° to wave propagation were shown to be sensitive to higher values of water saturation ($S_w > 0.7$). Previous studies (theoretical and experimental) have shown this fluid sensitivity of SWS at oblique angles to wave propagation in fully saturated fractured rocks. However, this is the first study to show that partial liquid/gas saturation could also have an effect on the measured SWS. Insights gained from theory suggest this effect is a result of frequency-dependent effects due to the presence of partial gas saturation. The quasi-shear wave in this direction is sensitive to the bulk modulus of the saturating fluid, and as such the effective bulk modulus of the saturated rock. This effective rock-fluid modulus is frequency-dependent due to wave-induced fluid flow mechanisms which act to stiffen the rock. This stiffening in turn affects the SWS in a frequency-dependent manner by increasing the velocity of the quasi-shear wave, and hence, reducing the observed SWS. The modelling only considered the frequency-dependent

effects due to partial saturation in the background material, apart from at full water saturation where dispersion from the fractures was also considered. Therefore, the modelling only predicts a subtle effect of saturation on SWS when the rock is partially saturated.

In chapter 5, the rock samples that were ground into octagonal prisms removed ambiguities due to inter-sample variations seen when cylindrical plugs were taken from different blocks, at different directions relative to the fracture normal. This allowed the investigation of water saturation effects on P-wave anisotropy using a single sample. A bench-top pulse-transmission setup was used to measure P-wave velocities at 0^{o}, 90^{o}, and 45^{o} to the fracture normal, at different water saturation states. P-wave anisotropy was found to be sensitive to water saturation, with the sensitivity increasing as wave propagation moved from parallel to perpendicular to the fractures. The concept of wave induced fluid flow was found useful in explaining these observations. The modelling study in Chapter 4 showed that frequency-dependent effects due to partial liquid/gas saturation in the background rock material can affect the observed fracture-induced anisotropy even though no fluid effects on the compliance of the fractures are considered. This was also shown to be the case for P-wave anisotropy; however, further insights from the modelling interpretation suggest dispersion effects from the fractures due to saturation distribution at the crack/pore scale could also be important. This effect was shown by using a non-Reuss averaged fluid modulus for the fractured rock model, which gave better agreement with the magnitude of dispersion observed. This has a physical interpretation in terms of non-equal fluid pressures.

The presence of equant porosity (background rock porosity) in fluid saturated rocks containing aligned fractures has been shown to affect the measured anisotropy due to wave induced fluid flow. However, the way in which the amount of equant porosity affects the observed anisotropy is still poorly understood. The work in Chapter 6 was designed to study the effect of porosity on P-wave anisotropy by creating synthetic rock samples having different background porosities but similar fracture properties (density, size). Increased consolidation of the samples during the manufacturing process meant the rocks could not be produced using the previous methods of leaching out aluminium discs to create voids. A compromise was made to use a material that would not require leaching out with acid, but would leave a weakened residue. Unfortunately, the results were ambiguous due to unexpected inconsistencies of

the effects of layering in the blank samples, which made interpretation of the fracture effects ambiguous. The study did however show that the porosity of the synthetic sandstones can be varied within a decent range (17% - 27%), something that is not trivial. Also, an interesting saturation dependence of layer-induced P-wave anisotropy was observed in the blank rock samples. However, this effect will require further investigation before any interpretations or conclusions can be made.

7.2 Discussion and conclusion

Understanding the seismic response of fluid saturated porous rocks containing aligned fractures is important for the interpretation of field measurements of seismic anisotropy in terms of the fracture properties (orientation, density), rock and fluid properties (Crampin et al., 1986, Thomsen, 1995, Hudson et al., 2001). Consequently, the effect of fluids on fracture-induced seismic anisotropy in porous rocks has been a focus of research for about 30 years, and is still actively developing. Various theories have been developed with varying degrees of limiting assumptions (e.g. single phase saturation, dilute concentrations of voids); however, there are only a handful of controlled experiments. Controlled laboratory experiments and suitable theoretical models are still lacking in the case of partial gas/liquid saturation effects in fractured rocks. Also, although the effects of porosity on frequency-dependent seismic anisotropy in saturated fractured rocks is developed theoretically (Jakobsen et al., 2003), experimental studies are still lacking. In a bid to partly address these issues, this work aimed to make initial observations which could help improve our understanding of these effects and ultimately help inform the development and/or validation of suitable theoretical models.

The attenuation results from Chapter 3 confirm the previously established notion that Q_s/Q_p ratios can be used to distinguish between full liquid saturation ($Q_s/Q_p \leq 1$) and full or partial gas saturation ($Q_s/Q_p > 1$) (Winkler and Nur, 1982, Klimentos, 1995, Koesoemadinata and McMechan, 2001). Attenuation is also sensitive to the presence of fractures and as such, attenuation anisotropy can also be used for fractured rock characterisation (Maultzsch et al., 2007, Zhu et al., 2007, Chichinina et al., 2009). The results for the rock containing fractures aligned parallel to wave propagation direction suggest that the saturation

relationship already established, and also observed in our experiments for non-fractured rocks could be violated in fractured rocks depending on the direction of propagation. Therefore, care must be taking when using attenuation ratios for fluid discrimination (e.g., Klimentos, 1995, Dvorkin and Mavko, 2006) in reservoirs containing fractures. Q_{s1}/Q_{s2} could be used for magnitude of fracturing while and Q_{s1}/Q_p could be used for saturation discrimination. It would be interesting to conduct these experiments on samples with different fracture densities (preferably higher) to observe how these relations evolve with fracture density.

The results for velocity anisotropy in both Chapters 4 and 5 where water saturation is seen to affect shear wave splitting at oblique angles of incidence, and P-wave anisotropy, respectively, have important practical implications. Insights from the modelling study showed that partial saturation effects in the background rock alone could affect the measured seismic anisotropy. These saturation effects are frequency-dependent due to wave induced fluid flow mechanisms which could be at the microscopic (squirt) or mesoscopic scale (patchy). Although these experiments were done at ultrasonic frequencies, these effects could also occur at lower sonic and seismic frequencies under suitable conditions. For example, studies have suggested that patchy saturation effects could be observed at seismic frequencies (1-100 Hz) if the saturation heterogeneities are large enough (tens of centimetres) (e.g., White, 1975, Mavko and Mukerji, 1998). There have also been studies showing evidence for patchy saturation at sonic frequencies from well logs in the literature (Brie et al., 1995, Dvorkin et al., 1999, e.g., Caspari et al., 2011). In the presence of aligned fractures in such conditions, it follows that the effects of patchy saturation in the background rock could have an effect (which would be frequency-dependent) on the measured anisotropy. Dispersion from the fractures could amplify these effects as was shown in Chapter 5. Without considering these dispersion effects by assuming uniform saturation distribution and using the Biot-Gassmann-Domenico relation, no fluid effect on anisotropy would be expected except at approximately full water saturation. This is because in assuming uniform saturation, the effective fluid modulus is given as the Reuss average of the gas and liquid, which is effectively the modulus of the gas from dry to approximately full liquid saturation. Therefore, in the presence of dispersion, seismic anisotropy can be more sensitive to degree of saturation and could be exploited as such.

Despite observing several new phenomena, there are still limitations that need to be addressed by future work. More experimental data is needed to better understand the effects presented here, and to isolate controlling mechanisms. For partial saturation effects, a very interesting study would be to observe the changes in saturation within the sample using X-ray CT scan. The presence of fractures complicate the effects of partial gas saturation as the elastic response (hence anisotropy) would depend on the saturation distribution within the rock background and within the fractures. Realistically, larger fractures (compared to the pores) would be expected to saturate differently as they would drain preferentially before the pores or microcracks. Consequently, the presence of fractures could itself cause saturation heterogeneities by causing preferential drainage of different regions, which could change the observed seismic response. Therefore, strictly speaking, two saturation values would be required in the modelling as the fracture saturation could differ from the background rock saturation and this would affect the seismic anisotropy. The information from the imaging could shed some light on the controlling mechanisms at different stages of saturation and help with interpretation of results. This could mean analysing the effect of water saturation on both the absolute velocities and the anisotropy could give more information about the saturation distribution. For example if the change in the velocity parallel to the fractures is negligible, but that perpendicular to the fractures is significant, this could indicate the fractures are draining preferentially. Likewise, if the velocities in both these directions change by similar amount and the change in anisotropy is negligible, then this could indicate that the fractures remain liquid saturated while the background rock saturation is becoming gas saturated. Experiments using different fracture densities would also be interesting to observe the changes of these effects with fracture density. Which of the effects would be amplified with an increase in fracture density? Would the saturation effects in the background rock material turn out to be more or less important compared to the saturation effects in the fractures? More studies are needed to better understand these effects.

The studies in this thesis have paved the way for further experimental studies on fracture-induced seismic anisotropy in fluid saturated porous rocks containing aligned fractures. The synthetic sandstones represent analogues of naturally occurring sandstones in terms of the background rock properties. The relatively high porosity, but low permeability of the samples might be counter-intuitive but this is consistent with observations in natural rocks and sediments. Porosity generally tends to increase with decreasing grain size for sands of

uniform grain size, while permeability decreases with decreasing grain size as pore throats are smaller in finer sediments, with the higher capillary attraction of the walls inhibiting flow (Chilingarian and Wolf, 1976, Selley, 2000). The manufacturing method allows for the variation of the fracture properties and now allows for the variation background rock porosity. However, limitations in the manufacturing process still exist, which when overcome would present significant opportunities. For example, making fractured rock samples without background layering effects would remove inter-sample ambiguities which prevented the interpretation of the experimental results of porosity effects on P-wave anisotropy in Chapter 6. Removing this inter-sample ambiguity due to layering would also allow for plugs to be cored at different directions and measured using the more accurate pulse-reflection method under confining pressure, enabling pressure effects to be studied.

A significant challenge associated with fractured rock experiments is the size of the fractures compared to the wavelength. These experiments violate the equivalent medium criterion which requires the wavelength to be much larger than the size of the fractures. Fracture sizes in these experiments are on the order of the measurement wavelengths and as such the fractures introduce scattering which is undesirable. Making samples with fractures that are much smaller than the wavelength (about ten times smaller) would be very challenging at ultrasonic frequencies. Therefore, reducing the measurement frequencies by using a resonant bar technique (e.g., Murphy, 1982, Winkler and Nur, 1982, Cadoret et al., 1995, Nakagawa et al., 2013) or low-frequency forced deformation stress-strain measurements (e.g., Spencer, 1981, Batzle et al., 2006) could be a way to get around that. These low frequency methods also present their set of challenges such as difficulty in making low frequency measurements, sample size, and measurements of shear wave splitting. However, if such measurements are achieved through either method, it would represent a significant advance, as scattering effects would be eliminated and only desirable intrinsic dispersion effects which are only accounted for in equivalent medium theories would be measured. Although in reality, fractures can occur at different scales, so the situation where the fractures are on the order of the wavelength could also occur in practice and is still relevant. However, the majority of fracture-induced anisotropy is believed to be caused by fractures much smaller than the wavelength, and are modelled as such using equivalent medium theories (Crampin and Peacock, 2005). Therefore, measurements that meet the equivalent medium criteria would be more ideal for comparison to equivalent medium

theories and their proposed mechanisms, without interference from scattering effects. Finally, isotropic diffraction corrections were used in this study even though the rocks were anisotropic. Although the expected errors from diffraction effects would be systematic and as such, the effect on the trends would be minimal in these experiments, although the absolute accuracy of the measurements could benefit from anisotropic diffraction corrections. This could be an area for further improvements in future studies.

Appendices

Appendix A : Pulse-reflection system overview

A.1 Introduction

The ultrasonic pulse-reflection (also known as pulse-echo) system used in this study was developed by McCann and Sothcott (1992) based on the technique of Winkler and Plona (1982). An overview of the system is given here as a detailed description of the entire system and its calibration can be found in McCann and Sothcott (1992), and Best (1992).

In the pulse-reflection system, the sample is sandwiched between two cylindrical Perspex buffer rods of 5 cm diameter. Ultrasonic transducers (compressional or shear) transmit pulses through the buffer rod into the rock sample, and into the second buffer rod. The same transducer is used to receive the reflections from the Perspex-rock interfaces, from which the velocity and attenuation can be calculated. A schematic of the system is shown in Figure A.1.

Placing the transducers at either end of the sample allows P- and S-wave measurements to be made sequentially. The entire system made up of the steel housing of the transducers, the Perspex buffer rods, and the rock sample is enclosed in a rubber jacket and placed inside a Hoek-type pressure cell where hydrostatic pressure of up to 70 MPa can be applied.

A significant advantage of the pulse-reflection system over the pulse-transmission system is its repeatability and accuracy, particularly for attenuation measurements (McCann and Sothcott, 1992). For instance, signal amplitudes are sensitive to the coupling between the transducer and the sample, and a change in the thickness of the couplant would change this coupling, thereby affecting the pulse amplitude. This would introduce errors in the calculation of attenuation using the pulse-transmission method, as this requires two separate measurements (one on the rock and another on a reference material). The pulse-reflection method does not suffer from this drawback as measurements depend on a single measurement of the amplitudes from the top and base of the rock sample. As such, any variations due to the transducer couplant affect both reflections equally.

In the setup used in this work, the S-wave transducer was installed in the upper part and the P-wave transducer was installed in the lower part of the assembly. The reflections from the Perspex-rock interfaces at the top and base of the sample are displayed on a digital oscilloscope for direct measurement of the travel times and amplitudes (for a single frequency source) and stored on the computer for spectral analysis (for a broadband source) (see McCann and Sothcott, 1992). The sample is always allowed to equilibrate at any effective pressure it is under for at least 30 minutes. The laboratory temperature and relative humidity are always maintained at 20°C and 55% respectively, using an air conditioning unit.

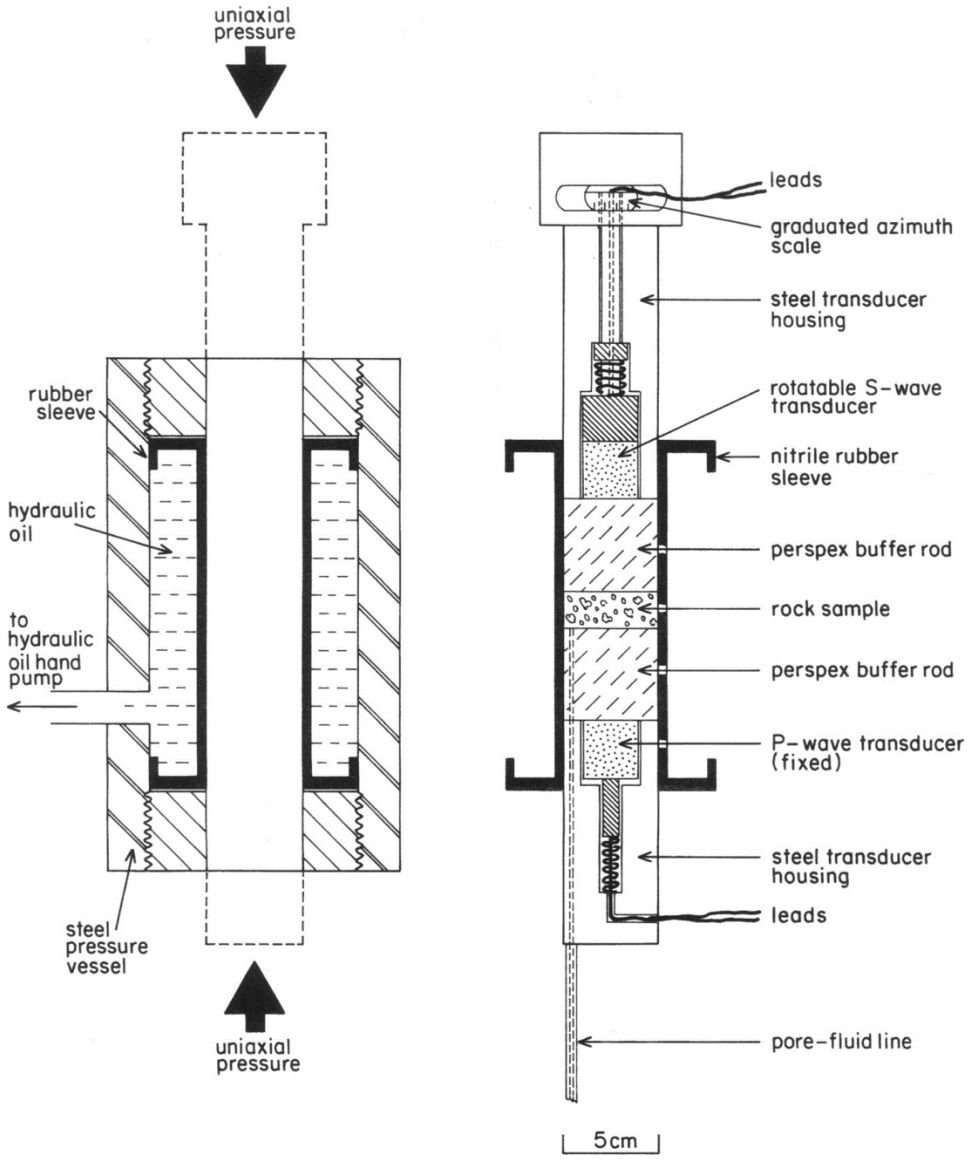

Figure A.1: Schematic of the ultrasonic pulse-echo system with rotating S-wave transducer mounting for measuring azimuthal S-wave anisotropy.

The sources of error in the pulse-reflection system are well discussed by Best (1992). Absolute errors can arise due to sample swelling (e.g. in clay rich samples) or sample compression, resulting in a change in sample length which could lead to errors in measurements if not accounted for. The other errors are systematic, and include sample flatness and parallelism, side wall reflections, and diffraction effects. Sample flatness and parallelism is needed to ensure a good welded contact between the buffer rods and the samples when under pressure. Side wall reflections due to beam spreading could cause the pulse to reflect off the walls and interfere with the direct pulses. However, this effect is expected to be significant only at low frequencies in this present setup, as it is possible to calculate the lowest frequency where side wall reflections are not expected. Diffraction effects which also introduce errors in the pulse-reflection system are discussed below.

The systematic errors were quantified by careful calibration using aluminium and brass samples, and it was found that velocity could be measured to an accuracy of ± 0.3% and attenuation to ± 0.2 dB/cm (see Best, 1992). Errors in calculations using the measured velocities or attenuations can be obtained by propagating the uncertainties in individual measured values (e.g., Taylor, 1982).

A.2 Pulse generators

Two separate sources were used to provide ultrasonic waves. An AVR-1-PW-C-P pulse generator was used to provide broadband pulses with frequency content between 500 to 1500 kHz. An Arenberg type PG650C pulse generator was used to generate single frequency pulsed-sine wave with internal frequencies in the range 0.4 MHz to 1.1 MHz (Best, 1992). An important advantage of making the high precision single-frequency measurements is to provide an absolute value to calibrate the velocity dispersion curve from the broadband measurements (McCann and Sothcott, 1992).

The pulses were displayed using a LeCroy digital oscilloscope and stacked 1000 times to improve the signal to noise ratio. The broadband signals were then saved onto a computer for subsequent processing. Figure A.2 show typical waveforms from the dry blank sample for the broadband and single frequency sources respectively.

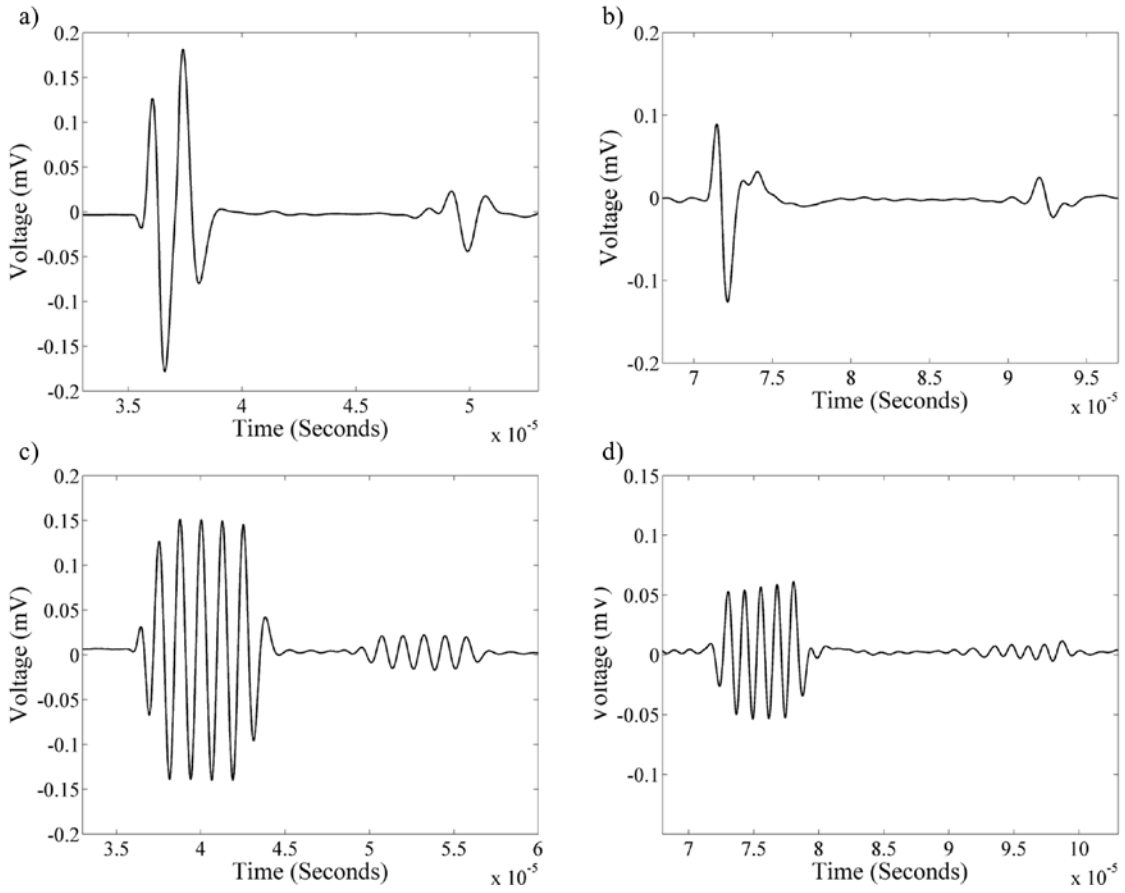

Figure A.2: Typical traces for a) P-wave and b) S-wave broadband traces, c) P-wave and d) S-wave toneburst traces.

A.3 Transducers and Couplants

The transducers used in the Pulse-reflection method in these experiments were a Panametrics type V102 P-wave transducer and a Panametrics type V152 S-wave transducer, both having a diameter of 2.54 cm and nominal frequency of 1 MHz.

Two different types of couplants were used to ensure good coupling between the transducers and the Perspex buffer rods. Ultragel couplant, a commercially available water-based gel was used as the P-wave couplant. Sonotech shear gel, a commercially available highly viscous honey-based compound was used as the S-wave couplant.

The shear wave transducer housing was designed to allow the transducer to be rotated on a thin film of shear-wave couplant while under confining pressure

(Figure A.3). The transducer is rotated manually using a thin metal rod inserted into pin holes in a metal ring at the top of the housing.

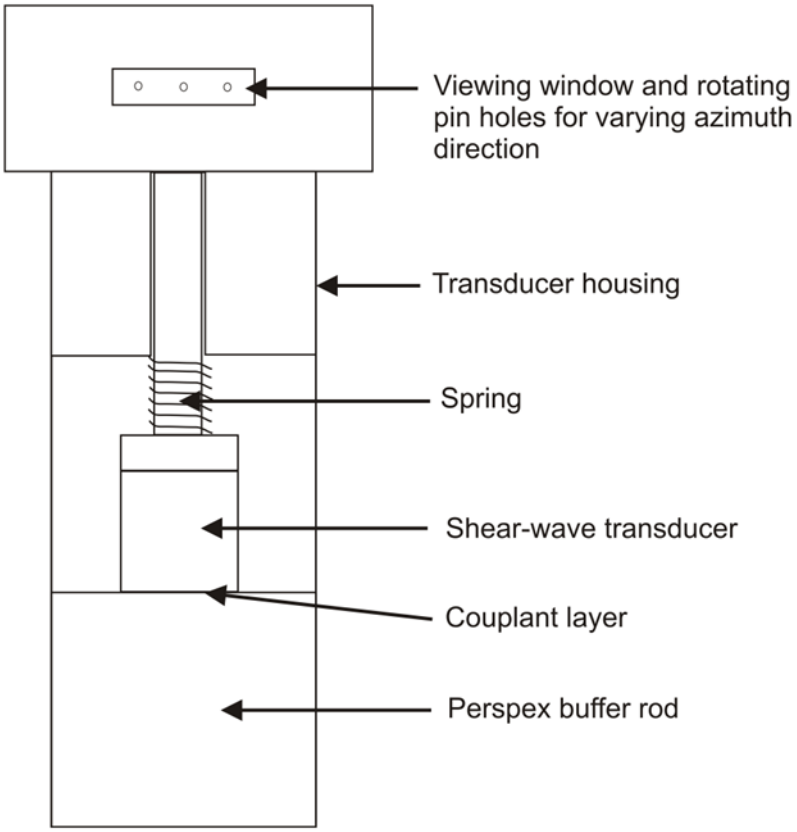

Figure A.3: Schematic of the shear-wave transducer housing. The design allows the transducer to be rotated for the measurement of azimuthal S-wave anisotropy under elevated pressures.

A.4 Diffraction (Beam spreading) corrections

The finite size of ultrasonic transducers causes diffraction. This wave interference effect causes phase and amplitude distortions which are a function of the transducer radius, the wave frequency and path length (distance from the transducer). The effect of the phase distortion is an apparent decrease in travel time (thus higher velocity). The effect of the amplitude distortion due to diffraction is an apparent amplitude reduction, leading to higher values of attenuation than the true value.

Papadakis (1972) formulated attenuation and phase corrections for ultrasonic pulses from a transducer of diameter a, at a distance z from the source, and a wavelength of λ. He defined a normalised distance S as:

$$S = \frac{z\lambda}{a^2} = \frac{zV}{a^2 f}\,, \tag{A1}$$

where f is the frequency and V is the velocity of the wave. The diffraction corrections Δt (*μs*) and $\Delta\alpha$ (*dB/cm*) for the travel times and attenuation coefficients respectively are then given as:

$$\Delta t = \frac{\Phi(S_B) - \Phi(S_A)}{2\pi f}\,, \tag{A2}$$

$$\Delta\alpha = \frac{\alpha(S_B) - \alpha(S_A)}{2L_R}\,, \tag{A3}$$

where Φ is the diffraction phase shift, L_R is the sample (rock) length, S_A and S_B are the normalised distances for the top and base reflections, respectively. The corrected travel times and attenuation coefficients are given as follows:

$$t = t' + \Delta t\,, \tag{A4}$$

$$\alpha = \alpha' - \Delta\alpha\,, \tag{A5}$$

where t' and α' are experimentally measured travel times and attenuation coefficients, respectively.

Using the relations of Papadakis (1972), Benson and Kiyohara (1974) produced tabulated values of Φ and $\Delta\alpha$. Although these corrections are strictly valid for P-waves propagating through an infinite medium, the same corrections have been shown to be reliable for S-waves (Best, 1992, McCann and Sothcott, 1992).

A.5 Calculation of Phase velocity

For single frequency measurements, velocities can be calculated from:

$$V(f) = \frac{2L_R}{t}\,. \tag{A6}$$

For broadband measurements, velocities can be calculated using:

$$V(f) = \frac{2L_R}{\left(t_B - \frac{\Phi_B(f)}{2\pi f} - \frac{1}{2f}\right) - \left(t_A - \frac{\Phi_A(f)}{2\pi f}\right)}\,, \tag{A7}$$

where $V(f)$ is the P- or S-wave velocity (m/s) at frequency f, t_A is the window start time for pulse A (top reflection), t_B is the window start time for pulse B (base reflection), $\Phi_A(f)$ is the Fourier phase angle spectrum for pulse A, $\Phi_B(f)$ is the Fourier phase angle spectrum for pulse B. The $\frac{1}{2f}$ term is included to account for the 180° phase change in the base reflection.

The travel time is corrected for diffraction effects at each frequency using equations A2 and A4.

A.6 Calculation of attenuation coefficient

The attenuation coefficient defined as the loss of amplitude per unit distance is given by

$$\alpha(f) = \frac{8.686}{2L_R} \ln\left\{\frac{A_A(f)}{A_B(f)} [1 - R^2(f)]\right\} \quad \text{(A8)}$$

where $\alpha(f)$ is the attenuation coefficient (*dB/cm*) at frequency f, $A_A(f)$ is the Fourier amplitude spectrum of the top reflection and $A_B(f)$ is the Fourier amplitude spectrum of the base reflection. $R(f)$ is the normal incidence reflection coefficient given as

$$R(f) = \frac{\rho_R V_R(f) - \rho_p V_p(f)}{\rho_R V_R(f) + \rho_B V_p(f)} \quad \text{(A9)}$$

where ρ isbulk density (*Kg/m³*) and subscripts *R* and *P* represent rock sample and Perspex buffer rods, respectively.

The quality factor Q is then given by

$$Q(f) = \frac{\pi f}{V(f)\alpha(f)} \quad \text{(A10)}$$

The attenuation coefficient is corrected for diffraction effects at each frequency using equations A3 and A5.

Appendix B : Saturation protocol

B.1 Introduction

When a rock is saturated by more than one fluid phase, it is known that seismic response is significantly affected by the spatial distribution of saturation in the sample, which has been shown could depend on the saturation protocol employed (Knight and Nolen-Hoeksema, 1990, Yin et al., 1992, Cadoret et al., 1995). The presence of saturation patches can cause dispersion due to wave induced fluid flow (White, 1975, Mavko and Mukerji, 1998). Elastic scattering could also become a problem when the seismic wavelength is comparable to the saturation patches (Gist, 1994b, Cadoret et al., 1998). Partial saturation can be achieved in various ways, notably: by imbibition and drainage; centrifugal desaturation; and rehydration in an atmosphere with controlled relative humidities.

The most common methods of achieving partial saturation is through imbibition (wetting fluid such as water displacing non-wetting fluid such as gas) and drainage (non-wetting fluid such as gas displacing wetting fluid such as water) (e.g. Knight and Nolen-Hoeksema, 1990, Cadoret et al., 1995). Imbibition begins with a dry sample which is then gradually saturated with water while drainage (or drying) begins with a fully saturated sample where gas displaces water or the sample is allowed to dry in order to achieve partial saturation. Advantages of these methods are: a wide range of achievable saturation; and it is relatively quick. However, the problem with these methods is the presence of saturation patches (saturation inhomogeneities), mainly during the drainage process (Le Ravalec et al., 1996, Cadoret et al., 1998, Knight et al., 1998).

Centrifuge desaturation is another method of achieving partial saturation. It is used predominantly in petrophysics and reservoir engineering studies for saturation profiles of relative permeability, wettability, capillary pressure effects and irreducible water saturation (e.g. Liu et al., 2006). Bourbie and Zinszner (1984) used this method to achieve partial saturation by placing totally saturated or partially saturated samples in a centrifuge which expels water from the sample by subjecting the sample to a centrifugal force. The water saturation is a function of acceleration and the length of the sample. The centrifuge method showed a

heterogeneous fluid distribution with gas bubbles clustered in zones where the pore entry radii are the largest (a function of capillary pressure) severely changing the seismic response compared to those obtained by drying and imbibition. The resulting effect was a more heterogeneous saturation distribution of liquid and gas.

Schmitt et al. (1994) investigated capillary phenomena in shaley rock samples to show the prime importance of capillary pressure in the behaviour of under-saturated materials. Saturation levels were achieved using three methods: 1) Immersion under vacuum which is equivalent to imbibition in a vacuum; 2) Saturation by capillary rise; 3) Equilibration in controlled atmosphere. Results showed that despite all the care taken to prevent heterogeneous saturation distribution, only equilibration in a controlled atmosphere sufficiently prevented this. They concluded that rehydrating the samples in a controlled atmosphere of known relative humidity while minimising heterogeneous saturation distribution could be carried out by water vapour condensation in the smallest pores. In their experiments, relative humidity was controlled in a desiccator using a sulphuric acid solution whose activity could be varied by adding water. Hydration was performed under a vacuum and the relative humidity was monitored using a hygrometer. Equilibration was monitored by continuous weighing of the samples and the weight measurements were converted to saturation. The drawbacks of this method are the length of time it takes for the samples to equilibrate and that full saturation cannot be achieved using this method.

B.2 Saturation protocol used in this thesis

In order to minimise heterogeneous saturation distribution, a similar method to that of Schmitt et al. (1994) was used. Partial saturation was achieved by placing the rock samples in an atmosphere of known relative humidity and left to absorb moisture until it reached equilibrium with the saturating environment. The equilibrium moisture content (EMC) was then determined by weighing the sample. This method was also successfully used by Papamichos et al. (1997) and Huang et al. (1986).

The rock samples were oven dried at 40 ^{o}C for 48 hours and then placed under a vacuum until a pressure of 10^{-4} Pa was achieved, ensuring the rock was completely dry. Ultrasonic wave measurements were then taken on the dry

samples. Partial water saturation (S_w) was achieved by placing the samples in an atmosphere of known and controlled relative humidity (RH) for between ten days to two weeks, until they had reached equilibrium. This method is known to give homogeneous S_w distributions for the lower S_w values (compared to imbibition and drainage); similar methods have been used elsewhere (Schmitt et al., 1994, King et al., 2000). Equilibration was monitored by weighing the samples at two-day intervals until the sample mass reached a constant value. The weighing scale used was an A&D GR-200-EC with accuracy up to 10^{-4} g; S_w can then be determined from rock porosity and dry weight using

$$S_w = \frac{M_s - M_d}{\rho_w \phi V_r} \tag{B1}$$

where M_s and M_d are the saturated and dry masses repectively, ρ_w is the density of water taken to be 1 gcm^{-3}, ϕ is the rock porosity, and V_r is the bulk volume of the rock.

The temperature and relative humidity in the laboratory was controlled at 20 ^{o}C and 55% respectively; as such, the samples were also weighed after the measurements to ensure no change in S_w had occurred as a result of exposure to a different RH atmosphere. There was hardly any loss of S_w, which was expected because of the much longer time for samples to absorb moisture and equilibrate compared to the relatively short time taken to make the ultrasonic measurements (< 2 hours in most cases). Also, measurements were not made with the sample directly exposed to the atmosphere as it was placed inside a high pressure rig (see McCann and Sothcott (1992) for detailed equipment setup).

Controlled relative humidity (RH) was achieved using aqueous saturated salt solutions. Greenspan (1977) gave a range of salt solutions that would maintain a given RH at a particular temperature. The salts used and their approximate RH values (at 20 ^{o}C laboratory temperature) were Magnesium Nitrate (54%), Ammonium Sulphate (82%), Sodium Carbonate Decahydrate (92%), and Potassium Sulphate (98%) respectively, giving four different S_w values. A saturated aqueous salt solution was placed at the base of a vacuum desiccator, over which a wire gauze held the rocks in suspension. A hygrometer was also placed on the wire gauze to monitor relative humidity. The desiccator was then placed under a vacuum for about two minutes and left to stand. This procedure was repeated whenever the rocks were taken out to be weighed. The maximum S_w achieved using this method was about 0.4 for both rocks.

The rocks were dried using the process described above, fully saturated in a vacuum with distilled, deionised and de-aired water and then pressurised to 7 MPa for at least 24 hours see (see McCann and Sothcott, 1992). Ultrasonic wave measurements were taken on the fully saturated samples. To achieve intermediate S_w values, we used a modified air/water drainage technique. In order to minimise effects of heterogeneous saturation distribution caused by drainage (Cadoret et al., 1995, Knight et al., 1998), the samples were wrapped in plastic ("cling") film after each drainage process. The wrapped samples were then placed in a desiccator containing the 98% RH solution, sealed (not vacuum sealed) and left for a minimum of 48 hours. The plastic film (and also the high RH atmosphere) prevents further air/water drainage, thus allowing capillary re-distribution over the length of time left to equilibrate (≥ 48 hours). Although steps were taken to avoid/minimize heterogeneous saturation, it should be pointed out that the objective was to observe differences between the fractured rock and the blank rock response as a function of saturation using identical saturation and measurement methods. The drainage method gave pre-determined saturations of approximately 0.90, 0.80, 0.70 and 0.55.

References

ADELINET, M., FORTIN, J., GUÉGUEN, Y., SCHUBNEL, A. & GEOFFROY, L. 2010. Frequency and fluid effects on elastic properties of basalt: Experimental investigations. *Geophysical Research Letters,* 37**,** L02303.

AGERSBORG, R., JAKOBSEN, M., RUUD, B. O. & JOHANSEN, T. A. 2007. Effects of pore fluid pressure on the seismic response of a fractured carbonate reservoir. *Studia Geophysica et Geodaetica,* 51**,** 89-118.

AL-HARRASI, O. H., KENDALL, J. M. & CHAPMAN, M. 2011. Fracture characterization using frequency-dependent shear wave anisotropy analysis of microseismic data. *Geophysical Journal International,* 185**,** 1059-1070.

ALFORD, R. M. Shear data in the presence of azimuthal anisotropy: Dilley, Texas. SEG Technical Program Expanded Abstracts 1986, 1986. 476-479.

ALLAN, J. & SUN, S. Q. 2003. Recovery factor in fractured reservoirs: lessons learned from 100 fractured fields. *Petroleum Exploration and Development,* 30**,** 129-136.

AMALOKWU, K., BEST, A. I., SOTHCOTT, J., CHAPMAN, M., MINSHULL, T. & LI, X.-Y. 2014. Water saturation effects on elastic wave attenuation in porous rocks with aligned fractures. *Geophysical Journal International,* 197**,** 943-947.

AMALOKWU, K., CHAPMAN, M., BEST, A. I., MINSHULL, T. A. & LI, X.-Y. 2015a. Water saturation effects on P-wave anisotropy in synthetic sandstone with aligned fractures. *Geophysical Journal International,* 202**,** 1088-1095.

AMALOKWU, K., CHAPMAN, M., BEST, A. I., SOTHCOTT, J., MINSHULL, T. A. & LI, X.-Y. 2015b. Experimental observation of water saturation effects on shear wave splitting in synthetic rock with fractures aligned at oblique angles. *Geophysical Journal International,* 200**,** 17-24.

ARTS, R., EIKEN, O., CHADWICK, A., ZWEIGEL, P., VAN DER MEER, L. & ZINSZNER, B. 2004. Monitoring of CO2 injected at Sleipner using time-lapse seismic data. *Energy,* 29**,** 1383-1392.

ASS'AD, J. M., TATHAM, R. H. & MCDONALD, J. A. 1992. A physical model study of microcrack-induced anisotropy. *Geophysics,* 57**,** 1562-1570.

AULD, B. A. 1973. *Acoustic fields and waves in solids*, Wiley.

BACKUS, G. E. 1962. Long-wave elastic anisotropy produced by horizontal layering. *J. Geophys. Res.,* 67**,** 4427–4440.

BAKULIN, A., GRECHKA, V. & TSVANKIN, I. 2000. Estimation of fracture parameters from reflection seismic data—Part I: HTI model due to a single fracture set. *Geophysics,* 65**,** 1788-1802.

BANIK, N. C. 1984. Velocity anisotropy of shales and depth estimation in the North Sea basin. *GEOPHYSICS,* 49**,** 1411-1419.

BATZLE, M., HAN, D. & HOFMANN, R. 2006. Fluid mobility and frequency-dependent seismic velocity — Direct measurements. *GEOPHYSICS,* 71**,** N1-N9.

BATZLE, M., HOFMANN, R., HAN, D.-H. & CASTAGNA, J. 2001. Fluids and frequency dependent seismic velocity of rocks. *The Leading Edge,* 20**,** 168-171.

BENSON, G. C. & KIYOHARA, O. 1974. Tabulation of some integral functions describing diffraction effects in the ultrasonic field of a circular piston source. *The Journal of the Acoustical Society of America,* 55**,** 184-185.

BERRYMAN, J. G. 1979. Long-wave elastic anisotropy in transversely isotropic media. *GEOPHYSICS,* 44**,** 896-917.

BERRYMAN, J. G. 1999. Origin of Gassmann's equations. *GEOPHYSICS,* 64**,** 1627-1629.

BERRYMAN, J. G. & WANG, H. F. 2000. Elastic wave propagation and attenuation in a double-porosity dual-permeability medium. *International Journal of Rock Mechanics and Mining Sciences,* 37**,** 63-78.

BEST, A. I. 1992. *The prediction of the reservoir properties of sedimentary rocks from seismic measurements.* Ph.D. thesis, University of Reading.

BEST, A. I., SOTHCOTT, J. & MCCANN, C. 2007. A laboratory study of seismic velocity and attenuation anisotropy in near-surface sedimentary rocks. *Geophysical Prospecting,* 55**,** 609-625.

BIOT, M. A. 1941. General Theory of Three-Dimensional Consolidation. *Journal of Applied Physics,* 12**,** 155-164.

BIOT, M. A. 1956. Theory of propagation of elastic waves in fluid-saturated porous solid, I. Low frequency range, II. Higher frequency range. *J. of the Acous. Soc. of America,* 28**,** 168-191.

BLAIR, D. P. 1990. A direct comparison between vibrational resonance and pulse transmission data for assessment of seismic attenuation in rock. *Geophysics,* 55**,** 51-60.

BOURBIE, T. & ZINSZNER, B. 1984. Saturation methods and attenuation versus saturation relationships in fontainebleau sandstone. *SEG Technical Program Expanded Abstracts*

BOURBIE, T. & ZINSZNER, B. 1985. Hydraulic and acoustic properties as a function of porosity in Fontainebleau Sandstone. *Journal of Geophysical Research: Solid Earth,* 90**,** 11524-11532.

BRIE, A., PAMPURI, F., MARSALA, A. & MEAZZA, O. 1995. Shear sonic interpretation in gas-bearing sands. SPE Annual Technical Conference and Exhibition, 1995.

BROWN, R. & KORRINGA, J. 1975. On The Dependence Of The Elastic Properties Of A Porous Rock On The Compressibility Of The Pore Fluid. *GEOPHYSICS,* 40**,** 608-616.

CADORET, T., MARION, D. & ZINSZNER, B. 1995. Influence of frequency and fluid distribution on elastic wave velocities in partially saturated limestones. *Journal of Geophysical Research: Solid Earth,* 100**,** 9789-9803.

CADORET, T., MAVKO, G. & ZINSZNER, B. 1998. Fluid distribution effect on sonic attenuation in partially saturated limestones. *Geophysics,* 63**,** 154-160.

CARCIONE, J., GUREVICH, B., SANTOS, J. & PICOTTI, S. 2013. Angular and Frequency-Dependent Wave Velocity and Attenuation in Fractured Porous Media. *Pure and Applied Geophysics,* 170**,** 1673-1683.

CARCIONE, J., HELLE, H. & PHAM, N. 2003. White's model for wave propagation in partially saturated rocks: Comparison with poroelastic numerical experiments. *GEOPHYSICS,* 68**,** 1389-1398.

CARCIONE, J. M. & PICOTTI, S. 2006. P-wave seismic attenuation by slow-wave diffusion: Effects of inhomogeneous rock properties. *GEOPHYSICS,* 71**,** O1-O8.

CASPARI, E., MÜLLER, T. & GUREVICH, B. 2011. Time-lapse sonic logs reveal patchy CO2 saturation in-situ. *Geophysical Research Letters,* 38.

CASTAGNA, J. P. 2001. Recent advances in seismic lithologic analysis. *GEOPHYSICS,* 66**,** 42-46.

CASTAGNA, J. P., SUN, S. & SIEGFRIED, R. W. 2003. Instantaneous spectral analysis: Detection of low-frequency shadows associated with hydrocarbons. *The Leading Edge,* 22**,** 120-127.

CHAPMAN, M. 2003. Frequency-dependent anisotropy due to meso-scale fractures in the presence of equant porosity. *Geophysical Prospecting,* 51**,** 369-379.

CHAPMAN, M. 2009. Modeling the effect of multiple sets of mesoscale fractures in porous rock on frequency-dependent anisotropy. *Geophysics,* 74**,** D97-D103.

CHAPMAN, M., MAULTZSCH, S., LIU, E. & LI, X.-Y. 2003. The effect of fluid saturation in an anisotropic multi-scale equant porosity model. *Journal of Applied Geophysics,* 54**,** 191-202.

CHAPMAN, M., ZATSEPIN, S. V. & CRAMPIN, S. 2002. Derivation of a microstructural poroelastic model. *Geophysical Journal International,* 151**,** 427-451.

CHAU, K. T. & WONG, R. H. C. 1997. Effective moduli of microcraked-rock: Theories and Experiments. *International Journal of Damage Mechanics,* 6**,** 258-277.

CHESNOKOV, E., BAYUK, I. O. & AMMERMAN, M. 2010. Determination of shale stiffness tensor from standard logs. *Geophysical Prospecting,* 58**,** 1063-1082.

CHICHININA, T., OBOLENTSEVA, I., GIK, L., BOBROV, B. & RONQUILLO-JARILLO, G. 2009. Attenuation anisotropy in the linear-slip model: Interpretation of physical modeling data. *GEOPHYSICS,* 74**,** WB165-WB176.

CHILINGARIAN, G. V. & WOLF, K. H. 1976. *Compaction of coarse-grained sediments, II (developments in sedimentology, 18 B)* Amsterdam, Elsevier.

CRAMPIN, S. 1981. A review of wave motion in anisotropic and cracked elastic-media. *Wave Motion,* 3**,** 343-391.

CRAMPIN, S. 1984. An introduction to wave propagation in anisotropic media. *Geophysical Journal of the Royal Astronomical Society,* 76**,** 17-28.

CRAMPIN, S. 1985. Evaluation of anisotropy by shear-wave splitting. *GEOPHYSICS,* 50**,** 142-152.

CRAMPIN, S. 1987. Geological and industrial implications of extensive-dilatancy anisotropy. *Nature* 328**,** 491–496.

CRAMPIN, S. 1989. SUGGESTIONS FOR A CONSISTENT TERMINOLOGY FOR SEISMIC ANISOTROPY. *Geophysical Prospecting,* 37**,** 753-770.

CRAMPIN, S. 1994. The fracture criticality of crustal rocks. *Geophysical Journal International,* 118**,** 428-438.

CRAMPIN, S. 1999. Calculable fluid–rock interactions. *Journal of the Geological Society,* 156**,** 501-514.

CRAMPIN, S., BUSH, I., NAVILLE, C. & TAYLOR, D. 1986. Estimating the internal structure of reservoirs with shear-wave VSPs. *The Leading Edge,* 5**,** 35-39.

CRAMPIN, S., EVANS, R., UCER, B., DOYLE, M., DAVIS, J. P., YEGORKINA, G. V. & MILLER, A. 1980a. Observations of dilatancy-induced polarization anomalies and earthquake prediction. *Nature,* 286**,** 874-877.

CRAMPIN, S. & LOVELL, J. H. 1991. A decade of shear-wave splitting in the Earth's crust: what does it mean? what use can we make of it? and what should we do next? *Geophysical Journal International,* 107**,** 387-407.

CRAMPIN, S., MCGONIGLE, R. & BAMFORD, D. 1980b. Estimating crack parameters from observations of P-wave velocity anisotropy. *Geophysics,* 45**,** 345-360.

CRAMPIN, S. & PEACOCK, S. 2005. A review of shear-wave splitting in the compliant crack-critical anisotropic Earth. *Wave Motion,* 41**,** 59-77.

DE FIGUEIREDO, J. J. S., SCHLEICHER, J., STEWART, R. R., DAYUR, N., OMOBOYA, B., WILEY, R. & WILLIAM, A. 2013. Shear wave anisotropy from aligned inclusions: ultrasonic frequency dependence of velocity and attenuation. *Geophysical Journal International*.

DELLINGER, J. & VERNIK, L. 1994. Do traveltimes in pulse-transmission experiments yield anisotropic group or phase velocities? *Geophysics,* 59**,** 1774-1779.

DETOURNAY, E. & CHENG, A. 1993. Fundamentals of poroelasticity, Comprehensive Rock Engineering, Vol 2: Analysis and Design Methods, Eds. Brown, ET, Fairhurst, CH and Hoek, E. Pergamon.

DOAN, M.-L., CONIN, M., HENRY, P., WIERSBERG, T., BOUTT, D., BUCHS, D., SAFFER, D., MCNEILL, L. C., CUKUR, D. & LIN, W. 2011. Quantification of free gas in the Kumano fore-arc basin detected from borehole physical properties: IODP NanTroSEIZE drilling Site C0009. *Geochemistry, Geophysics, Geosystems,* 12**,** Q0AD06.

DOMENICO, S. 1974. EFFECT OF WATER SATURATION ON SEISMIC REFLECTIVITY OF SAND RESERVOIRS ENCASED IN SHALE. *GEOPHYSICS,* 39**,** 759-769.

DOMENICO, S. N. 1976. Effect of brine-gas mixture on velocity in an unconsolidated sand reservoir. *Geophysics,* 41**,** 882-894.

DUTTA, N. & ODÉ, H. 1979a. Attenuation and dispersion of compressional waves in fluid-filled porous rocks with partial gas saturation (White model)—Part II: Results. *GEOPHYSICS,* 44**,** 1789-1805.

DUTTA, N. C. & ODÉ, H. 1979b. Attenuation and dispersion of compressional waves in fluid-filled porous rocks with partial gas saturation (White model); Part I, Biot theory. *Geophysics,* 44**,** 1777-1788.

DUTTA, N. C. & SERIFF, A. J. 1979. On White's model of attenuation in rocks with partial gas saturation. *Geophysics,* 44**,** 1806-1812.

DVORKIN, J., MAVKO, G. & NUR, A. 1995. Squirt flow in fully saturated rocks. *GEOPHYSICS,* 60**,** 97-107.

DVORKIN, J., MOOS, D., PACKWOOD, J. L. & NUR, A. M. 1999. Identifying patchy saturation from well logs. *GEOPHYSICS,* 64**,** 1756-1759.

DVORKIN, J., NOLEN-HOEKSEMA, R. C. & NUR, A. 1994. The squirt-flow mechanism; macroscopic description. *Geophysics,* 59**,** 428-438.

DVORKIN, J. & NUR, A. 1993. Dynamic poroelasticity: A unified model with the squirt and the Biot mechanisms. *GEOPHYSICS,* 58**,** 524-533.

DVORKIN, J. P. & MAVKO, G. 2006. Modeling attenuation in reservoir and nonreservoir rock. *The Leading Edge,* 25**,** 194-197.

ENSLEY, R. A. 1984. Comparison of P- and S-wave seismic data; a new method for detecting gas reservoirs. *Geophysics,* 49**,** 1420-1431.

ESHELBY, J. D. 1957. The Determination of the Elastic Field of an Ellipsoidal Inclusion, and Related Problems. *Proceedings of the Royal Society of London A: Mathematical, Physical and Engineering Sciences,* 241**,** 376-396.

FERNØ, M. A. 2012. *Enhanced Oil Recovery in Fractured Reservoirs*, INTECH Open Access Publisher.

GAISER, J. E. Advantages of 3-D PS-wave data to unravel S-wave birefringence for fracture detection. SEG Technical Program Expanded Abstracts 2000, 2000. 1201-1204.

GARBIN, H. & KNOPOFF, L. 1973. The compressional modulus of a material permeated by a random distribution of circular cracks. *Quarterly of Applied Mathematics,* 30**,** 453-464.

GARBIN, H. & KNOPOFF, L. 1975. ELASTIC-MODULI OF A MEDIUM WITH LIQUID-FILLED CRACKS. AMER MATHEMATICAL SOC 201 CHARLES ST, PROVIDENCE, RI 02940-2213.

GASSMANN, F. 1951. Elasticity of porous media. *Vierteljahrsschrder Naturforschenden Gesselschaft,* 96**,** 1-23.

GIST, G. A. 1994a. Fluid effects on velocity and attenuation in sandstones. *The Journal of the Acoustical Society of America,* 96**,** 1158-1173.

GIST, G. A. 1994b. Interpreting laboratory velocity measurements in partially gas-saturated rocks. *Geophysics,* 59**,** 1100-1109.

GRAY, D. & HEAD, K. 2000. Fracture detection in Manderson Field: A 3-D AVAZ case history. *The Leading Edge,* 19**,** 1214-1221.

GRECHKA, V. & TSVANKIN, I. 1998. 3-D description of normal moveout in anisotropic inhomogeneous media. *Geophysics,* 63**,** 1079-1092.

GREENSPAN, L. 1977. Humidity Fixed Points of Binary Saturated Aqueous Solutions. *J. Res. Nat. Bur. Stand. (U.S.) - A (Phys. And Chem.),* 81A**,** 89-96.

GREGORY, A. 1976. FLUID SATURATION EFFECTS ON DYNAMIC ELASTIC PROPERTIES OF SEDIMENTARY ROCKS. *Geophysics,* 41**,** 895-921.

GUREVICH, B. 2003. Elastic properties of saturated porous rocks with aligned fractures. *Journal of Applied Geophysics,* 54**,** 203-218.

GUREVICH, B., BRAJANOVSKI, M., GALVIN, R. J., MÜLLER, T. M. & TOMS-STEWART, J. 2009. P-wave dispersion and attenuation in fractured and porous reservoirs – poroelasticity approach. *Geophysical Prospecting,* 57**,** 225-237.

GUREVICH, B., MAKARYNSKA, D., DE PAULA, O. B. & PERVUKHINA, M. 2010. A simple model for squirt-flow dispersion and attenuation in fluid-saturated granular rocks. *Geophysics,* 75**,** N109-N120.

HELBIG, K. & THOMSEN, L. 2005. 75-plus years of anisotropy in exploration and reservoir seismics: A historical review of concepts and methods. *GEOPHYSICS,* 70**,** 9ND-23ND.

HESS, H. H. 1964. Seismic Anisotropy of the Uppermost Mantle under Oceans. *Nature,* 203**,** 629-631.

HILL, R. 1963. Elastic properties of reinforced solids: Some theoretical principles. *Journal of the Mechanics and Physics of Solids,* 11**,** 357-372.

HORNE, S. 2003. Fracture characterization from walkaround VSPs. *Geophysical Prospecting,* 51**,** 493-499.

HUANG , S. L., AUGHENBAUGH, N. B. & ROCKAWAY, J. D. 1986. Swelling pressure studies of shales. *Int. J. Rock Mech. Min. Sci. & Geomech. Abstr.,* 23**,** 371-377.

HUDSON, J. A. 1981. Wave speeds and attenuation of elastic waves in material containing cracks. *Geophysical Journal of the Royal Astronomical Society,* 64**,** 133-150.

HUDSON, J. A. 1986. A higher order approximation to the wave propagation constants for a cracked solid. *Geophysical Journal of the Royal Astronomical Society,* 87**,** 265-274.

HUDSON, J. A. & CRAMPIN, S. 2003. Comment on: 'The 3D shear experiment over the Natih field in Oman: the effects of fracture-filling fluids on shear propagation' by C.M. van der Kolk, W.S. Guest and J.H.H.M. Potters. *Geophysical Prospecting,* 51**,** 365-368.

HUDSON, J. A., LIU, E. & CRAMPIN, S. 1996. The mechanical properties of materials with interconnected cracks and pores. *Geophysical Journal International,* 124**,** 105-112.

HUDSON, J. A., POINTER, T. & LIU, E. 2001. Effective-medium theories for fluid-saturated materials with aligned cracks. *Geophysical Prospecting,* 49**,** 509-522.

JAKOBSEN, M. 2004. The interacting inclusion model of wave-induced fluid flow. *Geophysical Journal International,* 158**,** 1168-1176.

JAKOBSEN, M. & CHAPMAN, M. 2009. Unified theory of global flow and squirt flow in cracked porous media. *GEOPHYSICS,* 74**,** WA65-WA76.

JAKOBSEN, M. & HUDSON, J. 2003. Visco-Elastic Waves in Rock-Like Composites. *Studia Geophysica et Geodaetica,* 47**,** 793-826.

JAKOBSEN, M., JOHANSEN, T. A. & MCCANN, C. 2003. The acoustic signature of fluid flow in complex porous media. *Journal of Applied Geophysics,* 54**,** 219-246.

JOHNSON, D. L. 2001. Theory of frequency dependent acoustics in patchy-saturated porous media. *Journal of the Acoustical Society of America,* 110**,** 682-694.

JOHNSON, D. L., PLONA, T. J. & KOJIMA, H. 1994. Probing porous media with first and second sound. II. Acoustic properties of water-saturated porous media. *Journal of Applied Physics,* 76**,** 115-125.

JOHNSTON, D., TOKSÖZ, M. & TIMUR, A. 1979. Attenuation of seismic waves in dry and saturated rocks: II. Mechanisms. *GEOPHYSICS,* 44**,** 691-711.

KELDER, O. & SMEULDERS, D. M. J. 1997. Observation of the Biot slow wave in water-saturated Nivelsteiner sandstone. *GEOPHYSICS,* 62**,** 1794-1796.

KING, M. S., MARSDEN, J. R. & DENNIS, J. W. 2000. Biot dispersion for P- and S-wave velocities in partially and fully saturated sandstones. *Geophysical Prospecting,* 48**,** 1075-1089.

KLIMENTOS, T. 1995. Attenuation of P- and S-waves as a method of distinguishing gas and condensate from oil and water. *Geophysics,* 60**,** 447-458.

KLIMENTOS, T. & MCCANN, C. 1988. Why is the Biot slow compressional wave not observed in real rocks? *GEOPHYSICS,* 53**,** 1605-1609.

KNIGHT, R., DVORKIN, J. & NUR, A. 1998. Acoustic signatures of partial saturation. *GEOPHYSICS,* 63**,** 132-138.

KNIGHT, R. & NOLEN-HOEKSEMA, R. 1990. A laboratory study of the dependence of elastic wave velocities on pore scale fluid distribution. *Geophysical Research Letters,* 17**,** 1529-1532.

KOESOEMADINATA, A. & MCMECHAN, G. 2001. Empirical estimation of viscoelastic seismic parameters from petrophysical properties of sandstone. *Geophysics,* 66**,** 1457-1470.

KONG, L., GUREVICH, B., MÜLLER, T. M., WANG, Y. & YANG, H. 2013. Effect of fracture fill on seismic attenuation and dispersion in fractured porous rocks. *Geophysical Journal International,* 195**,** 1679-1688.

LE RAVALEC, M., GUÉGUEN, Y. & CHELIDZE, T. 1996. Elastic wave velocities in partially saturated rocks: Saturation hysteresis. *Journal of Geophysical Research: Solid Earth,* 101**,** 837-844.

LEBEDEV, M., GUREVICH, B., TOMS, J., CLENNEL, B. & PERVUKHINA, M. 2008. Direct laboratory observation of velocity-saturation relation transition during rocks saturation. *SEG Technical Program Expanded Abstracts***,** 1840-1844.

LEBEDEV, M., TOMS-STEWART, J., CLENNELL, B., PERVUKHINA, M., SHULAKOVA, V., PATERSON, L., MÜLLER, T. M., GUREVICH, B. & WENZLAU, F. 2009. Direct laboratory observation of patchy saturation and its effects on ultrasonic velocities. *The Leading Edge,* 28**,** 24-27.

LEFEUVRE, F. Fracture related anisotropy detection and analysis: “And if the P-waves were enough? ”. SEG Technical Program Expanded Abstracts 1994, 1994. 942-945.

LEI, X. & XUE, Z. 2009. Ultrasonic velocity and attenuation during CO2 injection into water-saturated porous sandstone: Measurements using difference seismic tomography. *Physics of the Earth and Planetary Interiors,* 176**,** 224-234.

LI, X. Y. 1999. Fracture detection using azimuthal variation of P-wave moveout from orthogonal seismic survey lines. *GEOPHYSICS,* 64**,** 1193-1201.

LIU, D., YUE, X., WANG, L., HOU, J. & ZHANG, J. 2006. Model study on the irreducible water saturation by centrifuge experiments. *Journal of Petroleum Science and Engineering,* 53**,** 77-82.

LIU, E., HUDSON, J. A. & POINTER, T. 2000. Equivalent medium representation of fractured rock. *Journal of Geophysical Research: Solid Earth,* 105**,** 2981-3000.

LIU, E. & MARTINEZ, A. 2013. *Seismic fracture characterization: Concepts and practical applications*, Eage publications bv.

LIU, E., QUEEN, J. H., LI, X. Y., CHAPMAN, M., MAULTZSCH, S., LYNN, H. B. & CHESNOKOV, E. M. 2003. Observation and analysis of frequency-dependent anisotropy from a multicomponent VSP at Bluebell-Altamont field, Utah. *Journal of Applied Geophysics,* 54**,** 319-333.

LYNN, H. B., BECKHAM, W. E., SIMON, K. M., BATES, C. R., LAYMAN, M. & JONES, M. 1999. P-wave and S-wave azimuthal anisotropy at a natural fractured gas reservoir, Bluebell-Altamont Field, Utah. *Geophysics,* 64**,** 1312-1328.

LYNN, H. B., SIMON, K. M., BATES, C. R. & DOK, R. V. 1996. Azimuthal anisotropy in P-wave 3-D (multiazimuth) data. *The Leading Edge,* 15**,** 923-928.

LYNN, H. B. & THOMSEN, L. A. Reflection shear-wave data along the principal axes of azimuthal anisotropy. SEG Technical Program Expanded Abstracts 1986, 1986. 473-476.

LYNN, H. B. & THOMSEN, L. A. 1990. Reflection shear-wave data collected near the principle axes of azimuthal anisotropy. *Geophysics,* 55**,** 147-156.

MACBETH, C. 1999. Azimuthal variation in P-wave signatures due to fluid flow. *Geophysics,* 64**,** 1181-1192.

MALLICK, S., CRAFT, K. L., MEISTER, L. J. & CHAMBERS, R. E. 1998. Determination of the principal directions of azimuthal anisotropy from P-wave seismic data. *GEOPHYSICS,* 63**,** 692-706.

MARSON-PIDGEON, K. & SAVAGE, M. K. 1997. Frequency-dependent anisotropy in Wellington, New Zealand. *Geophysical Research Letters,* 24**,** 3297-3300.

MAULTZSCH, S. 2005. *Analysis of frequency-dependent anisotropy in VSP data.* University of Edinburgh.

MAULTZSCH, S., CHAPMAN, M., LIU, E. & LI, X.-Y. 2007. Modelling and analysis of attenuation anisotropy in multi-azimuth VSP data from the Clair field. *Geophysical Prospecting,* 55**,** 627-642.

MAULTZSCH, S., CHAPMAN, M., LIU, E. & LI, X. Y. 2003a. Modelling frequency-dependent seismic anisotropy in fluid-saturated rock with aligned fractures: implication of fracture size estimation from anisotropic measurements. *Geophysical Prospecting,* 51**,** 381-392.

MAULTZSCH, S., HORNE, S., ARCHER, S. & BURKHARDT, H. 2003b. Effects of an anisotropic overburden on azimuthal amplitude analysis in horizontal transverse isotropic media. *Geophysical Prospecting,* 51**,** 61-74.

MAVKO, G. & JIZBA, D. 1991. Estimating grain-scale fluid effects on velocity dispersion in rocks. *Geophysics,* 56**,** 1940-1949.

MAVKO, G. & MUKERJI, T. 1998. Bounds on low-frequency seismic velocities in partially saturated rocks. *GEOPHYSICS,* 63**,** 918-924.

MAVKO, G., MUKERJI, T. & DVORKIN, J. 2009. *The Rock Physics Handbook*, Cambridge University Press.

MAVKO, G. & NOLEN-HOEKSEMA, R. 1994. Estimating seismic velocities at ultrasonic frequencies in partially saturated rocks. *GEOPHYSICS,* 59**,** 252-258.

MAVKO, G. & NUR, A. 1975. Melt squirt in the asthenosphere. *Journal of Geophysical Research,* 80**,** 1444-1448.

MAVKO, G. M. & NUR, A. 1979. Wave attenuation in partially saturated rocks. *Geophysics,* 44.

MCCANN, C. & SOTHCOTT, J. 1992. Laboratory measurements of the seismic properties of sedimentary rocks. *Geological Society, London, Special Publications,* 65**,** 285-297.

MIKSIS, M. J. 1988. Effects of contact line movement on the dissipation of waves in partially saturated rocks. *Journal of Geophysical Research: Solid Earth,* 93**,** 6624-6634.

MONSEN, K. & JOHNSTAD, S. E. 2005. Improved understanding of velocity–saturation relationships using 4D computer-tomography acoustic measurements. *Geophysical Prospecting,* 53**,** 173-181.

MUELLER, M. C. 1991. Prediction of lateral variability in fracture intensity using multicomponent shear-wave surface seismic as a precursor to horizontal drilling in the Austin Chalk. *Geophysical Journal International,* 107**,** 409-415.

MÜLLER, T., GUREVICH, B. & LEBEDEV, M. 2010. Seismic wave attenuation and dispersion resulting from wave-induced flow in porous rocks — A review. *GEOPHYSICS,* 75**,** 75A147-75A164.

MÜLLER, T. M. & GUREVICH, B. 2004. One-dimensional random patchy saturation model for velocity and attenuation in porous rocks. *Geophysics,* 69**,** 1166-1172.

MÜLLER, T. M., TOMS-STEWART, J. & WENZLAU, F. 2008. Velocity-saturation relation for partially saturated rocks with fractal pore fluid distribution. *Geophysical Research Letters,* 35**,** L09306.

MURPHY, W., WINKLER, K. & KLEINBERG, R. 1986. Acoustic relaxation in sedimentary rocks: Dependence on grain contacts and fluid saturation. *Geophysics,* 51**,** 757-766.

MURPHY, W. F. 1982. Effects of partial water saturation on attenuation in Massillon sandstone and Vycor porous glass. *J. Acoust Soc. Am.,* 71**,** 1458–1468.

MURPHY, W. F. 1984. Acoustic measures of partial gas saturation in tight sandstones. *Journal of Geophysical Research: Solid Earth,* 89**,** 11549-11559.

MURPHY, W. F. 1985. Sonic and ultrasonic velocities: Theory Versus experiment. *Geophysical Research Letters,* 12**,** 85-88.

NAKAGAWA, S., KNEAFSEY, T. J., DALEY, T. M., FREIFELD, B. M. & REES, E. V. 2013. Laboratory seismic monitoring of supercritical CO2 flooding in sandstone cores using the Split Hopkinson Resonant Bar technique with concurrent x-ray Computed Tomography imaging. *Geophysical Prospecting,* 61**,** 254-269.

NELSON, R. 2001. *Geologic analysis of naturally fractured reservoirs*, Gulf Professional Publishing.

NISHIZAWA, O. 1982. SEISMIC VELOCITY ANISOTROPY IN A MEDIUM CONTAINING ORIENTED CRACKS

TRANSVERSELY ISOTROPIC CASE. *Journal of Physics of the Earth,* 30**,** 331-347.

NOLEN-HOEKSEMA, R. C. 2000. Modulus—porosity relations, Gassmann's equations, and the low-frequency elastic-wave response to fluids. *GEOPHYSICS,* 65**,** 1355-1363.

NORRIS, A. N. 1993. Low-frequency dispersion and attenuation in partially saturated rocks. *The Journal of the Acoustical Society of America,* 94**,** 359-370.

O'CONNELL, R. J. & BUDIANSKY, B. 1974. Seismic velocities in dry and saturated cracked solids. *Journal of Geophysical Research,* 79**,** 5412-5426.

O'CONNELL, R. J. & BUDIANSKY, B. 1977. Viscoelastic properties of fluid-saturated cracked solids. *Journal of Geophysical Research,* 82**,** 5719-5735.

ODA, M., SUZUKI, K. & MAESHIBU, T. 1984. Elastic compliance for rock-like materials with random cracks. *Soils and Foundations,* 24**,** 27-40.

OLOFSSON, B., PROBERT, T., KOMMEDAL, J. H. & BARKVED, O. I. 2003. Azimuthal anisotropy from the Valhall 4C 3D survey. *The Leading Edge,* 22**,** 1228-1235.

ONISHI, K., TSUKADA, K., MATSUOKA, T. & YAMADA, Y. 2006. Measuring elastic wave of porous media in the freezing and thawing process of methane hydrate. *Proceedings of the 8th SEGJ International Symposium.*

PALMER, I. D. & TRAVIOLIA, M. L. 1980. Attenuation by squirt flow in undersaturated gas sands. *GEOPHYSICS,* 45**,** 1780-1792.

PAPADAKIS, E. P. 1972. Ultrasonic Diffraction Loss and Phase Change for Broad-Band Pulses. *The Journal of the Acoustical Society of America,* 52**,** 847-849.

PAPAGEORGIOU, G. & CHAPMAN, M. 2015. Multifluid squirt flow and hysteresis effects on the bulk modulus–water saturation relationship. *Geophysical Journal International,* 203**,** 814-817.

PAPAMICHOS, E., BRIGNOLI, M. & SANTARELLI, F. J. 1997. An experimental and theoretical study of a partially saturated collapsible rock. *Mechanics of Cohesive-frictional Materials,* 2**,** 251-278.

PEACOCK, S., MCCANN, C., SOTHCOTT, J. & ASTIN, T. 1994a. Experimental measurements of seismic attenuation In microfractured sedimentary rock. *GEOPHYSICS,* 59**,** 1342-1351.

PEACOCK, S., MCCANN, C., SOTHCOTT, J. & ASTIN, T. R. 1994b. Seismic velocities in fractured rocks: an experimental verification of Hudson's theory1. *Geophysical Prospecting,* 42**,** 27-80.

PLONA, T. J. 1980. Observation of a second bulk compressional wave in a porous medium at ultrasonic frequencies. *Applied Physics Letters,* 36**,** 259-261.

POINTER, T., LIU, E. & HUDSON, J. A. 2000. Seismic wave propagation in cracked porous media. *Geophysical Journal International,* 142**,** 199-231.

PRIDE, S. & BERRYMAN, J. 2003a. Linear dynamics of double-porosity and dual-permeability materials: Part II—Fluid transport equations. *Physical Review E,* 68**,** 036604.

PRIDE, S. R. & BERRYMAN, J. G. 2003b. Linear dynamics of double-porosity dual-permeability materials. I. Governing equations and acoustic attenuation. *Physical Review E,* 68**,** 036603.

PRIDE, S. R., BERRYMAN, J. G. & HARRIS, J. M. 2004. Seismic attenuation due to wave-induced flow. *Journal of Geophysical Research: Solid Earth,* 109**,** B01201.

PRIDE, S. R., HARRIS, J. M., JOHNSON, D. L., MATEEVA, A., NIHEL, K. T., NOWACK, R. L., RECTOR, J. W., SPETZLER, H., WU, R., YAMOMOTO, T., BERRYMAN, J. G. & FEHLER, M. 2003. Permeability dependence of seismic amplitudes. *The Leading Edge,* 22**,** 518-525.

QI, Q., MÜLLER, T. M., GUREVICH, B., LOPES, S., LEBEDEV, M. & CASPARI, E. 2014. Quantifying the effect of capillarity on attenuation and dispersion in patchy-saturated rocks. *Geophysics,* 79**,** WB35-WB50.

QIAN, Z., CHAPMAN, M., LI, X., DAI, H., LIU, E., ZHANG, Y. & WANG, Y. 2007. Use of multicomponent seismic data for oil-water discrimination in fractured reservoirs. *The Leading Edge,* 26**,** 1176-1184.

QUEEN, J. H. & RIZER, W. D. 1990. An integrated study of seismic anisotropy and the natural fracture system at the Conoco Borehole Test Facility, Kay County, Oklahoma. *Journal of Geophysical Research: Solid Earth,* 95**,** 11255-11273.

RAITT, R. W., SHOR, G. G., FRANCIS, T. J. G. & MORRIS, G. B. 1969. Anisotropy of the Pacific upper mantle. *Journal of Geophysical Research,* 74**,** 3095-3109.

RATHORE, J. S., FJAER, E., HOLT, R. M. & RENLIE, L. 1995. P- and S-wave anisotropy of a synthetic sandstone with controlled crack geometryl1. *Geophysical Prospecting,* 43**,** 711-728.

REISS, L. H. 1980. *The reservoir engineering aspects of fractured formations*, Editions Technip.

REUSS, A. 1929. Berechnung der Fließgrenze von Mischkristallen auf Grund der Plastizitätsbedingung für Einkristalle. *ZAMM - Journal of Applied Mathematics and Mechanics / Zeitschrift für Angewandte Mathematik und Mechanik,* 9**,** 49-58.

RICE, J. 1998. Elasticity of fluid-infiltrated porous solids (poroelasticity). *Stress,* 2**,** 2.

RUBINO, J., GUARRACINO, L., MÜLLER, T. M. & HOLLIGER, K. 2013. Do seismic waves sense fracture connectivity? *Geophysical Research Letters,* 40**,** 692-696.

RÜGER, A. 1997. P-wave reflection coefficients for transversely isotropic models with vertical and horizontal axis of symmetry. *Geophysics,* 62**,** 713-722.

RÜGER, A. & TSVANKIN, I. 1997. Using AVO for fracture detection: Analytic basis and practical solutions. *The Leading Edge,* 16**,** 1429-1434.

SAMS, M. S., NEEP, J. P., WORTHINGTON, M. H. & KING, M. S. 1997. The measurement of velocity dispersion and frequency-dependent intrinsic attenuation in sedimentary rocks. *GEOPHYSICS,* 62**,** 1456-1464.

SAYERS, C. M. 2002. Fluid-dependent shear-wave splitting in fractured media. *Geophysical Prospecting,* 50**,** 393-401.

SAYERS, C. M. 2009. Seismic characterization of reservoirs containing multiple fracture sets. *Geophysical Prospecting,* 57**,** 187–192.

SAYERS, C. M. & DASGUPTA, S. 2015. Elastic anisotropy of the Middle Bakken Formation. *GEOPHYSICS,* 80**,** D23-D29.

SAYERS, C. M. & KACHANOV, M. 1991. A simple technique for finding effective elastic constants of cracked solids for arbitrary crack orientation statistics. *International Journal of Solids and Structures,* 27**,** 671-680.

SAYERS, C. M. & RICKETT, J. E. 1997. Azimuthal variation in AVO response for fractured gas sands. *Geophysical Prospecting,* 45**,** 165-182.

SCHLUMBERGER 1991. *Log Interpretation Principles/Applications*, Schlumberger Educational Services.

SCHMITT, L., FORSANS, T. & SANTARELLI, F. J. 1994. Shale testing and capillary phenomena. *Int. J. Rock Mech. Min. Sci. & Geomech. Abstr.,* 31**,** 411 – 427.

SCHOENBERG, M. 1980. Elastic wave behavior across linear slip interfaces. *The Journal of the Acoustical Society of America,* 68**,** 1516-1521.

SCHOENBERG, M. 1983. REFLECTION OF ELASTIC WAVES FROM PERIODICALLY STRATIFIED MEDIA WITH INTERFACIAL SLIP*. *Geophysical Prospecting,* 31**,** 265-292.

SCHOENBERG, M. & DOUMA, J. 1988. ELASTIC WAVE PROPAGATION IN MEDIA WITH PARALLEL FRACTURES AND ALIGNED CRACKS1. *Geophysical Prospecting,* 36**,** 571-590.

SCHOENBERG, M. & MUIR, F. 1989. A calculus for finely layered anisotropic media. *GEOPHYSICS,* 54**,** 581-589.

SCHOENBERG, M. & PROTAZIO, J. 1992. "Zoeppritz" rationalized, and generalized to anisotropic media. *Journal of Seismic Exploration,* 1**,** 125-144.

SCHOENBERG, M. & SAYERS, C. M. 1995. Seismic anisotropy of fractured rock. *Geophysics,* 60**,** 204-211.

SELLEY, R. C. 2000. *Applied sedimentology*, Elsevier.

SHERLOCK, D. & SIGGINS, A. 2004. The development of synthetic CIPS sandstones for geophysical research. *SEG Technical Program Expanded Abstracts.*

SHERLOCK, D. H., DODDS, K. J. & WEIR, G. 2007. The development of Analog Reservoir Modelling for seismic and reservoir engineering research. *Journal of Petroleum Science and Engineering,* 57**,** 82–91.

SHUCK, E. L. 1991. Azimuthal anisotropy analysis from shear VSPs. *Geophysical Journal International,* 107**,** 639-647.

SIL, S., SEN, M. & GUREVICH, B. 2011. Analysis of fluid substitution in a porous and fractured medium. *GEOPHYSICS,* 76**,** WA157-WA166.

SIL, S., SRIVASTAVA, R. P. & SEN, M. K. 2010. Observation of shear-wave splitting in the multicomponent node data from Atlantis field, Gulf of Mexico. *Geophysical Prospecting,* 58**,** 953-964.

SIMIYU, S. M. 2000. Geothermal reservoir characterization: Application of microseismicity and seismic wave properties at Olkaria, Kenya rift. *Journal of Geophysical Research: Solid Earth,* 105**,** 13779-13795.

SMITH, T. M., SONDERGELD, C. H. & RAI, C. S. 2003. Gassmann fluid substitutions: A tutorial. *GEOPHYSICS,* 68**,** 430-440.

SODAGAR, T. M. & LAWTON, D. C. 2014. Time-lapse seismic modelling of CO2 fluid substitution in the Devonian Redwater Reef, Alberta, Canada. *Geophysical Prospecting,* 62**,** 518-529.

SPENCER, J. W. 1981. Stress relaxations at low frequencies in fluid-saturated rocks: Attenuation and modulus dispersion. *J. Geophys. Res.,* 86**,** 1803–1812.

TAYLOR, J. R. 1982. *An Introduction to Error Analysis: The Study of Uncertainties in Physical Measurements*, University science books.

TERZAGHI, K. V. 1923. Die berechnung der durchlassigkeitsziffer des tones aus dem verlauf der hydrodynamischen spannungserscheinungen. *Sitzungsberichte der Akademie der Wissenschaften in Wien, Mathematisch-Naturwissenschaftliche Klasse, Abteilung IIa,* 132**,** 125-138.

THOMSEN, L. 1986. Weak elastic anisotropy. *Geophysics* 51**,** 1954-1966.

THOMSEN, L. 1988. Reflection seismology over azimuthally anisotropic media. *Geophysics,* 53**,** 304-313.

THOMSEN, L. 1995. Elastic anisotropy due to aligned cracks in porous rock. *Geophysical Prospecting* 43**,** 805-829.

THOMSEN, L. 2002. *Understanding seismic anisotropy in exploration and exploitation*, Society of Exploration Geophysicist.

TIEN, Y. M. & TSAO, P. F. 2000. Preparation and mechanical properties of artificial transversely isotropic rock. *International Journal of Rock Mechanics and Mining Sciences,* 37**,** 1001–1012.

TILLOTSON, P., CHAPMAN, M., BEST, A. I., SOTHCOTT, J., MCCANN, C., SHANGXU, W. & LI, X.-Y. 2011. Observations of fluid-dependent shear-wave splitting in synthetic porous rocks with aligned penny-shaped fractures‡. *Geophysical Prospecting,* 59**,** 111-119.

TILLOTSON, P., CHAPMAN, M., SOTHCOTT, J., BEST, A. I. & LI, X.-Y. 2014. Pore fluid viscosity effects on P- and S-wave anisotropy in synthetic silica-cemented sandstone with aligned fractures. *Geophysical Prospecting,* 62**,** 1238-1252.

TILLOTSON, P., SOTHCOTT, J., BEST, A. I., CHAPMAN, M. & LI, X.-Y. 2012. Experimental verification of the fracture density and shear-wave splitting relationship using synthetic silica cemented sandstones with a controlled fracture geometry. *Geophysical Prospecting,* 60**,** 516-525.

TILLOTSON, P. R. 2012. *A laboratory investigation of frequency-dependent seismic anisotropy in fractured rocks.* Ph.D. thesis, University of Southampton.

TOMS, J., MÜLLER, T. M., CIZ, R. & GUREVICH, B. 2006. Comparative review of theoretical models for elastic wave attenuation and dispersion in partially saturated rocks. *Soil Dynamics and Earthquake Engineering,* 26**,** 548-565.

TOMS, J., MÜLLER, T. M. & GUREVICH, B. 2007. Seismic attenuation in porous rocks with random patchy saturation. *Geophysical Prospecting,* 55**,** 671-678.

TSVANKIN, I. 1997. Reflection moveout and parameter estimation for horizontal transverse isotropy. *Geophysics,* 62**,** 614-629.

TSVANKIN, I., HELBIG, K. & TREITEL, S. 2001. Seismic signatures and analysis of reflection data in anisotropic media.

TUTUNCU, A. N. & SHARMA, M. M. 1992. The influence of fluids on grain contact stiffness and frame moduli in sedimentary rocks. *GEOPHYSICS,* 57**,** 1571-1582.

VAN DER KOLK, C. M., GUEST, W. S. & POTTERS, J. H. H. M. 2001. The 3D shear experiment over the Natih field in Oman: the effect of fracture-filling fluids on shear propagation. *Geophysical Prospecting,* 49**,** 179-197.

VERDON, J. P. & KENDALL, J. M. 2011. Detection of multiple fracture sets using observations of shear-wave splitting in microseismic data. *Geophysical Prospecting,* 59**,** 593-608.

VISSER, R. 1988. *Acoustic Measurements on Real and Synthetic Reservoir Rock.* Ph.D. thesis, Delft University of Technology Delft.

WANG, Z. 2001. Fundamentals of seismic rock physics. *GEOPHYSICS,* 66**,** 398-412.

WANG, Z. 2002. Seismic anisotropy in sedimentary rocks, part 2: Laboratory data. *Geophysics,* 67**,** 1423-1440.

WANG, Z. & NUR, A. 1990. Dispersion analysis of acoustic velocities in rocks. *The Journal of the Acoustical Society of America,* 87**,** 2384-2395.

WANG, Z. & NUR, A. 1992. Elastic wave velocities in porous media: A theoretical recipe. *In:* WANG, Z. & NUR, A. (eds.) *Seismic and Acoustic Velocities in Reservoir Rocks, vol. 2, Theoretical and Model Studies.* Tulsa, Ok: Society of Exploration Geophysicists.

WEI, J. & DI, B. 2008. A physical model study of effect of fracture aperture on seismic wave. *Science in China Series D: Earth Sciences,* 51**,** 233-240.

WHITE, J. E. 1975. Computed seismic speeds and attenuation in rocks with partial gas saturation. *Geophysics,* 40**,** 224-232.

WHITE, J. E., MARTINEAU-NICOLETIS, L. & MONASH, C. 1983. MEASURED ANISOTROPY IN PIERRE SHALE*. *Geophysical Prospecting,* 31**,** 709-725.

WINKLER, K. 1985. Dispersion analysis of velocity and attenuation in Bera Sandstone. *Journal of Geophysical Research,* 90**,** 6793-6800.

WINKLER, K. & NUR, A. 1979. Pore fluids and seismic attenuation in rocks. *Geophysical Research Letters,* 6**,** 1-4.

WINKLER, K. & NUR, A. 1982. Seismic attenuation: Effects of pore fluids and frictional-sliding. *GEOPHYSICS,* 47**,** 1-15.

WINKLER, K. W. 1983. Frequency dependent ultrasonic properties of high-porosity sandstones. *Journal of Geophysical Research: Solid Earth,* 88**,** 9493-9499.

WINKLER, K. W. 1986. Estimates of velocity dispersion between seismic and ultrasonic frequencies. *GEOPHYSICS,* 51**,** 183-189.

WINKLER, K. W. & MURPHY, W. F. 1995. Acoustic velocity and attenuation in porous rocks. *Rock Physics and Phase Relations,* 3**,** 20-34.

WINKLER, K. W. & PLONA, T. J. 1982. Technique for measuring ultrasonic velocity and attenuation spectra in rocks under pressure. *Journal of Geophysical Research: Solid Earth,* 87**,** 10776-10780.

WINTERSTEIN, D. 1992. How shear-wave properties relate to rock fractures; simple cases. *The Leading Edge,* 11**,** 21-28.

WINTERSTEIN, D. F. 1986. Anisotropy effects in P-wave and SH-wave stacking velocities contain information on lithology. *Geophysics,* 51**,** 661-672.

WINTERSTEIN, D. F. 1990. Velocity anisotropy terminology for geophysicists. *GEOPHYSICS,* 55**,** 1070-1088.

WINTERSTEIN, D. F., DE, G. S. & MEADOWS, M. A. 2001. Twelve years of vertical birefringence in nine-component VSP data. *Geophysics,* 66**,** 582-597.

WINTERSTEIN, D. F. & PAULSSON, B. N. P. 1990. Velocity anisotropy in shale determined from crosshole seismic and vertical seismic profile data. *GEOPHYSICS,* 55**,** 470-479.

WU, X., CHAPMAN, M., LI, X.-Y. & BOSTON, P. 2014. Quantitative gas saturation estimation by frequency-dependent amplitude-versus-offset analysis. *Geophysical Prospecting,* 62**,** 1224-1237.

XU, S. 1998. Modelling the effect of fluid communication on velocities in anisotropic porous rocks. *International Journal of Solids and Structures,* 35**,** 4685-4707.

YAO, Q., HAN, D.-H., YAN, F. & ZHAO, L. 2013. Fluid substitution with dynamic fluid modulus: Facing the challenges in heterogeneous rocks. *SEG Technical Program Expanded Abstracts 2013.*

YIN, C. S., BATZLE, M. L. & SMITH, B. J. 1992. Effects of partial liquid/gas saturation on extensional wave attenuation in Berea sandstone. *Geophysical Research Letters,* 19**,** 1399-1402.

ZHU, Y., TSVANKIN, I., DEWANGAN, P. & WIJK, K. V. 2007. Physical modeling and analysis of P-wave attenuation anisotropy in transversely isotropic media. *Geophysics,* 72**,** D1-D7.

ZIMMERMAN, R. W. 1991. *Compressibility of sandstones*, Elsevier.